

The Pennsylvania State University

The Graduate School

College of Engineering

RIPARIAN HYDRAULIC GRADIENT AND WATER TABLE

DYNAMICS IN TWO STEEP HEADWATER STREAMS

A Thesis in

Civil Engineering

by

Thomas J. Voltz

© 2011 Thomas J. Voltz

Submitted in Partial Fulfillment
of the Requirements
for the Degree of

Master of Science

August 2011

The thesis of Thomas J. Voltz was reviewed and approved* by the following:

Michael N. Gooseff
Assistant Professor of Civil and Environmental Engineering
Thesis Co-advisor

Thorsten Wagener
Associate Professor of Civil and Environmental Engineering
Thesis Co-advisor

Kamini Singha
Assistant Professor of Geosciences

Peggy Johnson
Professor of Civil and Environmental Engineering
Head of the Department of Department or Graduate Program

*Signatures are on file in the Graduate School

ABSTRACT

Patterns of riparian hydraulic gradients and flows in headwater catchments provide the hydrologic context for important ecological processes, but are not well understood. Of particular importance is the relative dominance of down- and cross-valley hydraulic gradients, which are a primary control on stream-aquifer exchange dynamics and subsurface residence time of stream water. We investigate hydraulic gradient and water table dynamics over different time scales in the riparian zones of two steep, forested, headwater catchments in the H.J. Andrews Experimental Forest, Oregon. Groundwater level and stream stage data collected at high spatial and temporal resolutions over a period encompassing a 1.25-year storm and subsequent baseflow recession indicate that both riparian zones exhibit strong seasonal down-valley dominance in hydraulic gradients, and responses to rainfall input that do not adhere to simple conceptual models of riparian water table rise. Four constant-rate tracer injections in each stream showed a seasonal increase in the intrusion of tracer-labeled stream water into riparian aquifers as stream discharge receded. In one riparian zone this was linked to the seasonal changes observed in hydraulic gradients, which would tend to increase the potential for hyporheic exchange flows. The similar hydraulic gradient response of the same riparian area to the storm implied the potential for increased stream-groundwater exchange due to the storm, contrary to studies finding increased hyporheic exchange with decreased flows (otherwise supported by seasonal tracer data here). Despite similarity in size, location, and geology, only one watershed exhibited repeated diurnal fluctuations in stream flow and water table elevation during the dry summer, likely because the other lacked riparian vegetation.

Spatial and temporal patterns in water level fluctuations, showing increased magnitude with greater distance from the stream and increasing magnitudes through the season, support the idea that the stream has a buffering effect on water table dynamics that diminishes with distance. Time lag between minimum vapor pressure deficit and minimum water level increased in all cases throughout the season, but at a much faster rate in the stream than in the riparian wells. This points to the possible down-network accumulation of upstream ET signals that could distort the timing of minimum water level in the stream, as has been previously proposed.

TABLE OF CONTENTS

LIST OF FIGURES.....	viii
LIST OF TABLES.....	xvi
ACKNOWLEDGEMENTS.....	xvii
Chapter 1 Introduction	1
1.1 Prevalence of Headwater Streams	1
1.2 Ecologic Importance of Headwaters.....	1
1.3 Riparian Zones and the Terrestrial-Aquatic Interface	2
1.4 Movement of Water in Riparian Zones	3
1.5 Riparian Water Table Fluctuations – Diurnal, Storm, and Seasonal.....	5
1.6 Conclusion.....	7
1.7 Scope and Objectives.....	8
Chapter 2 Site Description	11
2.1 Physical Description	11
2.2 Climate	11
2.3 Geology and Soils.....	13
2.4 Vegetation and History of Management	14
2.5 Study Reaches	16
Chapter 3 Field Methods and Data Processing.....	20
3.1 Monitoring Networks.....	20
3.1.1 WS01 Monitoring Network.....	21
3.1.2 WS03 Monitoring Network.....	22
3.2 Constant-Rate Salt Tracer Injections	22
3.2.1 Injection of Salt Tracer.....	23
3.2.2 Manual Measurement of Well Electrical Conductivity.....	23
3.3 Instrumentation	24
3.3.1 Water Level Loggers	24
3.3.1.1 Pressure-based Water Level Loggers	24
3.3.1.2 Capacitance-based Water Level Loggers.....	26

3.3.1.3	Logger Deployment	28
3.3.1.4	Reference to Datum and Corroboration with Depth Sounder..	29
3.3.2	Electrical Conductivity (EC) Probes and Loggers	29
3.3.2.1	Handheld EC Meter	29
3.3.2.2	In-stream EC Loggers	30
3.4	Other Data Sources	30
3.4.1	Atmospheric Data	30
3.4.2	Flow Data	31
3.5	Water Level Data Processing	31
3.5.1	Disturbances to Water Level Records	31
3.5.2	Referencing Water Levels to a Common Datum	32
3.5.3	Removing Small Errors from EC Measurement Disturbance.....	33
3.5.4	Application of a Simple Smoothing Function	34
3.5.5	Lessons Learned.....	35
3.6	Interpolation of Water Elevations and Calculation of Hydraulic Gradients	35
3.6.1	Interpolation Scheme	35
3.6.2	Calculation of Gradients	36
3.6.3	Resolution of Gradients into Down- and Cross-valley Components...	37
3.7	Water Table Elevation Anomalies.....	37
3.8	Timing of Daily Peak and Trough Water Elevation	38
Chapter 4 Hydraulic Gradient Dynamics.....		39
4.1	Analysis over Three Time Scales	39
4.2	Spatial Definition of Gradients.....	40
4.3	Gradient Dynamics Over the Seasonal Time Scale	42
4.3.1	WS01 Gradient Time Series	42
4.3.2	WS01 Seasonal Salt Tracer Intrusion into Riparian Zone	46
4.3.3	WS03 Gradient Time Series	49
4.3.4	WS03 Seasonal Salt Tracer Intrusion into Riparian Zone	51
4.4	Gradient Dynamics Over the Storm Time Scale	54
4.4.1	WS01.....	54
4.4.2	WS03.....	57
4.5	Gradient Dynamics over the Daily Time Scale	61
4.5.1	WS01.....	61
4.5.2	WS03.....	65
4.6	Summary and Discussion	65
4.6.1	Seasonal Time Scale.....	65
4.6.2	Storm Time Scale	66
4.6.3	Daily Time Scale	67
4.6.4	Discussion of Related Literature.....	68

Chapter 5 Water Table Dynamics	73
5.1 Water Level Anomalies	73
5.1.1 WS01 Anomalies.....	73
5.1.2 Investigating Patterns in WS01 Riparian Anomalies	80
5.1.2.1 Relation of Connectivity to Distance from Stream in WS01	82
5.1.2.2 Consistency of Water Table Response in WS01.....	84
5.1.2.3 Possible Role of Tree Proximity in Anomaly Magnitude in WS01	86
5.1.3 WS03 Anomalies (or Lack Thereof)	87
5.1.4 Accounting for the Difference between WS01 and WS03	90
5.1.5 Timing of Daily Peak and Trough Water Levels	92
5.2 Discussion of WS01 Conceptual Models.....	97
5.3 Summary of Findings	101
Chapter 6 Conclusions	103
References	107
Appendix A Water Level Plots.....	115
A-1. WS01 - Uncorrected, Corrected, Smoothed, Mean, and Manual Readings	115
A-2. WS03 - Uncorrected, Corrected, Smoothed, Mean, and Manual Readings	126
Appendix B Down- and Cross-valley Gradient Magnitude Plots	133
B-1. WS01 – Down-valley Gradient Magnitudes	133
B-2. WS01 – Cross-valley Gradient Magnitudes	137
B-3. WS03 – Down-valley Gradient Magnitudes	140
B-4. WS03 – Cross-valley Gradient Magnitudes	143
Appendix C Anomaly Magnitude vs. Vapor Pressure Deficit in WS01.....	146
Appendix D Water Level Anomalies in WS03	148

LIST OF FIGURES

Figure 2-1 LIDAR image showing outlines of the study watersheds, stream networks, and locations of the study reaches. Inset from USGS Seamless Server.	12
Figure 2-2 WS01 study reach and surrounding riparian zone and lower hillslopes.	17
Figure 2-3 The study reach in WS03, with salient natural features and installed monitoring equipment.	18
Figure 4-1. Hyeto-hydrograph showing hydrologic conditions for the field season, and the time scales considered in our assessment. Vapor pressure deficit (measured at 4.5 meters above ground) is included (gray line) to give context to the diurnal streamflow fluctuations seen in WS01.	39
Figure 4-2. WS01 riparian area, divided into near-hillslope (NH), middle-riparian (MR) and stream-adjacent (SA) zones. Triangles with diagonal lines denote gradient records that ended before the end of the season, and red-shaded triangles are those that began par-way through the season.	41
Figure 4-3. WS03 riparian area, divided into near-hillslope (NH), stream-adjacent (SA), and through-stream (TS) zones. Triangles with diagonal lines denote gradient records that ended before the end of the season, and red-shaded triangles are those that began par-way through the season.	42
Figure 4-4. Illustration of the physical meaning of different hypothetical values of the cross- to down-valley ratio (CDVR), for a) WS01 and b) WS03. Note that the cross-valley sign convention for WS03 is opposite that of WS01, so that in both cases a positive CDVR indicates a gradient directed towards the stream channel.	43
Figure 4-5. WS01 cross- to down-valley gradient ratio (CDVR) for the entire field season, plotted according to the three zones labeled in Figure 4-2. The grey band indicates the region of down-valley dominance.	45
Figure 4-6. 48-hr EC in the WS01 riparian zone, normalized to the stream concentration of 1. Each time step marks the end of a constant-rate salt tracer injection. Gradients at each time step are displayed as arrows that grow darker in color and stack above the earlier arrows as time advances. The colored area diminishes in size as less data becomes available due to wells drying out. The salt tracer was	

injected about 40 meters above the upstream-most well transect. Flow is from bottom right to top left.	47
Figure 4-7. WS03 cross- to down-valley gradient ratio (CDVR) for the entire field season, plotted according to the zones defined in Figure 4-3. Note that the y-axis limits are from -3 to 3, rather than -1 to 1 as in the WS01 figure above. The grey band indicates the region of down-valley dominance.	50
Figure 4-8. 35-hr EC in the WS01 riparian zone, normalized to the stream concentration of 1. Each time step marks the 35 th hour of a 48-hr constant-rate salt tracer injection. Gradients at each time step are displayed as arrows that grow darker in color and stack above the earlier arrows as time advances. Blue circles denote wells. The salt tracer was injected about 40 meters above the upstream-most well transect. Note that the colorbar axis limits are from 0.25 to 1, unlike those in Figure 4-6 for WS01. Flow is from bottom right to top left.	52
Figure 4-9. WS01 cross- to down-valley gradient ratio (CDVR) for the June 1-8 storm period, plotted according to the three zones labeled in Figure 4-2. The grey band indicates the region of down-valley dominance.	55
Figure 4-10. Time-lapsed image of the riparian gradient storm response in WS01. Gradient arrows are plotted such that the arrow color transitions from light grey to black as time progresses over the storm response period. The colored background indicates the rise in water level from the pre-storm level, to show how water levels rose to produce the observed gradient changes. Flow is from bottom right to top left.	56
Figure 4-11. WS03 cross- to down-valley gradient ratio (CDVR) for the June 1-8 storm period, plotted according to the three zones labeled in Figure 4-3. The grey band indicates the region of down-valley dominance.	58
Figure 4-12. Time-lapsed image of the riparian gradient storm response in WS03. Gradient arrows are plotted such that the arrow color transitions from light grey to black as time progresses over the period displayed. The colored background indicates the rise in water level from the pre-storm level, to show how water levels rose to produce the observed gradient changes. Flow is from bottom right to top left.	60
Figure 4-13. WS01 cross- to down-valley gradient ratio (CDVR) for the June 1-8 storm period, plotted according to the three zones labeled in Figure 4-2. Tick marks are displayed at 00:00 on the day labeled.	62

Figure 4-14. WS01 cross- to down-valley gradient ratio (CDVR) for the June 1-8 storm period, plotted according to the three zones labeled in Figure 4-2. Tick marks are displayed at 00:00 on the day labeled. 64

Figure 5-1. Water level anomalies in the WS01 riparian wells, near-hillslope (NH) zone. The dark grey line is flow at the weir 75 m downstream, and the light grey dashed line is vapor pressure deficit at 4.5 m above the ground, recorded at a meteorological station several hundred meters away. The grey rectangles in the top panel indicate when each of the week-long sub-periods occurs. 74

Figure 5-2. Water level anomalies in the WS01 riparian wells, middle-riparian (MR) zone. The dark grey line is flow at the weir 75 m downstream, and the light grey dashed line is vapor pressure deficit at 4.5 m above the ground, recorded at a meteorological station several hundred meters away. The grey rectangles in the top panel indicate when each of the week-long sub-periods occurs. 75

Figure 5-3. Water level anomalies in the WS01 riparian wells, stream-adjacent (SA) zone. The dark grey line is flow at the weir 75 m downstream, and the light grey dashed line is vapor pressure deficit at 4.5 m above the ground, recorded at a meteorological station several hundred meters away. The grey rectangles in the top panel indicate when each of the week-long sub-periods occurs. 76

Figure 5-4. Water level anomalies for the WS01 in-stream loggers. The dark grey line is flow at the weir 75 m downstream, and the light grey dashed line is vapor pressure deficit at 4.5 m above the ground, recorded at a meteorological station several hundred meters away. The grey rectangles in the top panel indicate when each of the week-long sub-periods occurs. 77

Figure 5-5. 7-day mean water level anomalies plotted against distance from the stream. The points represent the mean anomaly magnitudes for the weeks of July 5-12 (red), July 21-28 (green), and August 5-12 (blue). In-stream loggers not shown. 79

Figure 5-6. Water level anomaly magnitude plotted against change in vapor pressure deficit for the same daily periods in the near-hillslope (NH) zone of WS01. 81

Figure 5-7. Maximum water level rise in WS01 riparian wells during the first peak of the storm on June 2 vs. perpendicular distance to the stream thalweg. 83

Figure 5-8. Seasonal drop in WS01 riparian water levels from June 15 to August 19 vs. perpendicular distance to the stream thalweg. 83

- Figure 5-9. 7-day mean water level anomalies plotted against maximum water level rise during the storm. The points represent the mean anomaly magnitudes for the weeks of July 5-12 (red), July 21-28 (green), and August 5-12 (blue)..... 85
- Figure 5-10. 7-day mean water level anomalies plotted against seasonal drop in water level from June 15 to August 19. The points represent the mean anomaly magnitudes for the weeks of July 5-12 (red), July 21-28 (green), and August 5-12 (blue). 85
- Figure 5-11. Mean water level anomalies over the period from July 18 to August 20 vs. the sum of the tree influence index (diameter/distance²) for each well. 87
- Figure 5-12. Water level anomalies in the WS03 riparian wells, near-hillslope (NH) zone. The dark grey line is flow at the weir 75 m downstream, and the light grey dashed line is vapor pressure deficit at 4.5 m above the ground, recorded at a meteorological station several hundred meters away. The grey rectangles in the top panel indicate when each of the week-long sub-periods occurs. 3-mm data logger tolerance is shown as black dashed lines..... 89
- Figure 5-13. WS01 near-hillslope (NH) zone. Timing of peak (blue) and trough (red) water levels through the baseflow recession period. The y-axis is shown with midnight at the center (hour 0). Their best-fit lines are black for wells (G1 = solid; F1 = dash; E1 = dot) and thick grey for stream flow. Timing of peak and trough stream flow values at the gauge weir are shown for context. Time of maximum vapor pressure deficit indicated by the sun symbol and dashed yellow line, minimum by the moon symbol and dashed dark blue line..... 93
- Figure 5-14. WS01 middle-riparian (MR) zone. Timing of peak (blue) and trough (red) water levels through the baseflow recession period. Their best-fit lines for wells are shown in black (H2 = solid; G2 = dash; F2 = dot; E2 = dot-dash) and in thick grey for flow. See Figure 5-13 caption for more details. 93
- Figure 5-15. WS01 stream-adjacent (SA) zone. Timing of peak (blue) and trough (red) water levels through the baseflow recession period. Their best-fit lines for wells are shown in black (H3 = solid; G3 = dash; F3 = dot; E3 = dot-dash; D3 = solid crossed) and in thick grey for flow. See Figure 5-13 caption for more details..... 94
- Figure 5-16. WS01 in-stream loggers. Timing of peak (blue) and trough (red) water levels through the baseflow recession period. Their best-fit lines for in-stream loggers are shown in black (IS0 = solid; IS1 = dash; IS2 = dot; IS3 = dot-dash; IS4 = solid crossed) and thick grey for flow. See Figure 5-13 caption for more details..... 94

Figure 5-17. Theil regression slopes for the timing of peaks (blue circles) and troughs (green x's) in riparian, in-stream, and down-stream flow at the weir.....	96
Figure A-1-1. Evolution of the water elevation record in well D2, WS01.	116
Figure A-1-2. Evolution of the water elevation record in well D3, WS01.	116
Figure A-1-3. Evolution of the water elevation record in well E1, WS01.....	117
Figure A-1-4. Evolution of the water elevation record in well E2, WS01.....	117
Figure A-1-5. Evolution of the water elevation record in well E3, WS01.....	118
Figure A-1-6. Evolution of the water elevation record in well F1, WS01.	118
Figure A-1-7. Evolution of the water elevation record in well F2, WS01.	119
Figure A-1-8. Evolution of the water elevation record in well F3, WS01.	119
Figure A-1-9. Evolution of the water elevation record in well G1, WS01.	120
Figure A-1-10. Evolution of the water elevation record in well G2, WS01.	120
Figure A-1-11. Evolution of the water elevation record in well G3, WS01.	121
Figure A-1-12. Evolution of the water elevation record in well H1, WS01.	121
Figure A-1-13. Evolution of the water elevation record in well H2, WS01.	122
Figure A-1-14. Evolution of the water elevation record in well H3, WS01.	122
Figure A-1-15. Evolution of the water elevation record of in-stream logger IS0, WS01.....	123
Figure A-1-16. Evolution of the water elevation record of in-stream logger IS1A, WS01.	123
Figure A-1-17. Evolution of the water elevation record of in-stream logger IS1B, WS01.	124
Figure A-1-18. Evolution of the water elevation record of in-stream logger IS2, WS01.....	124
Figure A-1-19. Evolution of the water elevation record of in-stream logger IS3, WS01.....	125
Figure A-1-20. Evolution of the water elevation record of in-stream logger IS4, WS01.....	125

Figure A-2-1. Evolution of the water elevation record of well D3, WS03.	126
Figure A-2-2. Evolution of the water elevation record of well D6, WS03.	126
Figure A-2-3. Evolution of the water elevation record of well E5, WS03.....	127
Figure A-2-4. Evolution of the water elevation record of well E6, WS03.....	127
Figure A-2-5. Evolution of the water elevation record of well G5, WS03.	128
Figure A-2-6. Evolution of the water elevation record of well G6, WS03.	128
Figure A-2-7. Evolution of the water elevation record of well H3, WS03.	129
Figure A-2-8. Evolution of the water elevation record of well H5, WS03.	129
Figure A-2-9. Evolution of the water elevation record of well H6, WS03.	130
Figure A-2-10. Evolution of the water elevation record of well I5, WS03.....	130
Figure A-2-11. Evolution of the water elevation record of well I6, WS03.....	131
Figure A-2-12. Evolution of the water elevation record of in-stream logger IS0, WS03.....	131
Figure A-2-13. Evolution of the water elevation record of in-stream logger IS2, WS03.....	132
Figure A-2-14. Evolution of the water elevation record of in-stream logger IS3, WS03.....	132
Figure B-1-1. WS01 down-valley gradient magnitude for the entire field season, plotted according to the three zones labeled in Figure 4-2.....	134
Figure B-1-2. WS01 down-valley gradient magnitude for the storm period, plotted according to the three zones labeled in Figure 4-2.....	135
Figure B-1-3. WS01 down-valley gradient magnitude for the week of July 24-31, plotted according to the three zones labeled in Figure 4-2.....	136
Figure B-2-1. WS01 cross-valley gradient magnitude for the entire field season, plotted according to the three zones labeled in Figure 4-2.....	137

Figure B-2-2. WS01 cross-valley gradient magnitude for the storm period, plotted according to the three zones labeled in Figure 4-2.....	138
Figure B-2-3. WS01 cross-valley gradient magnitude for the week of July 24-31, plotted according to the three zones labeled in Figure 4-2.....	139
Figure B-3-1. WS03 down-valley gradient magnitude for the entire field season, plotted according to the three zones labeled in Figure 4-3.....	140
Figure B-3-2. WS03 down-valley gradient magnitude for the storm period, plotted according to the three zones labeled in Figure 4-3.....	141
Figure B-3-3. WS03 down-valley gradient magnitude for the week of July 24-31, plotted according to the three zones labeled in Figure 4-3.....	142
Figure B-4-1. WS03 cross-valley gradient magnitude for the entire season, plotted according to the three zones labeled in Figure 4-3.....	143
Figure B-4-2. WS03 cross-valley gradient magnitude for the storm period, plotted according to the three zones labeled in Figure 4-3.....	144
Figure B-4-3. WS03 cross-valley gradient magnitude for the week of July 24-31, plotted according to the three zones labeled in Figure 4-3.....	145
Figure C-1. Water level anomaly magnitude plotted against change in vapor pressure deficit for the same daily period in the middle-riparian (MR) zone of WS01.....	146
Figure C- 2. Water level anomaly magnitude plotted against change in vapor pressure deficit for the same daily period in the stream-adjacent (SA) zone of WS01.....	147
Figure D-1. Water level anomalies in the WS03 riparian wells, stream-adjacent (SA) zone. The dark grey line is flow at the weir 75 m downstream, and the light grey dashed line is vapor pressure deficit at 4.5 m above the ground, recorded at a meteorological station several hundred meters away. The grey rectangles in the top panel indicate when each of the week-long sub-periods occurs. 3-mm data logger tolerance is shown as black dashed lines.....	149
Figure D-2. Water level anomalies in the WS03 riparian wells, in-stream loggers. The dark grey line is flow at the weir 75 m downstream, and the light grey dashed line is	

vapor pressure deficit at 4.5 m above the ground, recorded at a meteorological station several hundred meters away. The grey rectangles in the top panel indicate when each of the week-long sub-periods occurs. 3-mm data logger tolerance is shown as black dashed lines.150

LIST OF TABLES

Table 2-1. Physical attributes of study watersheds and stream reaches..... 12

ACKNOWLEDGEMENTS

This thesis is the result of earnest efforts by many individuals, none of which can be discounted. I thank Mike Gooseff for patiently seeing me through the entire four-semester journey and helping me maintain my sanity in the final days and hours. Thorsten Wagener always offered insightful and incisive feedback and criticism, and was an excellent motivational officer. Adam Ward and Michael Fitzgerald were surrogate older brothers to me afield in Oregon and at home in State College, and showed me many more than a useful thing or two about science and life. Kamini Singha offered excellent advice as the co-leader of our project group. Invaluable and frequent advice, assistance, encouragement, and camaraderie came from the other Water Resources grad students and associates, Keith Sawicz, Christa Kelleher, Susan Gregg, Mitch Weaver, George Holmes, Riddhi Singh, Joe Kasprzyk, Alisha Fernandez, Rachel Urban, Xuan Yu, Adam Wlostowski, Katy Gerech, Emily Bernzott, Jon Herman, Matt Woodruff, Melissa Ward, and Sarah Godsey. Generally kind tolerance was granted by my parents, siblings, and my girlfriend Lee, who often gave me a precious mental anchor and a much-needed dose of perspective.

Last but not least, the staff and scientists at the HJ Andrews Experimental Forest provided assistance and facilities and the American taxpayers through the National Science Foundation provided funding that made all of this work possible.

Chapter 1

Introduction

1.1 Prevalence of Headwater Streams

Many researchers in the fields of ecology, hydrology, biology, and chemistry have recognized the importance of first- and second-order headwater streams in the broader context of large stream networks and drainage basins. Early work by Horton [1945] and later contributions by Strahler [1957] established 'stream order' as a means of quantitatively measuring the prevalence of differently sized geomorphic features in drainage basins. Their work revealed that low-order, headwater streams greatly dominated stream networks both in terms of stream channel length and upstream drainage area. In the United States, headwater streams make up 70 to 80% of stream networks by channel length [Leopold et al., 1964; Meyer et al., 2007]. In an assessment of nitrogen pollution in European rivers Haycock et al. [1993] noted that it was commonly recognized that first- and second-order streams contribute more than 90% of flow to most rivers by the time they reach the ocean.

1.2 Ecologic Importance of Headwaters

Headwater streams' prevalence in terms of channel length and drainage area leads logically to their disproportionately large influence on downstream water quality. Regulating water quality in headwater streams is a priority first step in the larger scheme of remediating European rivers, strictly because of their dominant contribution to total river flow [Haycock et al., 1993]. Headwater streams perform a number of important functions, including maintaining

natural discharge regimes, regulation and retention of sediment and nutrients, processing organic matter, and determining the character of water quality in that region [Lowe and Likens, 2005]. Many studies demonstrate the role headwater streams play in retention of sediment [Dieterich and Anderson, 1998], dissolved organic carbon [McDowell, 1985], particulate organic matter [Jones and Smock, 1991; Webster et al., 1994], and nitrogen, typically as nitrate [Haycock et al., 1993; Jacobs and Gilliam, 1985; Triska et al., 1989; Valett et al., 1996; Dieterich and Anderson, 1998; Peterson et al., 2001; Thomas et al., 2001, Alexander et al., 2007].

Nitrogen, generated in large quantities by human activity [Thomas et al., 2001], can be toxic to humans and animals in high concentrations and is therefore classified as a pollutant. Alexander et al. [2007] find that headwater streams in the northeast U.S. contribute 55% of flow and 40% of nitrogen input to higher-order receiving rivers, highlighting the substantial downstream impacts of many headwater streams taken together. Effective transformation and retention of inorganic nitrogen in headwater streams can help to prevent eutrophication in downstream waters [Peterson et al., 2001], such as that which affects waters in the Lower Susquehanna Basin and Chesapeake Bay in the northeast U.S. [Millard et al., 2001].

1.3 Riparian Zones and the Terrestrial-Aquatic Interface

Riparian zones, commonly defined as the vegetated strips of land adjacent to stream channels in valley bottoms [Hill, 1996], play a special role in the transformation and retention of nutrients like nitrogen [Jacobs and Gilliam, 1985; Altman and Parizek, 1995; Hill, 1996; Burt et al., 1999; Vidon et al., 2010]. Riparian zones are also commonly thought of as the interface between the aquatic (stream) and terrestrial (hillslope and valley bottom) environments [Hill, 1996, Meyer et al., 2007], an interface identified as a critical point for nutrient flux and

chemical reactant availability and regulated by stream-groundwater exchange [Morrice et al., 1997; Dahm et al., 1998]. Presence of this interface leads to the development of so-called 'hot spots' and 'hot moments' in riparian or other areas of stream-groundwater exchange, where conditions are just right for substantial biogeochemical activity [Hill, 1996; McClain et al., 2003; Vidon et al., 2010]. Both time and space must favor this activity, however, as one without the other may fail to produce a beneficial outcome. For instance, Burt et al. [1999] showed that great potential existed for denitrification in the organic-rich upper soil horizon of a riparian zone, but it was largely underexploited because the timing of nitrogen-bearing water flowing from the hillslope seldom brought the water into that soil horizon to cause a 'hot moment'. Similarly, a lack of sufficient organic matter or other necessary biogeochemical reactants (i.e. those required to generate a 'hot spot') obviates the potential for flow of nutrient-bearing water through that space, since one half of the equation is missing. This underlines the importance of studying hydrologic flowpaths within riparian zones in order to establish the link between ecology and hydrology and to improve the prediction of the timing and location of hot spots and hot moments, with a view to undertaking management programs that use this knowledge to ultimately improve downstream water quality in affected regions [Haycock et al., 1993].

1.4 Movement of Water in Riparian Zones

Because riparian zones (particularly those in headwater catchments) tend to be nearly saturated with water much of the time and intimately connected with the streams they interface with, flow in these systems under varying climatic conditions can be complicated and sometimes counter-intuitive. The most notable aspect of flow in these systems that has been

studied and discussed in recent years is the link between groundwater and surface water, which had previously tended to be discussed and managed as though they were separate entities [Jones and Holmes, 1996; Winter, 1998]. Recognizing that streams and their adjacent riparian aquifers were frequently well connected required that conceptual models of flow in those systems be expanded to account for this exchange and the more complex gradients and flow paths it implied [Larkin and Sharp, 1992; Woessner, 2000]. An important aspect of this conceptual expansion was the recognition that valley-bottom riparian flow does not occur only in a perpendicular (cross-valley) direction relative to the stream, but is instead three-dimensional in nature, with groundwater often flowing oblique to the direction of streamflow [Harbaugh and Getzen, 1977; Prince, 1980; Alley, 1993; Haycock et al., 1993; Altman and Parizek, 1995; Hill, 1996]. Many researchers have recognized this and analyzed three-dimensional riparian flow systems in various headwater locations [Harvey and Bencala, 1993; Morrice et al., 1997; Wroblicky et al., 1998; Kasahara and Wondzell, 2003; Vidon and Hill, 2004; Wondzell, 2006]. But comparatively fewer have conducted seasonal monitoring of riparian water table elevations at high temporal and spatial resolution in order to provide a detailed characterization of the relative dominance of down- and cross-valley hydraulic gradients, and combined this with solute transport data from tracer injections to assess the impact of gradient changes on riparian stream-groundwater exchange.

The three-dimensional nature of riparian flow, and in particular the relative magnitudes of down- and cross-valley gradients has implications for studying and engineering the ecological function of riparian buffer zones. Alley [1993] suggests that in many cases it would be prudent to conduct several seasons of water level monitoring to establish patterns of gradients and

flowpaths prior to collecting water quality samples, so that transformation or retention of nutrients or other groundwater constituents can be tracked accurately for a given parcel of water along its flow path. From the perspective of riparian zones serving as buffers against nonpoint-source groundwater pollution, residence time is an important consideration that is directly determined by riparian hydraulic gradients [Haycock et al., 1993]. Riparian groundwater that tends to flow parallel to the streamflow direction (down-valley) will spend much more time in the soil before entering surface water (if it does at all), the impact being that even for narrow riparian corridors, actual retention times can be substantially greater than expected [Haycock et al., 1993]. Better understanding of the spatial and temporal distribution of down- and cross-valley gradient dominance in a riparian area can therefore greatly inform both scientific studies aimed at tracking biogeochemical cycling and management strategies for protecting headwater streams.

1.5 Riparian Water Table Fluctuations – Diurnal, Storm, and Seasonal

In addition to riparian-scale hydraulic gradient patterns that result from seasonal fluctuations in the water table, there are other aspects of riparian water table dynamics that have been studied and could teach us more about spatially characterizing riparian areas. In particular, numerous studies have focused on fluctuations in groundwater levels and stream stage and flow that occur in a diurnal cycle, of which Gribovski et al. [2010] provide a good review. Of these, the majority focus on diurnal fluctuations caused by regular variations in evapotranspiration (ET) demand from phreatophytic (water-loving) or other vegetation close enough to the saturated zone to produce effects on the groundwater level and stream stage. These studies approach this phenomenon from different perspectives, with most focusing on

estimation of streamflow volumes “lost” to vegetation through ET [White, 1932; Troxell, 1936; Dunford and Fletcher, 1947; Robinson, 1958; Tschinkel, 1963; Meyboom, 1964, 1967; Reigner, 1966; Weisman, 1977; Baird et al., 2005; Loheide et al., 2005; Lautz, 2007; Gribovski et al., 2008; Loheide, 2008], and others focusing more on what could be learned about physical watershed or riparian zone processes on the basis of the fluctuations or changes in them [Weisman, 1977; Burt, 1979; Bren, 1997; Butler et al., 2007]. A number of studies have also been conducted at the H.J. Andrews Experimental Forest (HJA) field sites used in this work, aimed at assessing the extent of vegetation influence on ET-induced fluctuations in streamflow and hillslope groundwater flow [Bond et al., 2002; Barnard et al., 2010] and how they fit into conceptual models about riparian zone hydrology [Gooseff et al., 2008; Wondzell et al., 2009] and the headwater stream hydrology on the whole [Wondzell et al., 2007].

The study of diurnal fluctuations in riparian water tables is useful in management of water resources and for improving hydrogeologic and eco-hydrologic characterization of watersheds [Gribovski et al., 2010]. Water table fluctuations that occur also in response to storm events, seasonal drying, and the accumulated effect of many consecutive diurnal fluctuations, found to speed flow recession [Federer, 1973; Weisman, 1977], are of similar interest and can be useful in learning more about the behavior of riparian zones and their role in mediating stream-terrestrial linkages. Here, we seek to use high resolution water elevation data supplemented by thorough literature review to comment on the work performed at our field sites in HJA, in order to both test and refine, if necessary, conceptual models already proposed based on past (recent) data collected there. Our objectives include assessing diurnal, storm, and seasonal water table fluctuations.

1.6 Conclusion

Since processes like denitrification tend to be focused in localized hot spots of low oxygen and high organic carbon [Parkin, 1987; Murray et al., 1995; Hill, 1996], for example, and hydrologic flowpaths are essential in creating and carrying nutrients and biochemical reactants and products to and from these sites [McCain et al., 2003; Vidon et al., 2010], understanding how water is likely to flow in morphologically and hydrologically distinct headwater catchments will enable us to predict how the efficacy of nutrient cycling and other ecological processes varies between regions. Furthermore, due to the complex nature of groundwater flow in headwater riparian areas, there is a need for studies that assess patterns of hydraulic gradients and potential hydrologic flowpaths at the spatial scale of the riparian zone. Although several researchers in the last few decades have shown experimentally and through the use of models that the down-valley gradient plays a prominent role in determining the complex combinations of hydraulic gradient magnitudes and directions that can occur in headwater riparian areas, none have explicitly examined the relative dominance of down- and cross-valley gradient components as they vary both in space across the riparian zone and in time throughout seasonally varying flow conditions. Such variation in flow and water table elevation is found in the baseflow recession that occurs during summers in the western Cascades of Oregon, at our study sites located within the H.J. Andrews Experimental Forest LTER site.

This work serves as an initial step towards improving our ability to predict and assess the extent of stream-groundwater interaction in steep, narrow headwater streams with the use of experimental field water elevation and solute transport data. It also probes the potential of using temporal dynamics in a network of riparian water elevation records to detect spatial

patterns in the riparian zone that may be indicative of similar behavior in other headwater riparian zones. Lastly, it is part of a larger body of experimental work performed at two well-studied headwater streams in the H.J. Andrews Experimental Forest (HJA), and will complement with new data what has already been learned there, while providing a clearer conceptual understanding of how these systems work that can inform and aid the planning of future work at these sites.

1.7 Scope and Objectives

The scope of this work consists of high-resolution temporal measurement of groundwater-level and stream-stage elevations in spatially dense monitoring networks in two steep, second-order headwater stream reaches in western Oregon, USA. Interpretation of water table elevation data is limited to evaluation of hydraulic gradients based on the 3-dimensional phreatic water surface as measured in wells and the open stream channel. No vertical hydraulic gradients are analyzed at point locations in the stream to study upwelling and downwelling of water. We also use fluid electrical conductivity (EC) data collected from the monitoring well networks during a series of constant-rate salt tracer injections into both streams conducted throughout the summer of 2010. Our research objectives can be divided into two primary categories:

1. **Hydraulic gradients.** Although many researchers have acknowledged the down-valley gradient in their studies of floodplain and riparian water table dynamics, many continue to assume, often implicitly through 2-dimensional elevation-view diagrams (i.e. lateral cross-sections), that groundwater in riparian areas flows perpendicularly towards or away from stream channels. Additionally, while numerous researchers have studied

nutrient cycling and retention along groundwater flowpaths from upland agricultural or other sites through riparian areas to streams, relatively fewer have examined transport of solutes and nutrients from the stream to the riparian zone, and of these few have assessed how the spatial extent of this exchange zone varies through time and with changing flow conditions. Therefore, the research objectives for this first part of our work are:

- 1a. To gain better understanding of how down- vs. cross-valley dominance in hydraulic gradients varies in space across headwater riparian zones and in time across both long (seasonal baseflow recession) and short (storm, daily) time scales
 - 1b. To assess the impact of seasonal baseflow recession on the extent of stream water intrusion into the riparian areas adjacent to streams receiving the salt tracer injections
2. **Spatial and Temporal Water Table Dynamics.** A significant volume of work exists that documents and analyzes various aspects of diurnal fluctuations in groundwater levels, stream stage, and discharge, but few studies focus on small, spatially dense networks of water table elevation measurements. Additionally, there is utility in work aimed at characterizing hydraulic behavior of different areas of a riparian zone by specifically seeking to identify small-scale spatial patterns in relationships between different measures of water table dynamics over seasonal time scales and in view of proximity to sources of evapotranspiration (ET) demand and the position within the valley bottom (i.e. distance from stream thalweg). Our objectives in this second part of the work are:

- 2a. To evaluate how diurnal water table fluctuation magnitudes are organized spatially and how they change throughout the baseflow recession period
- 2b. To track how, if at all, the timing of the daily peak and trough water levels change throughout the baseflow recession season
- 2c. To assess whether the magnitude of the diurnal water table fluctuations (maximum minus minimum value) correlates with proximity of wells to nearby trees, which may act as localized sources of ET water withdrawal
- 2d. To assess whether the proximity of a well to the stream thalweg correlates with the following aspects of water table dynamics:
 - i. Magnitude of diurnal water table fluctuations
 - ii. Seasonal drop in water level over the summer baseflow recession
 - iii. Total rise in water level in response to a 1.25-year storm event
- 2e. To assess whether any correlation exists in comparing the following water table dynamics to each other:
 - i. Magnitude of diurnal water table fluctuations vs. seasonal drop
 - ii. Magnitude of diurnal water table fluctuations vs. storm rise

Chapter 2

Site Description

2.1 Physical Description

The two headwater catchments used in this study are watershed one (WS01) and watershed three (WS03), located in the H.J. Andrews Experimental Forest (HJA) in the western Cascade Mountains, about 80 km east of the city of Eugene, Oregon (**Figure 2-1**). Basic physical parameters of the watersheds and study reaches are given below in **Table 2-1**. Both watersheds are markedly dissected by their streams, with very steep hillslopes (> 50%) and high-gradient stream channels (\approx 15%). Valley bottom riparian areas tend to be narrow and constrained by the adjacent hillslopes. The two stream reaches used in this study were located at the very bottom of the watersheds, within 100 meters of the flow gauging stations. These reaches were chosen because they contain established riparian well networks.

2.2 Climate

The HJA has a Mediterranean climate, with very wet, mild winters and unusually dry, cool summers. Average monthly temperatures at the elevation of WS01 and WS03 vary between 1°C in January and 20°C in July [Rothacher et al., 1967]. Snow packs form at lower elevations, but seldom last beyond two weeks. Most of the precipitation (about 2300 mm annually) falls mainly as rain between the months of October and May [Swanson and Jones, 2002], resulting in a baseflow recession period that begins sometime in mid to late June and

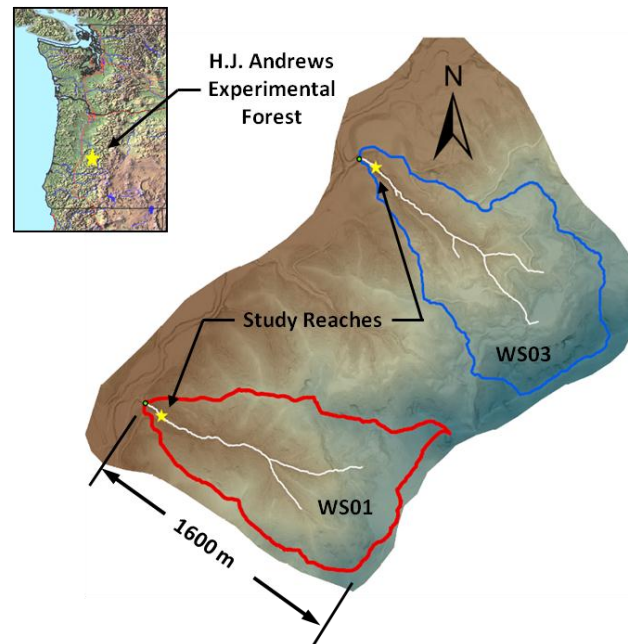


Figure 2-1. LIDAR image showing outlines of the study watersheds, stream networks, and locations of the study reaches. Inset from USGS Seamless Server.

Table 2-1. Physical attributes of study watersheds and stream reaches.

Physical Attribute	Watershed 1	Watershed 3
--- Whole Watershed ---		
¹ Area (hectares)	95.8	97.2
*Aspect (true north-azimuth)	290°36' (WNW)	314°24' (NW)
² Elevation above m.s.l.		
Maximum (m)	1018	1077
Minimum (m) [at flume]	432	472
³ Lee's Radiation Index	41.9	36.5
--- Study Reach and Riparian Area ---		
Length (m) [along stream]	24	24
Width (m) [perpendicular to stream]	10	4
Mean Channel Slope (%)	11.9	13.8
Strahler Stream Order	2	2

¹Calculated in ESRI ArcMap using 2010 1-m LIDAR

²Based on 2010 1-m LIDAR

³Higher number indicates greater incident solar radiation [Lee, 1963]

*Data taken from Rothacher et al. [1967]

lasts until late August or September. This offers an opportunity to study the change in riparian hydraulic gradients and water table elevations over a range of flow conditions that occur in one continuous period.

2.3 Geology and Soils

The surface bedrock underlying HJA is geologically young, consisting of various derivatives of volcanic lava, mud, or pyroclastic flows [Swanson and James, 1975]. The bedrock in WS01 and WS03 is dominated by reddish (in the study reaches and lower elevations) and greenish (at higher elevations) breccias and tuffs deposited by the last volcanic activity during the Oligocene and lower Miocene epochs about 24 million years ago. These formations are readily weatherable, resulting in thick layers of unconsolidated, weathered rock on top of solid rock, and they lend themselves to extensive mass movements in the steep terrain found in WS01 and WS03. More solid andesite forms the drainage divide at the top of the ridge, and smaller flows of basalt are scattered throughout both watersheds [Rothacher et al., 1967].

Overall, soils in WS01 and WS03 are predominately shallow (1-2 meters) with limited profile development and considerable gravel and cobbles, although these are often underlain by thick layers of unconsolidated, weathered parent material, likely allowing substantial water storage and making them 'deep' from a hydrologic perspective. Depth to relatively impermeable bedrock is not obvious, and in some locations may exceed 15 meters. These deep weathered deposits may be important for maintaining baseflow during the summer dry spells. Although all soils found in WS01 and WS03 are texturally classified as loam and contain significant percentages of fines (> 20%), they tend to display massive, well-aggregated structure that contributes to high porosity (> 50% in all cases, up to 75%) and infiltration rates (about 500

cm/hr, but variable). The high porosity nearly eliminates the possibility of overland flow, and ensures that both watersheds respond rapidly to rainfall [Rothacher et al., 1967, Dyrness, 1969].

2.4 Vegetation and History of Management

Prior to the 1960s, forests in both WS01 and WS03 were predominantly made up of 400 to 500-yr-old Douglas fir trees, with varying amounts of western hemlock mixed interspersed throughout. Between 1962 and 1966, WS01 was completely clearcut, and then prescribed burned in 1967, whereas 25% of WS03 was clearcut and controlled burned in three sections from 1962 to 1963 and the rest left undisturbed [Swanson and Jones, 2002; Lutz and Halpern, 2006]. Following the experimental cutting and burning of all vegetation, WS01 was aerially reseeded with Douglas fir on two separate occasions with limited success, and was ultimately re-planted with 2-yr-old Douglas fir saplings at 3-m spacing. In WS03, the cut and burned areas were replanted with 3-yr-old Douglas fir saplings [Lutz and Halpern, 2006]. In the intervening 40 years, Douglas fir grew up over the vast majority of WS01 and the disturbed areas of WS03, with the exception of the near-stream riparian areas in WS01, in which red alder, big-leaf maple, and other deciduous trees out-competed Douglas fir and grew to relative maturity (breast-height diameter \approx 30 cm in our study reach). In February of 1996, the largest storm event on record in the HJA produced mass movements throughout HJA, and WS03 experienced a large debris flow that scoured most of the upper stream channel to bedrock, removing vegetation and ultimately depositing much of the displaced soil in the lower stream channel, including our reach. [Swanson and Jones, 2002]. Since then, red alder and big-leaf maple have

regenerated in parts of the riparian zone, including about half of our WS03 study reach, achieving diameters of about 5-8 cm.

The distribution of coniferous and deciduous vegetation can be explained by the adaptations made by large, long-lived conifers like Douglas fir to living in the extreme precipitation regime of the Pacific Northwest. Intense drought during the majority of the growing season from April to October greatly stresses hardwood species that depend on those months to produce while their leaves are on, while evergreen conifers are able to photosynthesize the whole year round [Waring and Franklin, 1979]. Conifers are also better adapted to drought conditions, since they are more water-efficient on average than deciduous trees, and it has been estimated that the water storage in the sapwood of a large Douglas fir tree could sustain photosynthesis-induced transpiration for up to 10 consecutive days [Running et al., 1975]. Douglas fir have additionally been found to require fewer nutrients than hardwoods, and are better able to access the nutrients stored in soil and litter during the non-growing season when copious rainfall promotes nutrient leaching [Waring and Franklin, 1979]. Some hardwood species like red alder have nitrogen-fixing abilities that give them some advantage [Waring and Franklin, 1979], but even with this they are restricted to very wet valley-bottom sites where they have ample access to water during the growing season, as observed in both study reaches of WS01 and WS03.

As it pertains to the ability of trees to access groundwater and cause diurnal level fluctuations through transpiration demand in the dry summers, it bears mentioning that despite their tremendous height, mature Douglas firs typically have 90% of their rooting mass within the first meter of the soil, rarely exceeding two meters in all [Santantonio et al., 1977],

and 75% of fine roots – through which most transpired water is drawn [Sollins et al., 1980] – occur in the upper 30 cm of soil [Santantonio, 1979]. Other studies found similar results [Heilman, 1990; Curt et al., 2001]. Heilman [1990] found that typical maximum rooting depth for red alder was also about one meter. In a study of transpiration in six small hardwoods Woods and O’Neal [1965] found that water was overwhelmingly drawn from the upper 30 cm of soil. However, many researchers have documented that water is drawn first from where it is most available and is later drawn from progressively greater depths as conditions require [Ogata et al., 1960; Running et al., 1975; Waring and Running, 1976].

2.5 Study Reaches

A detailed map of the WS01 study reach studied in this work is shown below in **Figure 2-2**. Steep hillslopes outside of the riparian area give way to a more level valley bottom. Other features of the area include ubiquitous rotten logs, much of them remnants of the 1960s clearcut, and many large boulders, which are concentrated in the stream channel.

The stream spatial extent shown in **Figure 2-2** reflects conditions in March, towards the end of the wet season. The thalweg is indicative of the deepest part of the stream channel, and consequently where water flowed throughout the baseflow recession period, while the two right-hand channel splits (looking downstream) at 1) the highest part of the stream and 2) between piezometers G4 and F4 went dry sometime in mid-summer. In general, the character of the stream in this reach with 11.9% slope can be described as a series of steps (often formed by downed trees), pools, and riffles, and the channel is subject to frequent reordering owing to the high rainfall and steep channel gradient. The channel is therefore less well-defined than

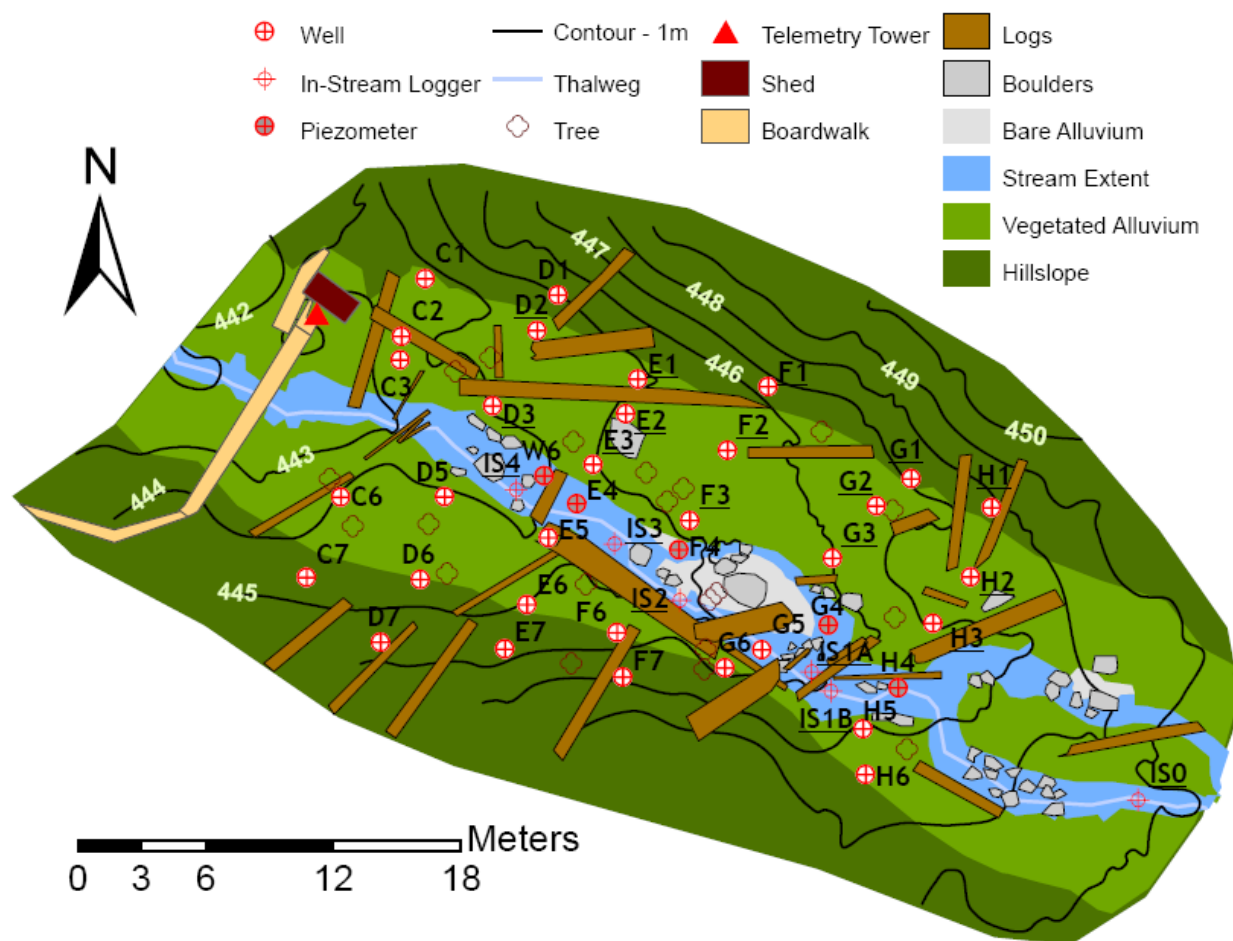


Figure 2-2. WS01 study reach and surrounding riparian zone and lower hillslopes.

headwater streams in more gently sloped watersheds. A number of 50-year old deciduous (mostly red alder) trees have grown up in the riparian zone, providing considerable shading of the site and exerting an ET demand on the riparian groundwater, where it is closer to the surface.

This valley bottom of WS03 (**Figure 2-3**) is much narrower and more confined by steep hillslopes and occasional bedrock outcrops than that of WS01, affording a more limited opportunity to monitor the riparian zone to the same cross-valley extent as in WS01. The two

streams are otherwise morphologically similar, and like WS01 the stream in WS03 is a series of steps, riffles, and pools, and generally does not follow a well-defined channel. WS03 seems to have a greater concentration of boulders in the stream channel, which play a central role in

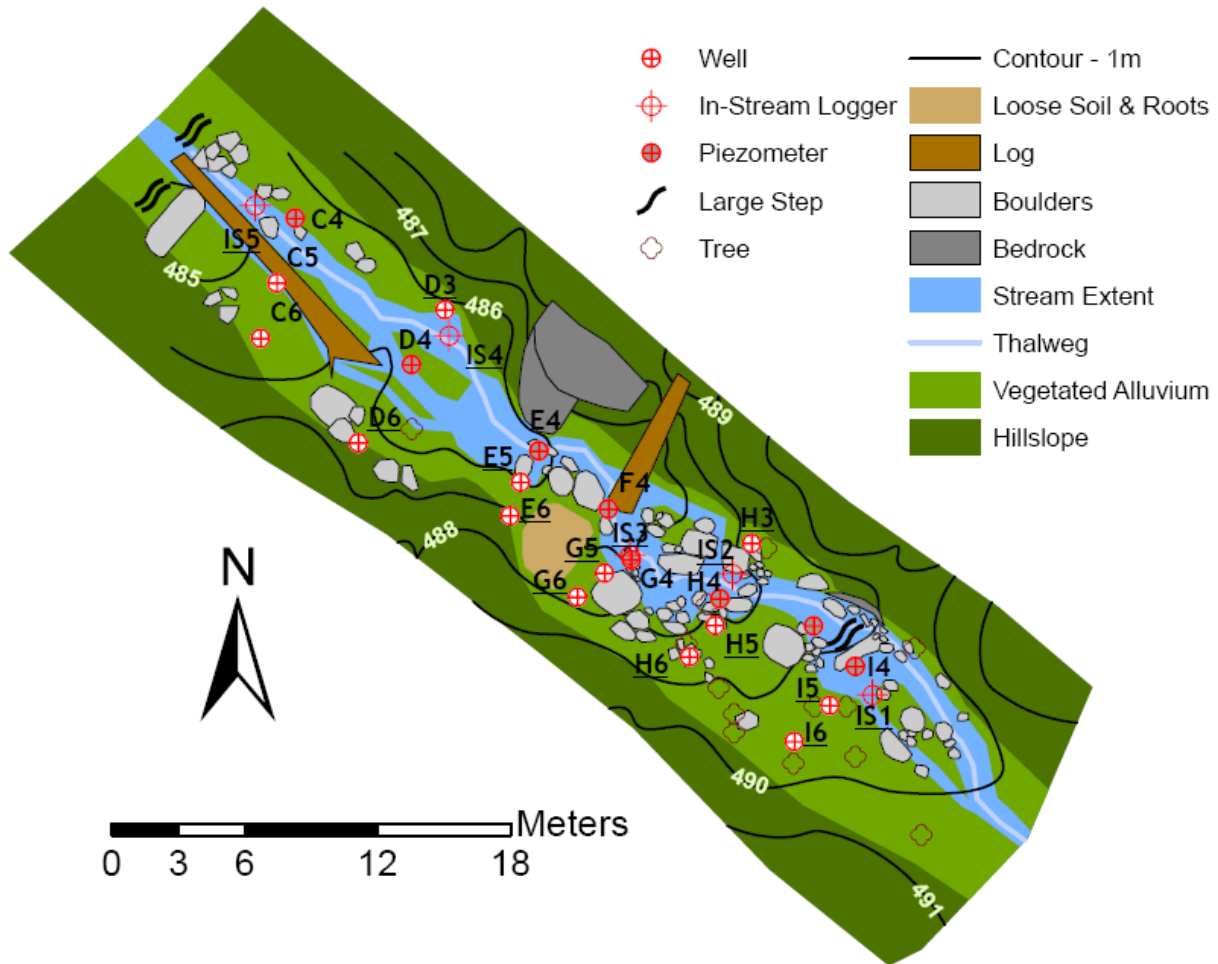


Figure 2-3. The study reach in WS03, with salient natural features and installed monitoring equipment.

controlling the downstream path of flowing streamwater. The stream is subject to reordering of sediments and boulders during large rainfall events, and evidence of the 1996 flood and mudslide is quite apparent in the eroded hillslopes, occasional exposed bedrock, relative lack of woody debris (compared to WS01) and presence of only young deciduous trees in some parts of the riparian zone. Due to the relative lack of vegetation, the WS03 study reach receives much more direct solar radiation and water temperatures are higher than in WS01. As with the above map of WS01, the spatial extent of the wetted stream channel shown in **Figure 2-3** represents wet conditions, and by mid-summer flowing water was generally only found in the channel delineated by the thalweg line.

Chapter 3

Field Methods and Data Processing

3.1 Monitoring Networks

To examine both the down- and cross-valley dominance of riparian hydraulic gradients (research objective 1a) and other spatial and temporal patterns in riparian water table dynamics (research objectives 2a-e), we collected groundwater level measurements at a high spatial density using shallow monitoring well networks that were installed by Steve Wondzell [Wondzell, 2006] in the summer of 1997 in the riparian areas along each of the two stream reaches (see **Figures 2-2 and 2-3**). The well casings were constructed from 1.25-inch diameter PVC pipe, screened over the bottom 50 cm by drilling 0.32-cm diameter holes at a density of about 0.25 holes/cm². Wells were driven in directly by hand, owing to the rugged nature of both sites, and penetrated to depths between 0.75 and 1.5 meters below the ground surface. Wondzell also installed a series of piezometers (screened over the bottom 5 cm only) in the streambed above and below salient geomorphic step features to assess vertical hydraulic gradients, but data collected from these piezometers were not used, since they were less likely to be representative of the phreatic (unconfined) water table elevation at those locations. In the intervening 13 years some wells and piezometers were destroyed or rendered unusable, leaving 32 and 13 riparian wells in WS01 and WS03 respectively available during our 2010 summer field season. We could not instrument all available wells, but still sought to record data in both watersheds. Of the remaining wells, 14 on the right bank of the WS01 study reach

and 11 mostly on the left bank of the WS03 reach were outfitted with data loggers that continuously recorded water level and temperature (generally at the bottom of wells) from June 1 to August 20, 2010. Following pre-season well development to re-engage the wells with the surrounding soil, we found that all wells were generally well-connected the surrounding groundwater, and re-filled with water relatively quickly when bailed for measurement purposes. We also placed in-stream loggers to record stream stage (and by extension water table elevation) in pools in both stream reaches -- 5 in WS01 and 4 in WS03 (one of which recorded no reliable data).

3.1.1 WS01 Monitoring Network

The riparian wells in WS01 were placed in transects roughly perpendicular to the stream, at a spacing of about 2-3 meters. Spacing between transects in the down-valley direction ranges from 6 to 8 meters. The wells outfitted with water level loggers are shown with underlined labels in **Figure 2-2**, covering a continuous region from transect D up to transect H (well D1 was dry except during a storm on June 2-4). In-stream loggers were generally placed in pools between the five well transects, although this had to be adjusted to ensure that the water would be deep enough to last throughout the summer baseflow recession. Nevertheless, since some of the wells and one in-stream pool went dry at various points during the summer, some of the well loggers' records ended before the end of the field season (H1 and D2), and one in-stream logger needed to be relocated (IS1). Due to its isolation from the rest of the monitoring network, the upstream-most logger IS0 was not considered during analysis.

3.1.2 WS03 Monitoring Network

Well placements in WS03 were necessarily constrained by the narrow width of the valley bottom between the steep hillslopes, and in the five transects instrumented (transect D to I, omitting F) well spacing was about 1.5-2 meters. It was also normally feasible to place only two wells in the adjacent riparian zone, rather than three as in WS01. Spacing between transects in WS03 also ranged from 6 to 8 meters. Wells instrumented with loggers are shown with underlined labels in **Figure 2-3**. In-stream loggers were placed more or less in line with well transects, again subject to adjustment in whichever direction promised deeper water. In one location the monitored area extended beyond the stream channel to well H3, the record for which begins after June 20. Otherwise, all loggers recorded data uninterrupted for the entire field season. Data from IS5 in transect C was not used in analysis, due to its being far removed from the rest of the monitoring network.

3.2 Constant-Rate Salt Tracer Injections

To address research objective 1b of assessing the influence of changing riparian hydraulic gradients on stream-groundwater exchange, this work was done in conjunction with a data collection campaign aimed at mapping and imaging the spatial and temporal extent of the hyporheic zone around both stream reaches. This was accomplished by conducting a series of continuous 48-hour tracer injections coupled with frequent measurement of fluid electrical conductivity (EC) in the networks of wells and piezometers. The well EC readings relative to the measured in-stream EC can be used to gauge what effects seasonally varying gradient patterns exert on the extent of tracer-labeled stream water intrusion into the riparian zones.

3.2.1 Injection of Salt Tracer

We injected a dissolved high-concentration NaCl solution into the stream to trace the movement of stream water into riparian aquifers. The goal of each injection (only approximately met) was to raise the EC of the receiving streamwater 100 $\mu\text{S}/\text{cm}$ above the background, which was about 40 $\mu\text{S}/\text{cm}$ at the start of the season, increasing to about 55 $\mu\text{S}/\text{cm}$ over the field season. Based on flow estimates from gauging stations located about 75 m downstream of each study reach, an appropriate mass of salt was dissolved in water (taken from the stream) and pumped into the stream non-stop for 48 hours, starting and ending at exactly 1pm (approximately solar noon). The continuous nature of the injections allowed enough time for salt-labeled streamwater to travel spatially and temporally longer-scale hyporheic flowpaths, allowing us to potentially approach an EC plateau in the riparian subsurface. Both injection points in WS01 and WS03 were located about 40 m upstream of the upstream end of both study reaches, allowing sufficient channel distance for complete mixing in the stream and transport of salt-labeled water into flowpaths that might begin upstream of the study reach monitored by wells. Injections were spaced a minimum of two weeks apart to ensure that EC in wells and the stream returned to a background condition, in other words that the tail of one injection's tracer breakthrough curve did not interfere with the rising limb of the next.

3.2.2 Manual Measurement of Well Electrical Conductivity

Fluid EC was measured in all water-bearing wells using a hand-held EC probe (described in detail below). All readings were taken following the evacuation of approximately one well volume of water in order to compensate for possible lack of rapid flow through wells and to

achieve a more representative reading of the EC in the groundwater surrounding the well. Readings were taken as quickly as possible to minimize time lag between the first and last measurement in a well network. Measurements (combination of all individual well readings) of EC across both monitoring networks were carried out at high frequency (20-30 minutes) during the few hours immediately following start and end of the injection and every 3 hours otherwise during and for several days after the injection. Sampling thereafter grew less frequent until enough of the breakthrough curve tail had been captured.

3.3 Instrumentation

3.3.1 Water Level Loggers

We used a variety of automated water level data loggers and one electronic depth sounder to record groundwater levels and stream stages throughout the field season. The automated loggers used a proxy measurement to indirectly measure water level, while the depth sounder had metric measurements printed on the wire and simply relied on completion of a circuit to make a sound and indicate that water had been found at that depth. The two types of automated loggers used pressure and electrical capacitance to record changes in water level, and are described below.

3.3.1.1 Pressure-based Water Level Loggers

The pressure-based loggers measure overlying pressure of water, and use a simple linear relationship to compute the height of the water column at that time. The constant of proportionality is the water's unit weight, which varies as a function of temperature. All of our pressure loggers therefore also recorded temperature, which was used to compute unit weight assuming uniform temperature in the water column. Temperature was also used by the

interfacing programs to automatically compensate the logged pressure measurements for a known temperature dependence, using calibration constants specific to each logger.

Pressure Compensation. Since the loggers measured absolute pressure, it was also necessary to record barometric pressure on site in order to account for both the additional pressure of the overlying air column and any air pressure changes caused by weather (which were quite significant). This was accomplished by suspending one logger beneath a covered shed in WS01 (depicted in **Figure 2-2**), out of direct sunlight and buffered somewhat against rapid changes in temperature, as recommended by the manufacturer (Onset Corporation, 2006). One barometric logger was used for compensating records from both watersheds, since at about 2-km distant WS03 is well within the 15-km and 30-km maximum radii recommended by two of the logger manufacturers (Onset Corporation, 2006; Solinst Canada Ltd., 2010). In the final step the compensated pressure record is converted to a water height based on the temperature-dependent unit weight of water.

Logger Specifications. The three brands of pressure loggers used were HOBO model U20-001-04 (range 0 – 4 m) by Onset, Levellogger Gold model (range 0 – 5 m) by Solinst, and CTD Diver (range 0 – 30 m) by Van Essen Instruments, a subsidiary of Schlumberger. The stated typical accuracy of the HOBOs and Levelloggers is ± 3 mm, while that of the CTD Divers is ± 30 mm. The stated resolutions are 1.4 mm, 0.05 mm, and 6 mm respectively. All three brands of logger are calibrated for temperature ranges of 0 to 40°C.

Accuracy of Diurnal Fluctuations. It has been demonstrated that small diurnal fluctuations observed in stream stage using this combination of two pressure loggers (one submerged, one external) can be exaggerated if placement of the external barometric logger is

not done very carefully [Cuevas et al., 2010]. This is due to the known temperature dependence of HOBO pressure readings (present in other brands as well), whereby (despite factory-calibrated temperature compensation) pressure measurements are slightly overestimated at temperatures above about 16°C and slightly underestimated below that (Onset Corporation, 2010). The authors show that when the barometric logger records temperatures ranging from 10°C to 30°C on a daily basis, the slight errors conspire to inflate maximum water depths and deflate minimum depths recorded by nearby submerged loggers. Using a HOBO model U20-001-01 (range 0 – 9 m, accuracy ± 5 mm, resolution 2.1 mm) to record stream stage at a v-notch weir gauging a small coastal watershed in Chile, they found a 20% exaggeration in streamflow fluctuation amplitude when the barometric logger was placed 1.5 m above ground (out of direct sunlight, but subject to large daily temperature changes) versus being placed in the stand pipe with the submerged weir logger where air temperature very closely tracked water temperature. However, this 20% exaggeration error in flow likely exaggerates the depth measurement error, since typical v-notch weir equations (none was given by the authors) employ a power of about 2.5 to the depth above the notch. Back-calculated, this 20% error in flow likely represents about a 3.3% error in water depth, which does not seem to threaten too greatly the accuracy of our measurements, despite our barometric logger placement above ground. Nevertheless, this is a consideration that should be kept in mind when performing these studies.

3.3.1.2 Capacitance-based Water Level Loggers

Several water level loggers used in this study use electrical capacitance as the proxy for water depth. Capacitance (stored charge) is calculated as the product of the common area of

the two (normally parallel) capacitor plates, the inverse of the distance between those plates, the dielectric constant of a vacuum, and the dielectric constant – relative to a vacuum – of the material between the plates, called the dielectric. In the case of a water level logger, one of the conducting plates is a metal filament, and it is coated with a uniform thickness of the dielectric material, commonly Teflon. The water that surrounds the Teflon-coated filament upon submergence serves as the second conducting plate. Therefore since the dielectric constant of Teflon, the thickness of the coating (and thus the distance between the two plates), and the surface area of the coated filament are fixed, a change in water depth yields a change in the common plate area, and a linear relationship between water depth and resulting capacitance can be established. Many loggers use a two-point calibration to establish this relationship, with the user specifying the known height (typically two endpoints of a logger's coated filament) of water that corresponds to whatever capacitance is registered at that level. Like the pressure loggers, capacitance loggers also have a temperature dependence that must be compensated for in processing raw readings.

We used only TruTrack brand capacitance rod loggers in this study, which have the capacitance cable housed in a rigid stainless steel tube and two different operational lengths of 1000 mm and 250 mm. According to the manufacturer (TruTrack, 2010), this corresponds to accuracies of ± 10 mm and ± 2.5 mm, respectively. The stated resolution for both sizes of logger is 1 mm. The known dependence on air and water temperature that affect measurements can be removed automatically in the interfacing program if both air and water temperature are recorded along with water depth, as was done in this study. All loggers were calibrated prior to deployment.

3.3.1.3 *Logger Deployment*

All water level loggers used in the study recorded data at a temporal resolution of five minutes, which both necessitated multiple intermediate downloads throughout the summer and offered opportunities to verify that data was in fact being collected, and correctly. All loggers in WS01 were downloaded prematurely after about two weeks of deployment as an initial check prior to continuation of the season. Where applicable, care was taken to place all loggers such that their operational ranges would not be exceeded (whether due to too much or too little water) during the season, which influenced choice of wells to instrumented and placement of in-stream loggers.

In Wells. All loggers hung in wells were suspended using simple chain affixed to the top of the logger with a steel key ring. Each well was capped with a loose-fitting PVC cap having a hole drilled through the center. This hole had two purposes, allowing the chain holding each logger to pass through and be held above the cap with a second steel key ring, and in the case of pressure loggers ensuring that air pressure was equalized within and without the well casing. In WS01, all wells were outfitted with HOBO loggers with the exception of well E2, which had a 1000-mm TruTrack logger. In WS03, a mixture of HOBOS and Leveloggers were used in wells, and the CTD Diver, which was less accurate due to its wider measurement range, was placed in well I6.

In the Stream. In-stream loggers were installed in two ways. In WS01 and at transect D in WS03, rebar was threaded through one end a short piece of PVC pipe and driven into the streambed. A HOBO logger was then placed inside the pipe, in such a way that it remained in

the same position throughout the season. A tight-fitting cap was placed on the other end of the pipe, with a drilled hole facing up to allow air bubbles to escape that might otherwise affect the pressure reading. For the other in-stream loggers in WS03, rebar was driven into the streambed and a short (250 mm) TruTrack logger was fastened to them using plastic zip ties.

3.3.1.4 Reference to Datum and Corroboration with Depth Sounder

In order to relate all water height records to a common elevation datum, we took manual depth sounder measurements periodically throughout the field season. The manual measurements were made relative to the tops of well casings or the stream surface, the elevations of which were measured using land surveying equipment. Manual measurements were made before and after each download event, in some cases for redundancy and in other cases because logger deployment elevations (chain lengths) were adjusted before being re-deployed for the next period of time. Measurements were also made at a few other intermediate times throughout the season, simply as a means of corroborating the logger-recorded measurements when all data records were ultimately processed and pieced together. The procedure for measurements involved first removing the logger and waiting 10-15 minutes for the water level to stabilize before taking a reading.

3.3.2 Electrical Conductivity (EC) Probes and Loggers

3.3.2.1 Handheld EC Meter

The EC meter used to take readings in the wells during tracer injections was the EC300, by YSI Incorporated. When operating within its lowest EC range of 0 – 500 $\mu\text{S}/\text{cm}$ (which was never exceeded during any injection), the stated accuracy and resolution of the EC300 are $\pm [1\%$ of reading + 2 $\mu\text{S}/\text{cm}]$ and 0.1 $\mu\text{S}/\text{cm}$, respectively. Since EC also varies as a function of

temperature, this device measures temperature and automatically corrects the reported EC reading according to known temperature-dependency coefficients. All values presented here or used in analyses were corrected for temperature.

3.3.2.2 *In-stream EC Loggers*

During and after stream tracer injections electrical conductivity of the stream water was measured at 30-second intervals by a pair of Campbell Scientific CS547A EC probes, connected to Campbell CR-1000 data loggers. As with the handheld probe, temperature is measured alongside EC and is used to compensate for the dependence EC has on temperature. These in-stream readings serve as the benchmark peak EC to which the well EC readings are normalized in fulfilling research objective 1b and assessing extent of salt tracer intrusion into the riparian aquifer.

3.4 Other Data Sources

3.4.1 Atmospheric Data

Atmospheric data for the time period covering our field season were collected at a meteorological station (Primary Met) located several hundred meters west-northwest of the WS01 study reach. Temperature was recorded every 15 minutes at various heights above the ground using temperature sensors protected from direct solar radiation by ventilated Gill shields. Relative humidity was recorded hourly in Gill shields at 1.5 m and 4.5 m. The resulting water vapor pressure deficit, relevant to research objectives 2b and 2c, was calculated hourly for the heights at which relative humidity and temperature were recorded, 1.5 m and 4.5 m. Precipitation was recorded in 5-minute intervals by a tipping bucket located 1 m above the ground, and was resolved into hourly and daily totals for presentation purposes. For additional

details see <http://andrewsforest.oregonstate.edu/data/studies/ms01/meta/template.cfm?page=provisionaldata&topnav=135>.

3.4.2 Flow Data

About 75 m below each of the study reaches are flow gauging stations that record stream stage using a float recorder and Campbell CR-10X datalogger. The stations use permanently installed trapezoidal flumes to funnel flow and permit debris to pass during most of the year, and custom-made v-notch weirs to gauge flow during the low-flow summer months. Stage data from WS01 and WS03 covering our field season were converted to volumetric flow rates using empirically derived rating curves (for both the flumes and v-notch weirs) developed by USFS hydrology technicians at the H.J. Andrews Experimental Forest.

3.5 Water Level Data Processing

3.5.1 Disturbances to Water Level Records

Apart from the necessary barometric pressure adjustments for the pressure-based water level loggers, all of the water level records required some amount of post-processing and quality control before they could be turned into continuous records of water table elevation. This was most commonly due to changes in the length of chain or depth of the logger, which occurred for multiple reasons. One reason was an intentional lowering or raising of a logger (typically between data downloads), in order to make sure it was not sitting on the bottom where it could be fouled by mud, or to make sure it was sufficiently submerged and would continue to accurately record changing water levels.

The other reason was unintentional disturbance caused by the frequent down-well EC measurements, which could not be taken without removing and replacing the loggers each

time, both for lack of sufficient water depth to fit both the water level logger and the EC meter and because our configuration connected the logger chain to the well cap. These disturbances resulted in occasional kinking and snagging of the chain on the well caps, temporarily altering the logger depth by a discrete amount which was usually apparent in the water level record, thanks largely to the presence of downward spikes in recorded depth often recorded while the logger was out of water. This was greatly diminished once the problem was recognized and care was taken to replace the loggers in the wells without affecting the logger suspension system. On rare occasions, a logger chain came apart and a logger was temporarily dropped at the bottom of a well, or a team member forgot to replace the logger after taking an EC reading. These rare periods were simply clipped from those loggers' data records, while the smaller-scale discrete changes in chain length and logger depth necessitated a somewhat more elaborate approach.

3.5.2 Referencing Water Levels to a Common Datum

The first step in processing the records was to assign one of the discrete logger data points from a given record a reference water elevation, as measured manually with the depth sounder. In all cases, a data point was chosen that was recorded 15-20 minutes before or after the time of the depth sounder measurement, to ensure that the logger had achieved temperature compensation and that the water level had stabilized before choosing a reference data point. This elevation would then be applied to the rest of the water level record, adjusting the values according to the differences between all other data points and the reference point. Since each total water level record was broken up into at least two sub-records, this process was carried out multiple times using several individual depth sounder readings. Due to possible

human and instrument error, the resulting sub-records of water elevation did not always line up properly, and some minor adjustments needed to be made to ensure that the total record was continuous.

3.5.3 Removing Small Errors from EC Measurement Disturbance

To remove the more numerous minor errors in the water level record, we made extensive use of MATLAB in automating some basic methods that could be repeatedly and quickly applied to all data time series. The first target was the occurrence of negative spikes in recorded water level, which were created when removal of a logger from a well coincided with a discrete 5-minute measurement. These were either removed by deleting all readings below a certain elevation, or by searching for and removing isolated readings that deviated from the previous and next measurements above a certain threshold. The other types of errors amounted to temporary step changes in water level, in which case records, proceeding from times of reliable accuracy, were automatically searched to find step changes above a certain threshold over any given 5-minute period from one reading to the next. When found, the deviating portions of record would be adjusted in the opposite direction by the magnitude of the step change detected. The threshold step change magnitude was varied until satisfactory removal of errors was achieved without compromising the quality of the data.

While these two semi-automated methods eliminated most errors, some still remained, and it was occasionally necessary to visually inspect the record to remove likely errors. As often as possible we sought to adhere to the several manual depth sounder measurements taken throughout the season. In general, the records were adjusted so that they contained no discontinuities across times when loggers were downloaded and redeployed, and that as many

minor errors were removed as possible, without compromising the data's integrity. It must be emphasized, however, that great care was taken to avoid allowing predilections about the data 'ought' to look obstruct the quality control process, and that in very few cases did the adjustment very substantially alter the recorded values, by more than a centimeter at certain points. In any case, the hydraulic gradients resulting from interpolation of these water table elevations are not very sensitive to changes on the order of a few centimeters, since the differences in ground elevations around the monitoring networks were so great as to dwarf relatively minor changes in water table elevation.

3.5.4 Application of a Simple Smoothing Function

Before being used in any analyses, the corrected water elevation records underwent slight smoothing by means of a simple moving average function. This was done to improve both the appearance and palatability of the water elevation records to some of our algorithms used in analysis (described below). This allowed for sampling of our data at longer time intervals than recorded without the risk of losing quality due to short time-scale noise, which was present in all records, particularly the pressure-based logger records. It also allowed us to rely on the ability of an algorithm to accurately locate true local maxima and minima, rather than being obscured or led astray by minor noise that represent false maxima and minima. The smoothing function computed a basic, balanced weighted moving average for each data point that weighted adjacent data points by a factor of three and points two time steps distant by a factor of five. This function was applied 20 times, an amount determined strictly by visual inspection and adherence to the goal of solely reducing noise without compromising the actual values of water elevation.

Appendix A contains plots of all water level records used in the subsequent analysis. The black line represents the final, corrected, slightly smoothed water elevation record, the dark grey the unsmoothed final record, the grey the raw, unadjusted record after being stitched together from sub-records, and the discrete red x's are the manual depth sounder measurements.

3.5.5 Lessons Learned

As a word of caution to those undertaking similar studies in the future, in which wells are used for the dual purpose of monitoring both groundwater levels and conductivity (or some other parameter), we recommend that as much effort as possible be made to eliminate the need to remove water level loggers from the wells. Whether through installing deeper wells, so that ample water is in the column to accommodate multiple devices, or installing large-diameter wells that can fit them side by side, for the sake of time spent in quality control and the ultimate credibility of the data, minimal disturbance of these long-term logger records is an ideal to be strived for. Additionally, the use of chain or cable less prone to becoming kinked or snagged would eliminate concerns that may arise from handling the loggers during download.

3.6 Interpolation of Water Elevations and Calculation of Hydraulic Gradients

3.6.1 Interpolation Scheme

The interpolation algorithm chosen for analysis of hydraulic gradients (as per research objective 1a) was a linear interpolation on triangular planes generated by a Delaunay triangulation of all points in the monitoring network where water elevation was recorded. The Delaunay triangulation has the property that the circumcircle of any triangle in the triangulation contains in its interior no point in the set of points being triangulated [Delaunay, 1934 via Lee

and Schachter, 1980]. In practical terms, this means that triangles are drawn such that minimum angles of all triangles are maximized, and that triangles approaching an equilateral condition are favored over skinny triangles. Once the triangular planes were established for our monitoring networks, MATLAB was used to generate a uniformly spaced grid ($\Delta x = \Delta y = 0.25$ m), over which the interpolated surface with its triangular facets was sampled to generate a 3-D surface at each time step. Although collected at a 5-minute interval, we sampled the lightly smoothed water elevation data at a 30-minute interval to speed the computationally intense interpolation process.

3.6.2 Calculation of Gradients

Since our interpolated surface is only as precise as the underlying triangulation, when calculating hydraulic gradients we computed only one gradient per triangular plane. We ensured that the point on the uniform sampling grid used in gradient calculation (generally close to the triangle centroid) was located such that four orthogonally adjacent grid points, used to calculate the component magnitudes in both grid directions, were all located on the same triangular plane. This guarantees that we did not rely on an interpolation of an interpolation, and that we do not analyze gradient information at a higher resolution than was recorded by the networks of water level loggers. Additionally, we used our judgment to exclude a certain number of triangular planes from analysis, in the event that they were especially skinny, or represented an interpolation over a very large area that seemed too coarse to be reliable.

3.6.3 Resolution of Gradients into Down- and Cross-valley Components

Because the original gradient calculation was done in the spatial context of the site surveys, where the y-axis was approximately equal to magnetic north, basic geometric manipulation of these gradient components was done in accordance with research objective 1a to establish down- and cross-valley gradients in each watershed. To do this, we first chose a line for each study reach that basically represented the down-valley axis (not necessarily parallel to the stream channel in all places), rotated each resultant gradient by the angular difference between magnetic north and the down-valley direction, and resolved that gradient into two new components that correspond to down-valley and cross-valley gradient components.

3.7 Water Table Elevation Anomalies

Here, we define “anomaly” to mean the deviation of a water elevation time series from its mean. For the purposes of this study, anomalies refer to the diurnal water table fluctuations observed primarily in WS01 after about July 1, which are the focus of research objectives 2a – e. To isolate and study these anomalies as a separate entity from the entire water elevation record at a given location, we first applied a smoothing function to our post-June 20 data similar to the one described above in section 3.5.4, this time with weighting coefficients of 5 (adjacent) and 10 (two time steps distant) to speed the process. This was applied to each record 4000 times, which by visual inspection and comparison to the original was just enough to remove all sign of the diurnal fluctuations and obtain the mean water elevation without causing it to shift vertically up or down. These ultra-smoothed mean time series are plotted along with the other incarnations of our water elevation time series in **Appendix A**. To isolate

the anomalies, we simply subtracted this mean time series from the lightly smoothed time series (described in section 3.5.4 above), yielding a time series that oscillated about zero, representing only the deviation in water elevation from the mean for each location.

3.8 Timing of Daily Peak and Trough Water Elevation

To fulfill research objective 2b, aimed at examining the seasonal change in timing of the daily maximum and minimum water levels, we constructed an algorithm that automatically searched each day for the two times at which the water level reached its peak and trough. Since peaks and troughs typically occurred during the hours of 7:00 - 12:00 and 14:00 – 17:00, respectively, we divided each post-July 1 lightly smoothed 5-minute record into 24-hour periods between noon and noon. This allowed us to easily and automatically capture the timings of a vast majority of daily peaks and troughs. The algorithm worked by seeking out the maximum and minimum values over each 24-hour interval, but these values also needed to satisfy the condition of being local maxima and minima, to ensure that the algorithm did not locate a value of the time series coming from or going to the next day that happened to be above or below the local peak or trough for that day. This was accomplished by guaranteeing that the slope between, for example, the maximum and next highest value was below a certain threshold and sufficiently close to zero. Points were removed from consideration until this condition was met, and both points used to check the slope were within 30 minutes of each other. Since some of the time series were inherently noisier than others, this algorithm was not always successful, and some ‘outliers’ result from unexpected events or disturbance-caused errors in the record. On the whole we were able to extract the timings of the vast majority of daily peaks and troughs.

Chapter 4

Hydraulic Gradient Dynamics

4.1 Analysis over Three Time Scales

In assessing hydraulic gradient dynamics in the riparian areas of WS01 and WS03, we chose three time scales over which to analyze dynamics. Depicted below in **Figure 4-1**, they are (1) seasonal, covering the majority of baseflow recession from prior to the June 2 storm to about August 20; (2) storm, which occurred as two consecutive rainfall events on June 2 and June 3-4 (return period of about 1.25 years, largest in WY2010), an analysis period of 7 days; and (3) daily, covering a typical 7-day series of diurnal rise and fall in stream stage and groundwater levels, from July 24 to 31. Research objective 1a is to assess to what extent and in

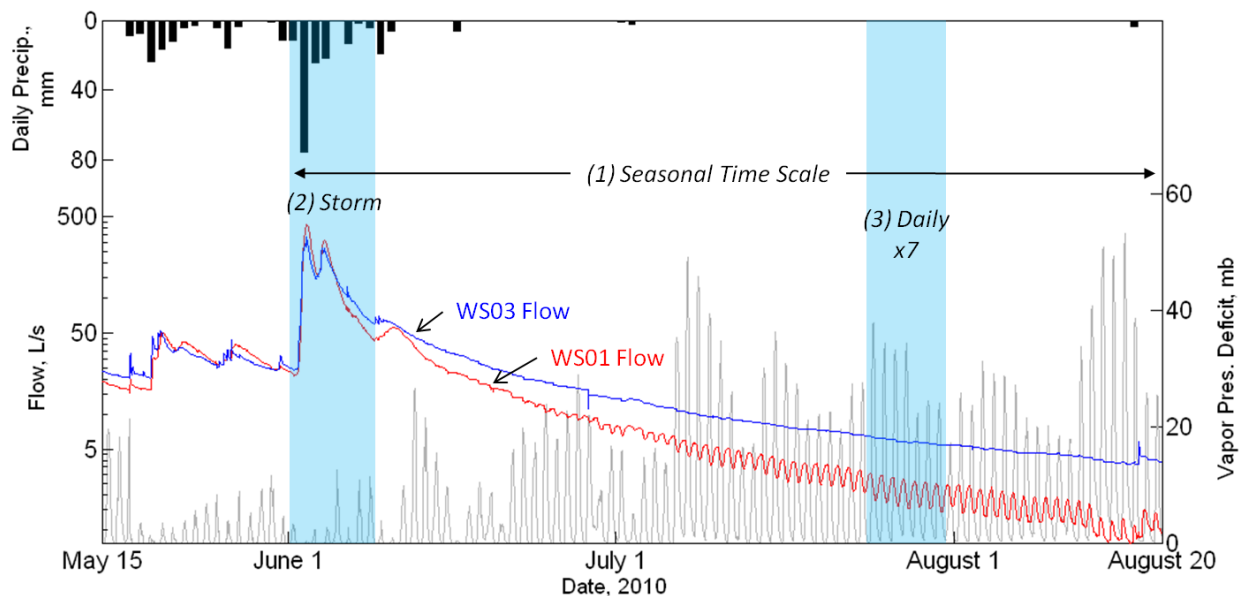


Figure 4-1. Hyeto-hydrograph showing hydrologic conditions for the field season, and the time scales considered in our assessment. Vapor pressure deficit (measured at 4.5 meters above ground) is included (gray line) to give context to the diurnal streamflow fluctuations seen in WS01.

what way spatial patterns in down- and cross-valley hydraulic gradients change in response to the water table dynamics occurring over these time scales, which reflect seasonal baseflow recession due to lack of precipitation and (primarily in the case of WS01) drying by increased evapotranspiration (ET), rise and fall in response to a large precipitation input, and diurnal rise and fall due to evapotranspiration in trees connected directly (submerged roots) or indirectly (via soil moisture gradients) to the saturated groundwater zone.

We seek to explore the relative importance of these processes with regard to the potential for riparian-stream water exchange to occur on these different time scales. Supporting this is our analysis addressing research objective 1b, which will for the seasonal time scale incorporate field measurements of salt tracer concentration (measured as EC) in the riparian wells (normalized to the stream EC), as recorded at the same point during four equal-length constant-rate tracer injections (see chapter 3, section 3.2). This will enable us to describe links between seasonal changes in riparian hydraulic gradients and the changes observed in stream water intrusion into the riparian zone, as indicated by the changing distributions of riparian tracer concentration.

4.2 Spatial Definition of Gradients

As explained in chapter 3, we performed linear interpolation of water table elevation over the triangular planes produced by a Delaunay triangulation of the active riparian monitoring network along the WS01 and WS03 study reaches (**Figures 4-2 and 4-3**). This resulted in a number of time series of gradient magnitudes, each time series representing a single triangular plane between a certain group of three monitoring points (wells and in-stream loggers). To establish a down- and cross-valley context, we resolved the gradient of each

triangular plane into two down-valley and cross-valley components. To plot the time series data, we established sign conventions as shown in **Figures 4-2 and 4-3**. The down-valley gradient is positive if pointed in the direction of streamflow, whereas the cross-valley gradient is positive if pointing towards the stream channel, and negative when pointing away. We also divided each riparian area into three zones along the down-valley axis to ease comprehension, giving each triangular plane an individual name that links it to the time series plotted below.

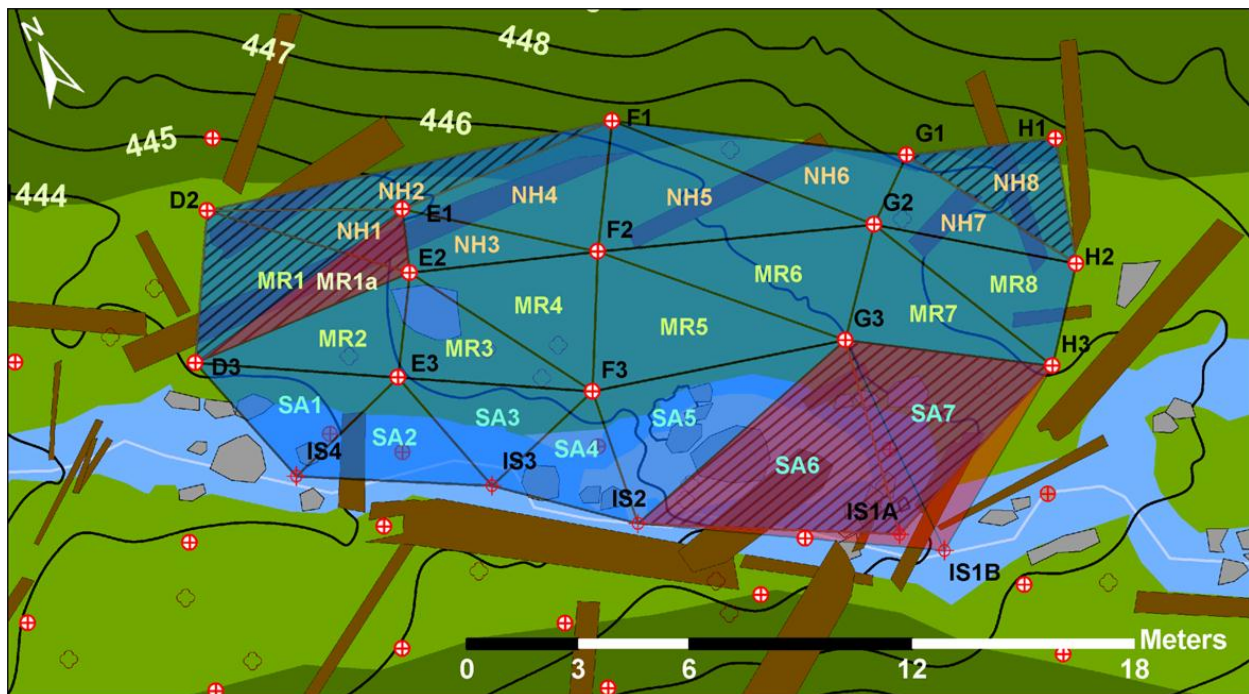


Figure 4-2. WS01 riparian area, divided into near-hillslope (NH), middle-riparian (MR) and stream-adjacent (SA) zones. Triangles with diagonal lines denote gradient records that ended before the end of the season, and red-shaded triangles are those that began par-way through the season.

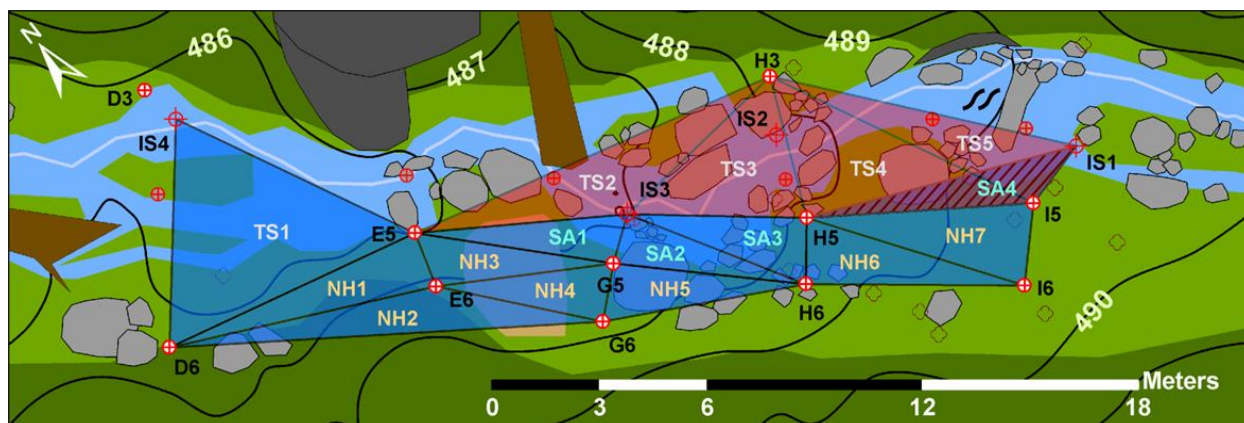


Figure 4-3. WS03 riparian area, divided into near-hillslope (NH), stream-adjacent (SA), and through-stream (TS) zones. Triangles with diagonal lines denote gradient records that ended before the end of the season, and red-shaded triangles are those that began par-way through the season.

In reporting the time series of the gradient components, we include three figures for each time scale, presenting (1) the down-valley gradient magnitude, (2) the cross-valley gradient magnitude, and (3) the ratio of the cross- to down-valley gradient magnitude. Each figure is divided into three plots according to the zones defined in **Figures 4-2 and 4-3**. It is expected that in these steep, narrow headwater valleys the time series of cross- to down-valley gradient ratio (CDVR) will be predominantly less than 1 throughout the baseflow recession, indicating a dominance of down-valley transport. Absolute gradient magnitudes are presented in **Appendix B** only, to provide context for more detailed discussion of some of the CDVR ratio time series.

4.3 Gradient Dynamics Over the Seasonal Time Scale

4.3.1 WS01 Gradient Time Series

A key to interpreting the cross- to down-valley gradient ratio (CDVR) is presented in **Figure 4-4**. An important dividing line of the CDVR value occurs at 1 or -1, indicating that the

cross- and down-valley gradient components are equal in magnitude. As seen in the figure, a gradient with this CDVR value is angled at 45 degrees either towards or away from the stream. A CDVR exceeding an absolute value of 1 indicates cross-valley gradient dominance, whereas the region bounded by 1 and -1 is indicative of down-valley gradient dominance.

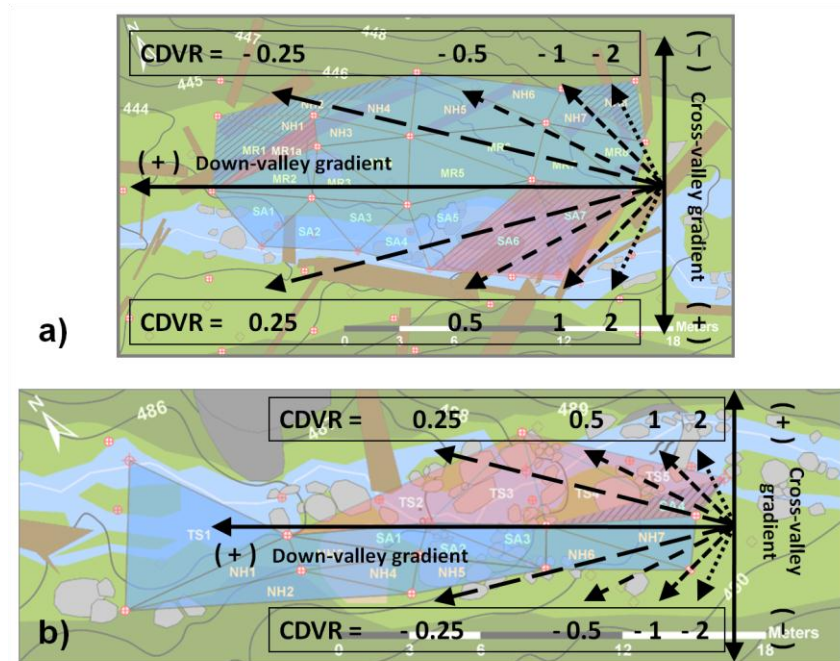


Figure 4-4. Illustration of the physical meaning of different hypothetical values of the cross- to down-valley ratio (CDVR), for a) WS01 and b) WS03. Note that the cross-valley sign convention for WS03 is opposite that of WS01, so that in both cases a positive CDVR indicates a gradient directed towards the stream channel.

The WS01 CDVR time series for the entire field season are presented in **Figure 4-5**. A glance at the figures reveals the spatial diversity recorded in hydraulic gradient dynamics throughout the entire season. The most striking result is that no CDVR (with the exception of one, during the storm) in any of the three zones (near hillslope [NH], middle riparian [MR], and stream adjacent [SA]) exceeds an absolute value of 1, indicating that at all times gradients were down-valley dominant. A majority of CDVRs fell within an absolute value of 0.5, particularly in

the SA zone, which is to be expected. Interestingly, all but one of the seven CDVRs in the SA zone were both negative for the majority of the season and ultimately trended towards a more negative value. This indicates a gradual rotation away from the stream in riparian gradients near the stream, possibly portending increased movement of water out of the stream and into the riparian zone. A few of the gradients (namely NH6, NH7, and SA2) showed CDVRs that crossed the zero axis of the plot during the storm, before returning to the values closer to which they began. This indicates that some gradients responded to the storm by rotating across the down-valley axis, but at most other times and at more prevalent lower flows favor one cross-valley direction over the other. Some gradients (e.g. NH3, MR6, SA2, SA3, SA4, SA5) responded to the storm by increasing cross-valley magnitude towards the stream, and then counter-intuitively showed the same tendency over the season, even as stream flow continued to recede. Others responded more intuitively (NH6, NH7, MR1), increasing cross-valley magnitude in one direction during the storm, and then tending toward the down-valley direction as flow decreased through the season. A number of gradients (NH2, NH3, MR1a, MR2, SA1, SA2) showed diurnal fluctuations in CDVR after approximately mid-July, some larger than others.

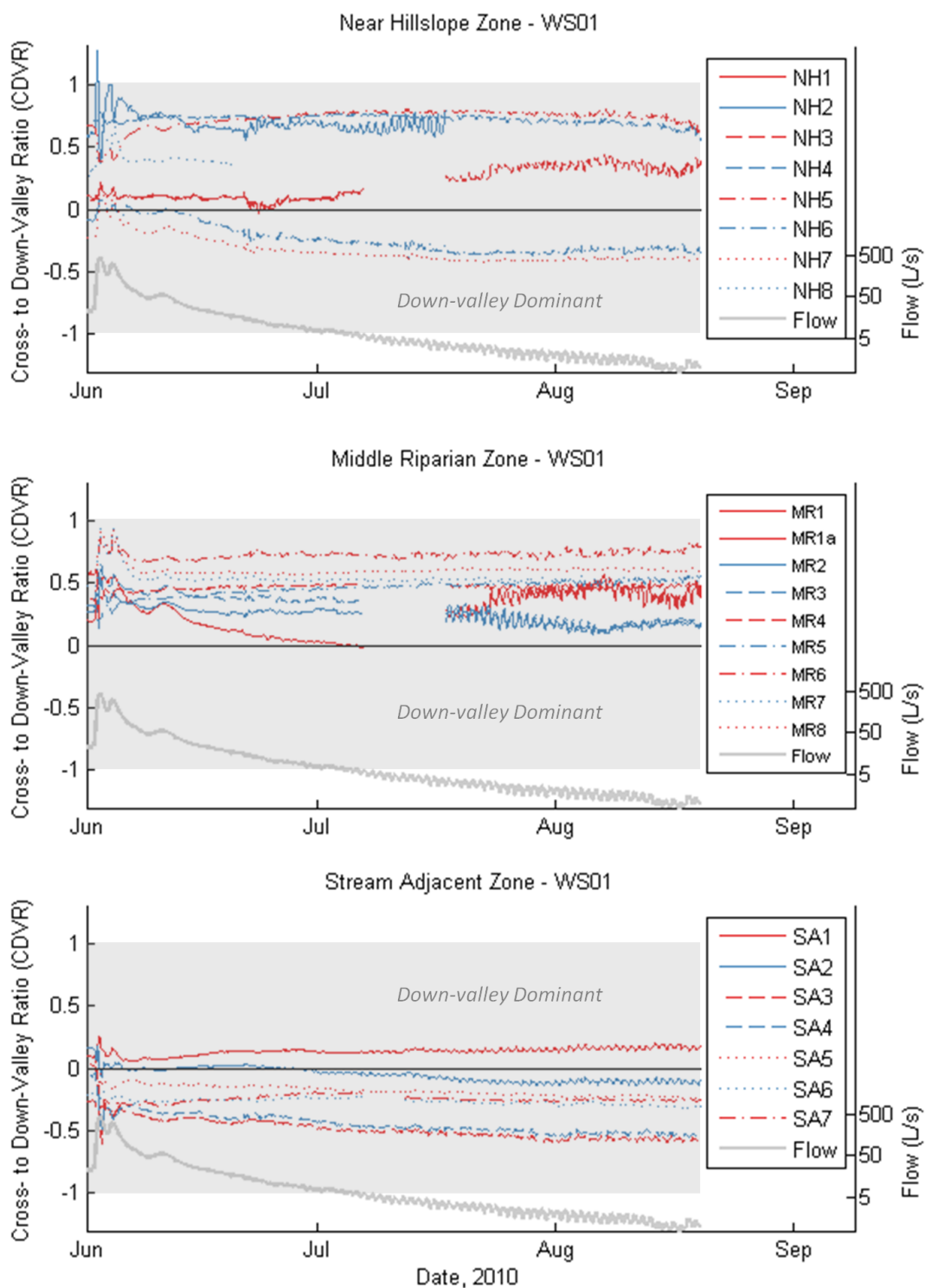


Figure 4-5. WS01 cross- to down-valley gradient ratio (CDVR) for the entire field season, plotted according to the three zones labeled in **Figure 4-2**. The grey band indicates the region of down-valley dominance.

Overall, most gradients showed substantially larger changes in response to the storm than to the seasonal flow recession, although there were exceptions (NH3, NH6, NH7, MR1). All gradients exhibited down-valley dominance, to the greatest extent in the SA and MR zones. Most interesting was the tendency for most of the CDVRs in the SA zone and some in the NH zone to gradually turn away from the stream as the season progressed, as it may have implications for changing patterns of stream-groundwater exchange.

4.3.2 WS01 Seasonal Salt Tracer Intrusion into Riparian Zone

To test whether the seasonal changes in hydraulic gradients can produce noticeable changes in the extent of stream-groundwater exchange in the WS01 riparian zone, we plotted the relative EC measured in the riparian well network at the end (before the pump was shut down) of each of the four 48-hr constant-rate tracer injections along with the hydraulic gradients as they changed through the season (**Figure 4-6**). This view of the gradients also gives a more visceral sense of the spatial pattern of hydraulic gradients and how they varied throughout the season. The riparian EC values were normalized to the stream EC (at a plateau condition), which varied little along the reach. Despite our best efforts, the increase in EC reached in the stream was not the same during each injection (as shown in the figure), and this must be taken in account when considering the results. Additionally, we assume that it is meaningful to compare the condition at the end of each injection, given that the same amount of time elapsed in each case. Although this does not take into account the effect of seasonally decreasing stream and groundwater velocities, a somewhat stable plateau was reached in most wells after 48 hrs of injection. The EC in wells prior to each injection was nearly the same as or

lower than that in the stream, within a few $\mu\text{S}/\text{cm}$, so any change observed in EC was assumed to be due to the introduction of the salt tracer.

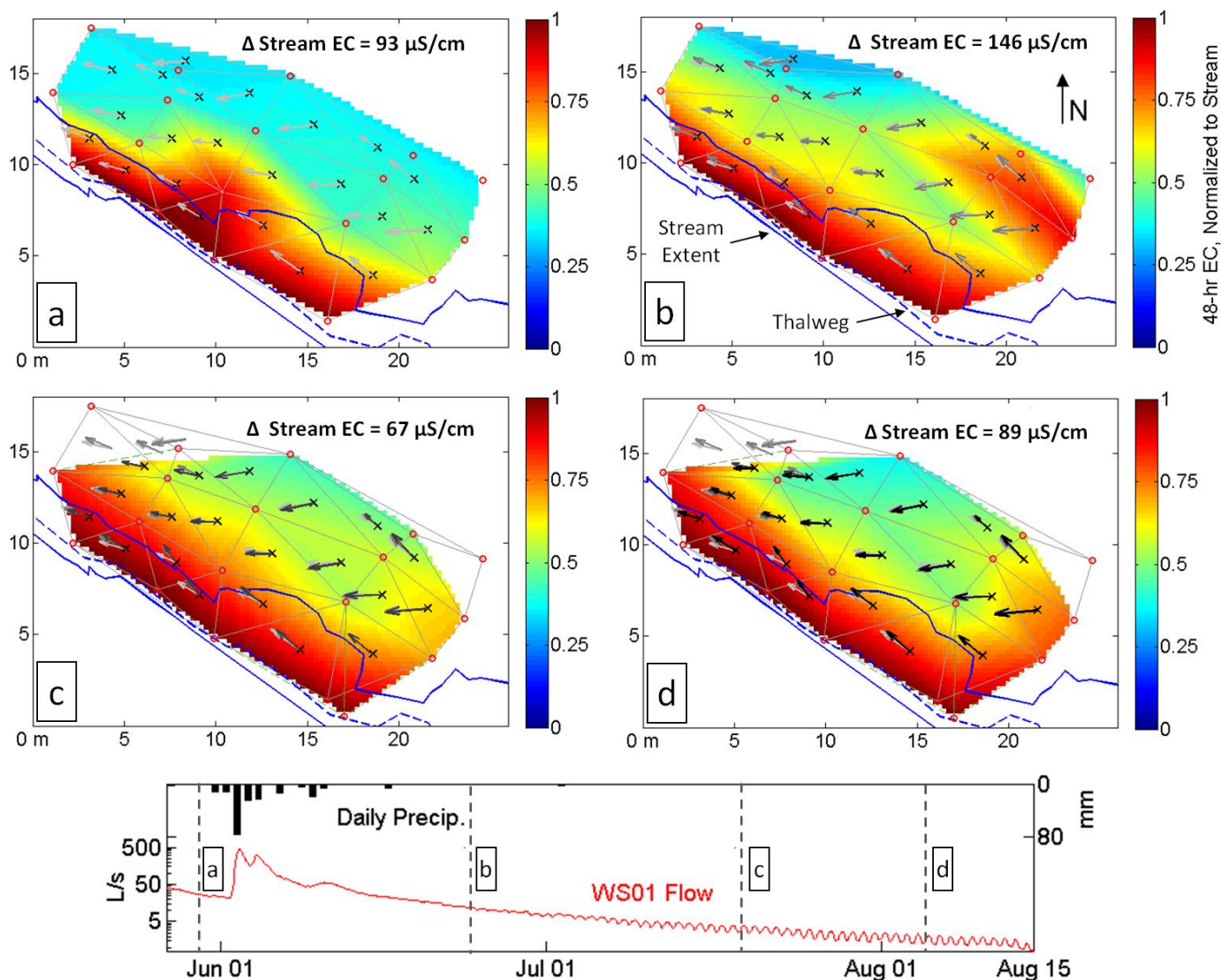


Figure 4-6. 48-hr EC in the WS01 riparian zone, normalized to the stream concentration of 1. Each time step marks the end of a constant-rate salt tracer injection. Gradients at each time step are displayed as arrows that grow darker in color and stack above the earlier arrows as time advances. The colored area diminishes in size as less data becomes available due to wells drying out. The salt tracer was injected about 40 meters above the upstream-most well transect. Flow is from bottom right to top left.

The increasing intrusion of salt-labeled stream water in the riparian zone is readily apparent in the progression through the four injections. The changes are most obvious in the first three injections, where salt-labeled water gradually creeps further into the riparian area until the lowest relative EC is about 0.4, occurring in the well furthest from the stream, F1 (x-y position 14m, 15m in **Figure 4-6 a, b, c**). It is interesting to note that the upstream-most transects of wells showed a special vulnerability to intrusion of salty water, despite being located as distant from the main channel (thalweg) as most other transects. It is conceivable that the side channel above the study reach, which is forced to turn back towards the main channel just upstream of these transects, conveyed enough salty water that this bend caused a substantial influx of stream water into the groundwater there, which resulted in elevated EC. This explanation is consistent with the lower EC observed in wells just downstream, since the hydraulic gradients calculated for that area would seem to send water on a flow path back to the stream. The gradual turning of the near-stream hydraulic gradients away from the stream also appears consistent with the increased salt intrusion, although it is difficult to directly attribute the observed changes in EC to the gradient changes, especially considering that there were 40 meters of stream channel and riparian zone between the tracer injection point and the monitored riparian area. It is possible, for instance, that a cumulative effect of slight gradient changes, similar to those observed in the study area, propagated the salty water further and further into the riparian groundwater as it progressed downstream from the injection point. All in all, it appears that there is a link between the seasonal changes in riparian hydraulic gradients and the observed changes in the extent of salt-labeled stream water intrusion into the riparian zone.

4.3.3 WS03 Gradient Time Series

Shown below are the CDVR time series for the entire field season in WS03 (**Figure 4-7**).

The most striking feature of the results is that of 16 gradients in all, the CDVR for three gradients (NH1, NH3, NH4) always exceed an absolute value of 1, nearly approaching 3 during the storm, while three others (NH2, NH5, SA1) reach absolute values substantially beyond 1 during the storm before returning to the condition of down-valley dominance. Gradient TS1 also fits into the first group, but is a special case owing to its very small component gradient magnitudes (see **Appendix B**), which inflate its apparent importance. This tendency reflects the steeper nature of some of the riparian sideslopes in WS03, particularly in the lower part of the monitored area. Almost all gradients triangles also show CDVRs that do not vary very much throughout the season, and with the exception of NH7 and TS5, they all share a tendency to rotate slightly towards the down-valley axis. Thus, there appears to be a gentle 'straightening out' of gradients occurring over the season. Most gradients responded intuitively by tending in the opposite direction of the way they responded to the storm, but NH3 (from about June 8 to July 5) and NH6 showed the same sort of response to both the storm and the ensuing seasonal dry period. With regard to CDVR sign, all gradients in the more distant NH zone showed a positive CDVR, pointing towards the stream, while 3 of the 4 gradients in the SA zone had primarily negative CDVRs, pointing away from the stream. SA4 exhibited the behavior seen in WS01, by rotating across the down-valley axis towards the stream solely in response to the storm, and then returning to its more common condition of pointing away from the stream. With the exception of TS1, all of the CDVRs within the through-stream (TS) zone were very close to zero, indicating a strong down-valley dominance in the stream channel itself.

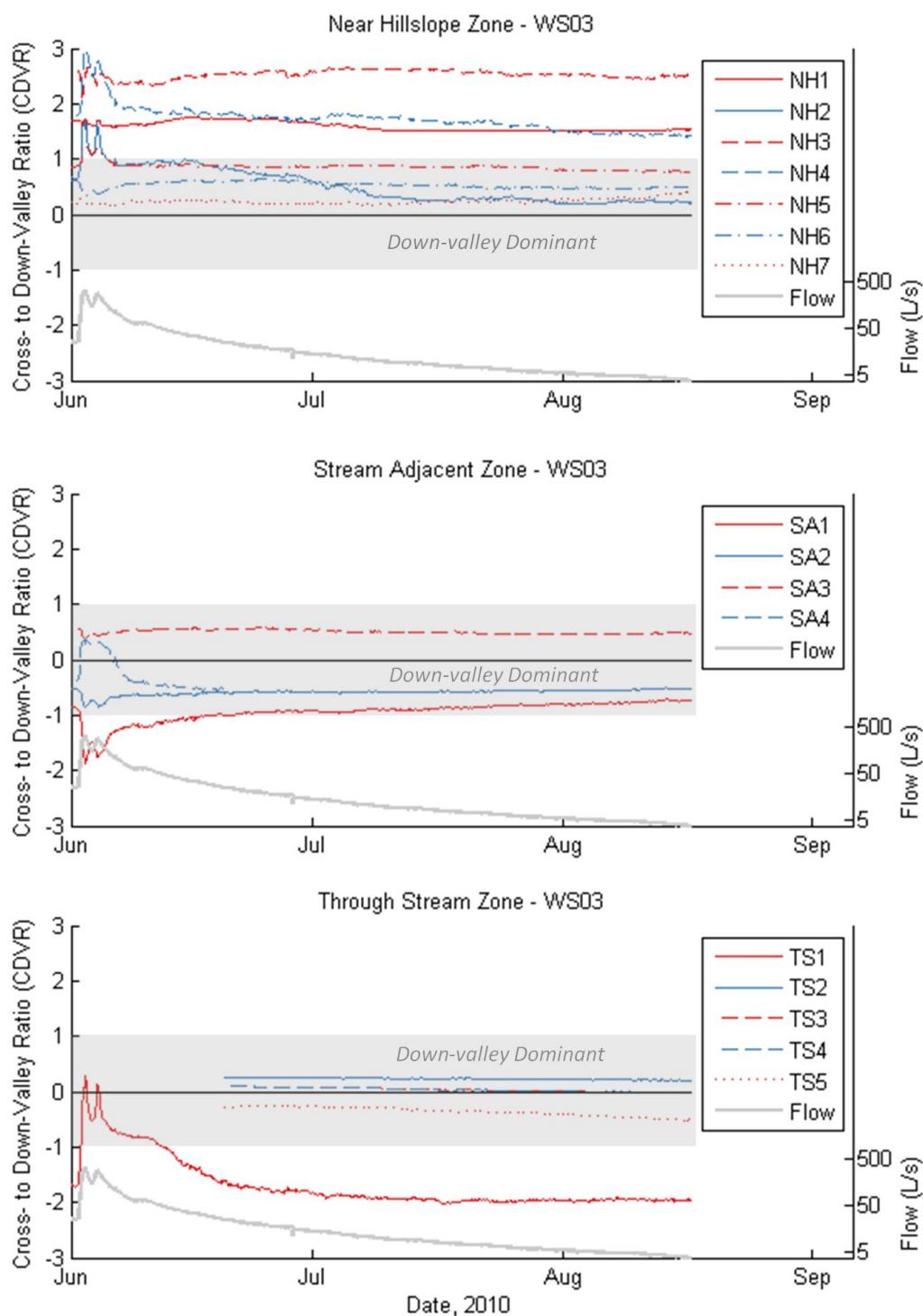


Figure 4-7. WS03 cross- to down-valley gradient ratio (CDVR) for the entire field season, plotted according to the zones defined in Figure 4-3. Note that the y-axis limits are from -3 to 3, rather than -1 to 1 as in the WS01 figure above. The grey band indicates the region of down-valley dominance.

Overall, the salient features of seasonal CDVR changes in WS03 were that, contrary to WS01, not all gradients exhibited down-valley dominance all of the time, that seasonal changes tended to be more subtle than those in WS01, and that there was a general tendency for gradients to 'straighten out' and align themselves more with the down-valley axis.

4.3.4 WS03 Seasonal Salt Tracer Intrusion into Riparian Zone

As with WS01, the impacts of gradients on the extent of salty stream water intrusion into the WS03 riparian zone can be assessed by plotting the riparian EC (normalized to the stream) at the same point during each of the four constant-rate injections together with the hydraulic gradients at those times (**Figure 4-8**). This also provides a straightforward perspective of the spatial arrangement of gradients, more so than the CDVR time series alone. All assumptions described above for WS01 hold here as well, and the increase in stream EC was also different from one injection to the next. The 48-hr mark could not be used in this analysis, because during the first injection the pump malfunctioned towards the end, resulting in rapid changes in both stream and riparian EC that would have impaired our ability to make comparisons between injections. We instead used a time of 35 hours, at midnight of the second injection day, when EC was relatively stable in the stream and wells.

Across the narrow riparian zone of WS03, the general patterns of stream water penetration do not change greatly (**Figure 4-8**). Upon closer inspection, however, there are a few locations that showed increased penetration of salt with each injection as the season advances. Wells D3, E5 and H5 all showed markedly lower EC than the rest of the

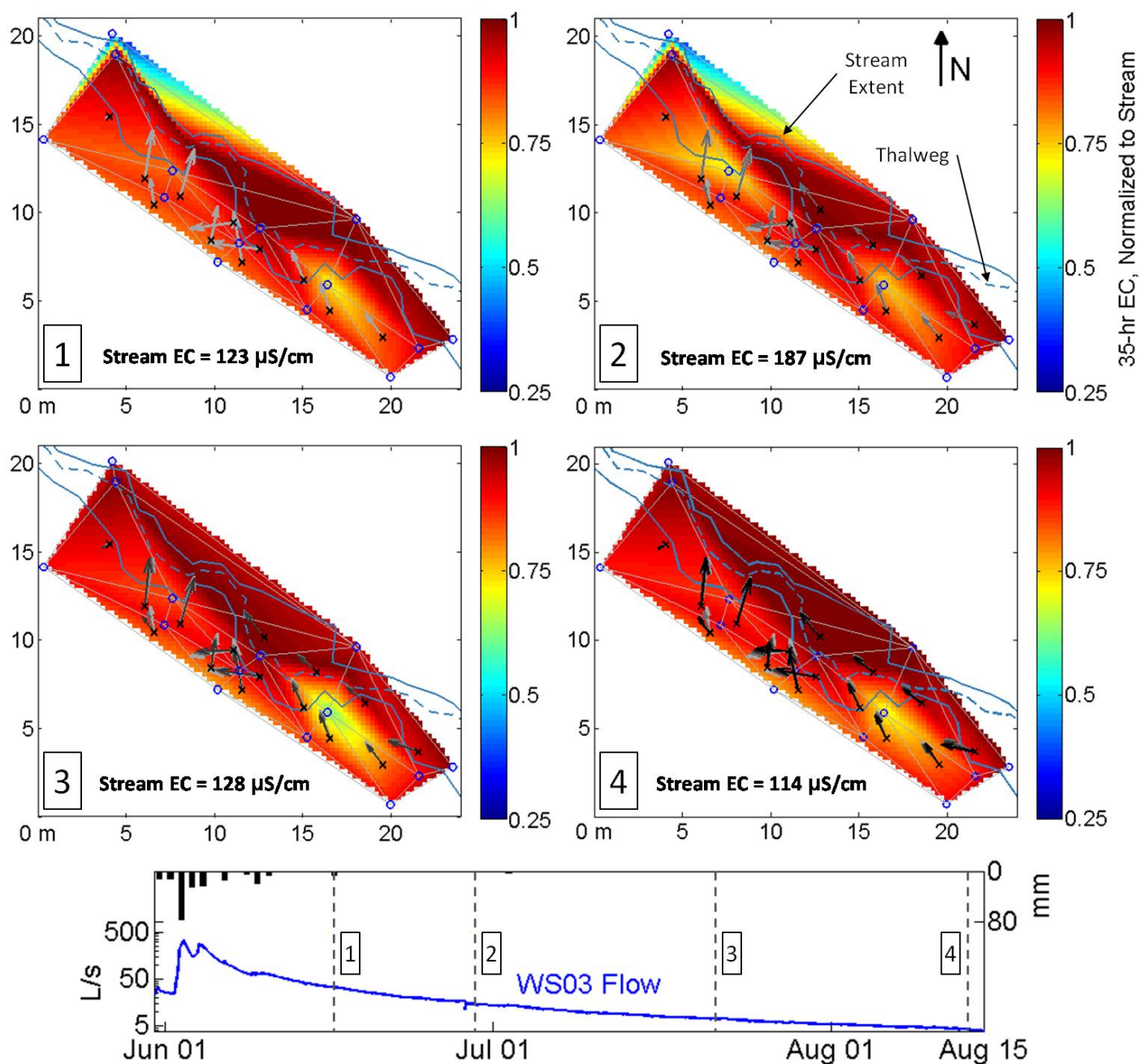


Figure 4-8. 35-hr EC in the WS01 riparian zone, normalized to the stream concentration of 1. Each time step marks the 35th hour of a 48-hr constant-rate salt tracer injection. Gradients at each time step are displayed as arrows that grow darker in color and stack above the earlier arrows as time advances. Blue circles denote wells. The salt tracer was injected about 40 meters above the upstream-most well transect. Note that the colorbar axis limits are from 0.25 to 1, unlike those in **Figure 4-6** for WS01. Flow is from bottom right to top left.

riparian well network during the first two tracer injections (less so in E5 for injection 1), but by the third injection the salty water completely broke through into well D3 (x-y position 5m, 20m in **Figure 4-8**) and penetrated considerably further into well E5 (position 8m, 12.5m). Well H5 (position 17m, 6m) continued to show a considerably lower relative EC (between 0.6 and 0.7) through the final injection. It is difficult to attribute any of these changes to the changes observed in hydraulic gradient direction throughout the season. For example, well E5 was down-gradient (see gradients NH1 and NH3) of the more impacted well E6 (position 7m, 11m) of the riparian zone and eventually showed more intrusion of the salt tracer. But, well H5 was similarly down-gradient of wells I5 and I6 (positions 22m, 2.5m, and 20m, 1m, respectively), both of which exhibited high relative EC, and it remained substantially less affected. Given the valley constraints in the cross-valley direction (2-3 times as narrow as the WS01 riparian area), it is also difficult to identify the extent to which stream water exchanges along the cross-valley axis. There is a hint of a boundary, in that well G6 (position 10m, 7.5m) showed a relative EC of about 0.8 for all injections, but this is very close to the stream EC and still indicates great intrusion of salt into the riparian zone. However, the absence of clear definition in the lateral extent of this stream water exchange is in itself very informative, considering that wells were placed across almost the entire lateral expanse of the valley bottom. Beyond the wells most distant from the stream were very steep hillslopes, so we can reasonably conclude that the greater part of the WS03 valley bottom riparian area (in the studied reach, at least) is very intimately connected with the stream water. Since this is the area closest to both the saturated zone and the actively flowing stream, this has implications for biogeochemical cycling in this and other similar systems with narrow and constrained valley bottoms.

4.4 Gradient Dynamics Over the Storm Time Scale

Examining changes in hydraulic gradient patterns as both study areas respond to the 1.25-year storm event that occurred on June 1-4 offers a valuable opportunity to gauge how down- and cross-valley gradient dominance varies with short-time scale, large rainfall inputs. This can aid the prediction of what biogeochemical responses may occur due to rapidly changing hydraulic gradients and the resulting flow paths. It also affords an opportunity to test field observations against conventional conceptual models that predict a headwater response to large rainfall events in which riparian water tables rise and cause dominantly cross-valley gradients to induce lateral flow towards the stream (a relatively 2-dimensional view). Similar to the seasonal time scale analysis, we focus on changes observed in the CDVRs through time, but the actual down- and cross-valley gradient magnitudes can be found in **Appendix B**.

4.4.1 WS01

The CDVR for the riparian gradients in WS01 spanning the first eight days of June, 2010 are presented in **Figure 4-9**. During this period, two consecutive large rainfall events delivered about 13 cm of rain to the area. The expected response of riparian hydraulic gradients to such an input of water would be an increase in the gradients pointing towards the stream, and a general dominance of cross-valley flow. Many gradients in the NH (6 of 8) and MR (6 of 8) zones fit this model and show positive increases in CDVR (towards the stream), but only 1 of 7 in the SA zone exhibits this behavior (SA1). All other gradients show the opposite effect, either diminishing the cross-valley component angled towards the stream (e.g. NH2, NH5) or amplifying the cross-valley component already angled away from the stream (e.g. SA3-6).

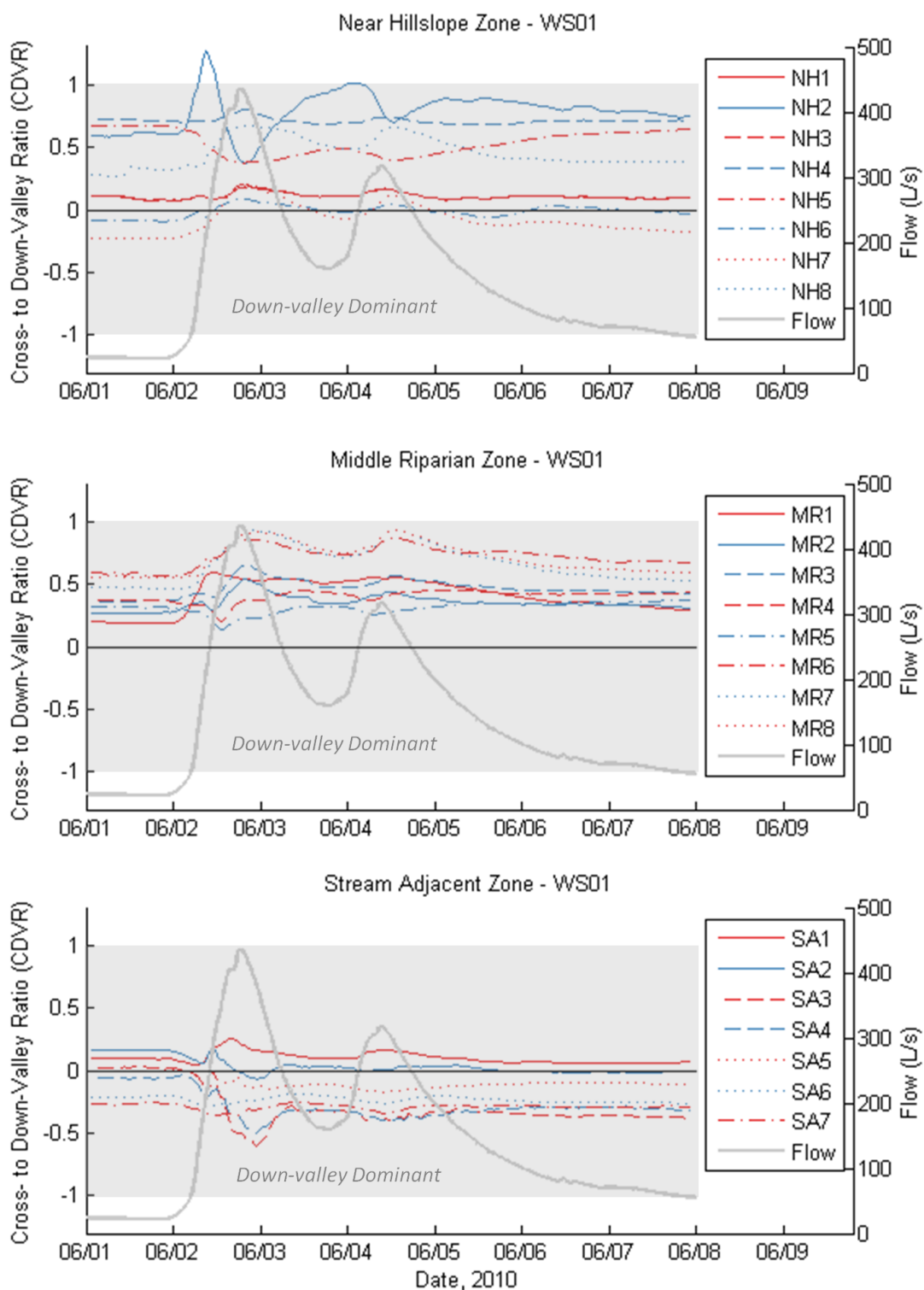


Figure 4-9. WS01 cross- to down-valley gradient ratio (CDVR) for the June 1-8 storm period, plotted according to the three zones labeled in **Figure 4-2**. The grey band indicates the region of down-valley dominance.

Moreover, only one gradient (NH2) ever leaves the state of down-valley dominance during the storm, and the majority of CDVRs stay below 0.75 even at the storm peaks. So, even with the strong cross-valley response observed in most gradients, the down-valley gradient always dominated. A time-lapsed image showing the change in gradient direction and magnitude from the time prior to the hydrograph rise to the first and highest peak provides a better assessment of the variability in storm response across the WS01 riparian zone (**Figure 4-10**).

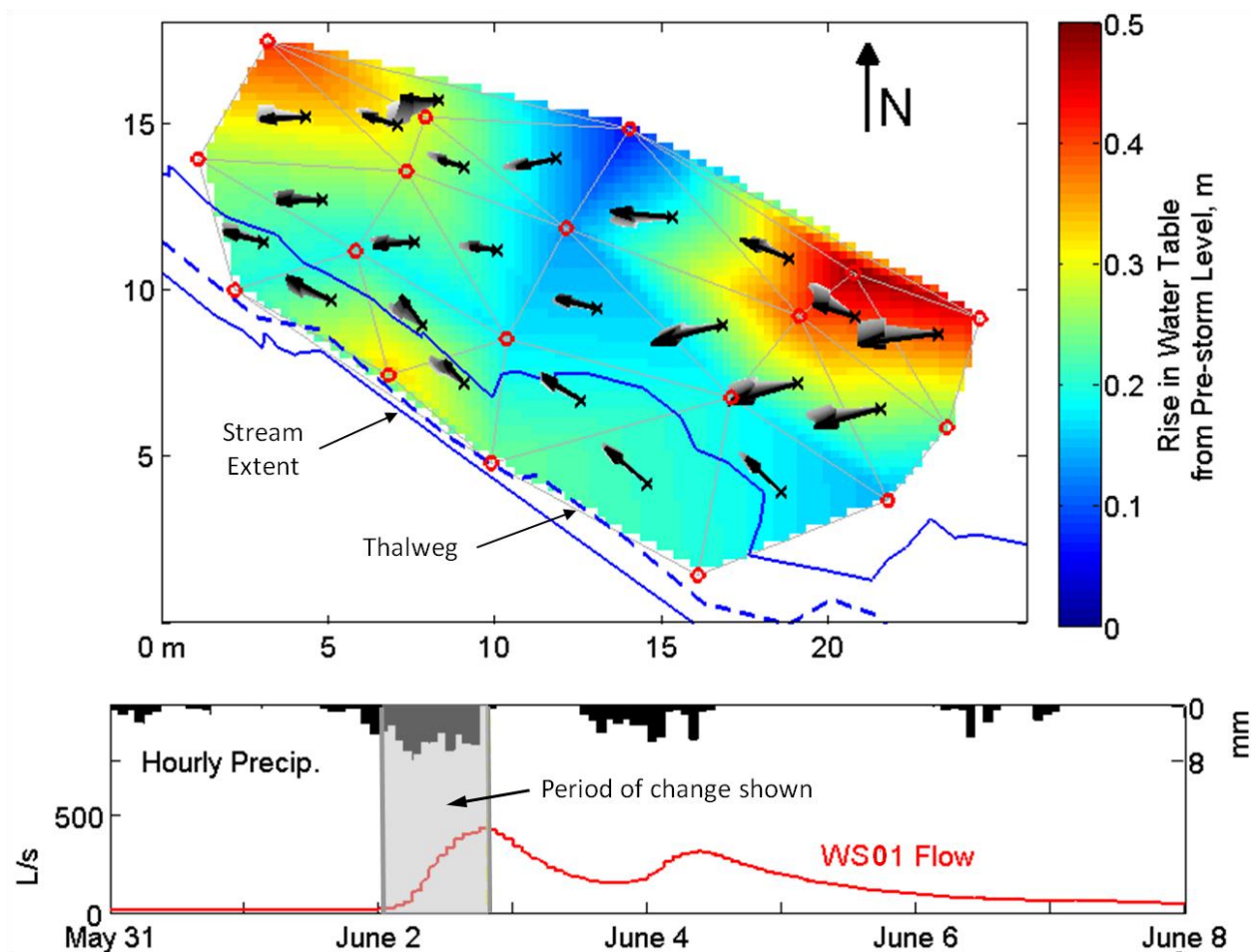


Figure 4-10. Time-lapsed image of the riparian gradient storm response in WS01. Gradient arrows are plotted such that the arrow color transitions from light grey to black as time progresses over the storm response period. The colored background indicates the rise in water level from the pre-storm level, to show how water levels rose to produce the observed gradient changes. Flow is from bottom right to top left.

The diversity of response observed throughout the WS01 riparian area, with some water levels rising high and others rising hardly at all, is demonstrated in **Figure 4-10**. It is difficult to attribute this variability of response to topographic features, since none were very apparent. For instance, it is unclear why well F1 (x-y position 14m, 15m in figure) showed almost no rise, and well G1 (position 21m, 11m) seven meters upstream rose almost 0.5 meters. Most interesting from the perspective of stream-groundwater exchange is that nearly all of the gradients nearest the stream turned farthest from the stream at the peak of flow. This seems to imply that, perhaps despite the gradients in the NH and MR zones turning towards the stream, more stream water is driven into the riparian subsurface in response to rainfall events, contrary to what conventional conceptual models would predict. Also, the persistent down-valley dominance in all gradients is possibly a telling feature of steep headwater streams in general, in that even during storm events most subsurface flow occurs parallel or at otherwise oblique angles to the stream, not directly towards the stream.

4.4.2 WS03

The plots of CDVR for WS03 (**Figure 4-11**) show similar behavior to that of WS01, but with a greater tendency for more intense responses in the cross-valley direction, due to the steeper riparian slopes in much of the riparian area (see **Figures 2-3 and 4-3**). As with WS01, most gradients in the NH zone show positively increasing CDVR (reaching values between 1 and 3) in response to the storm, turning more intensely towards the stream, except for NH6, which showed the opposite behavior, and NH7, which showed almost no reaction to the storm. All NH zone gradients maintained a positive CDVR during and after the storm. In the MR zone, three of four gradients showed decreasing CDVR in response to the storm peaks. One (SA3)

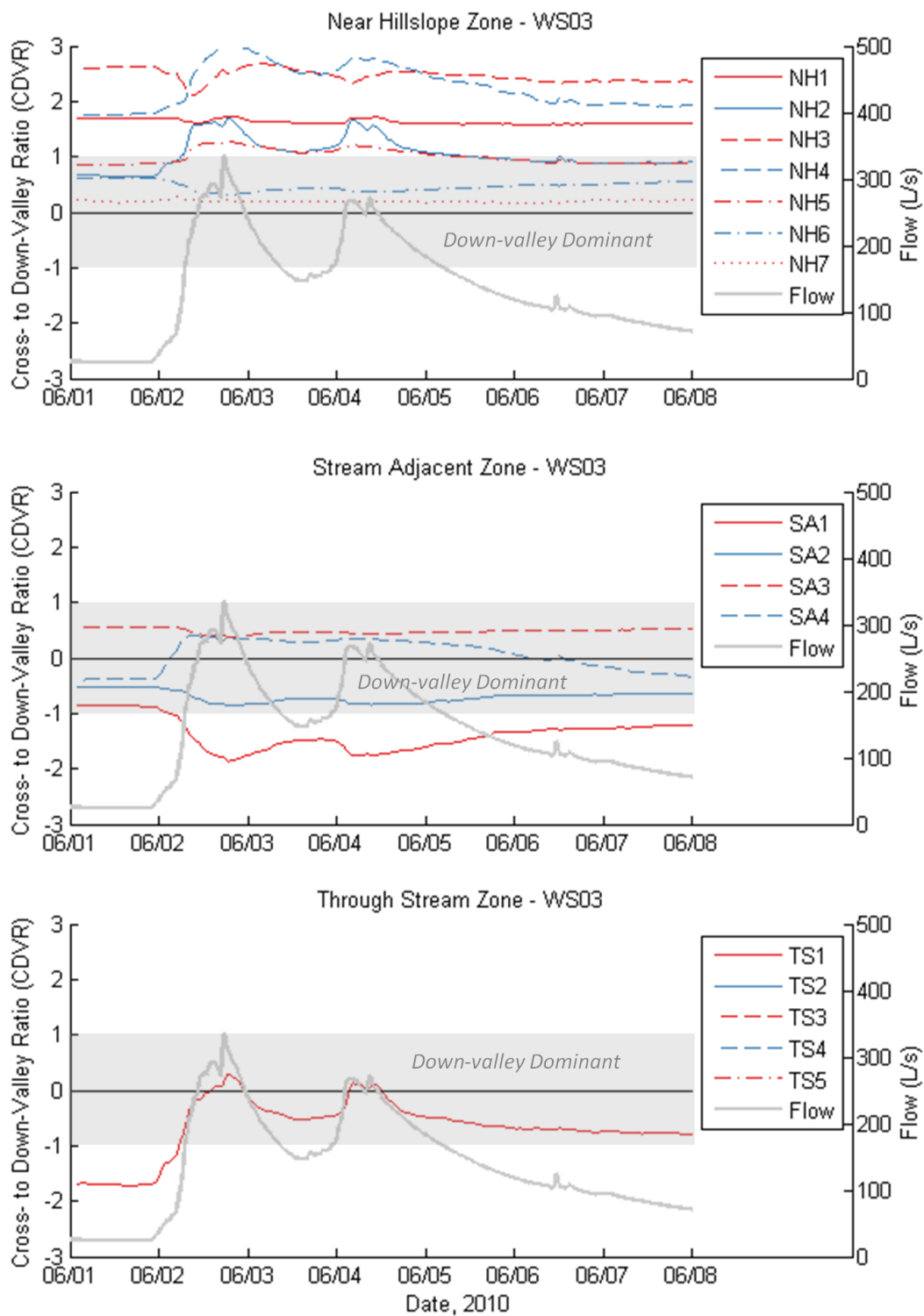


Figure 4-11. WS03 cross- to down-valley gradient ratio (CDVR) for the June 1-8 storm period, plotted according to the three zones labeled in **Figure 4-3**. The grey band indicates the region of down-valley dominance.

simply showed a less positive CDVR, but two (SA1 and SA2) began negative and became increasingly so, turning even further away from the stream. The fourth gradient (SA4) began with a negative CDVR and turned across the down-valley axis to have a cross-valley component pointing towards the stream during the storm peaks. The small-magnitude gradient TS1 showed a response analogous to that of SA4, beginning with a negative CDVR and just crossing the down-valley axis into the positive CDVR region, angling towards the stream.

The changes discussed here and shown in the time series plots can be more readily understood by looking at **Figure 4-12** below, showing a time-lapse image of the WS03 response to the first storm peak. As with WS01, the time-lapse image of the riparian storm response in WS03 reveals at a glance the diversity of responses among hydraulic gradients, produced by the varying heights to which the water table rose in the monitored wells. The steep gradients with high CDVR values in the NH zone can be seen along the left bank. Interestingly, one change not apparent in the CDVR plots (but evident in the gradient magnitude plots in **Appendix B**) is the substantial decrease in total gradient magnitude of NH1 and NH3, caused by the relatively large rise at well E5. The most striking feature is large, opposing gradients found in the pairs NH4, NH5, and SA1, SA2, centered around well G5 (x-y position 12m, 13m in the figure). These two pairs of gradient triangles would seem to funnel water to the area just downstream of well G5, indicating a possible hot spot for stream water to enter the subsurface. However, the salt tracer data shown in **Figure 4-8a** do not seem to imply anything remarkable about that location for subsurface entrance of stream water. Whatever the consequence, the opposing tendencies of these gradients become intensified during the storm, thanks in part to the virtually negligible response shown by the water level in well G5. Elsewhere in the WS03 riparian area, some of

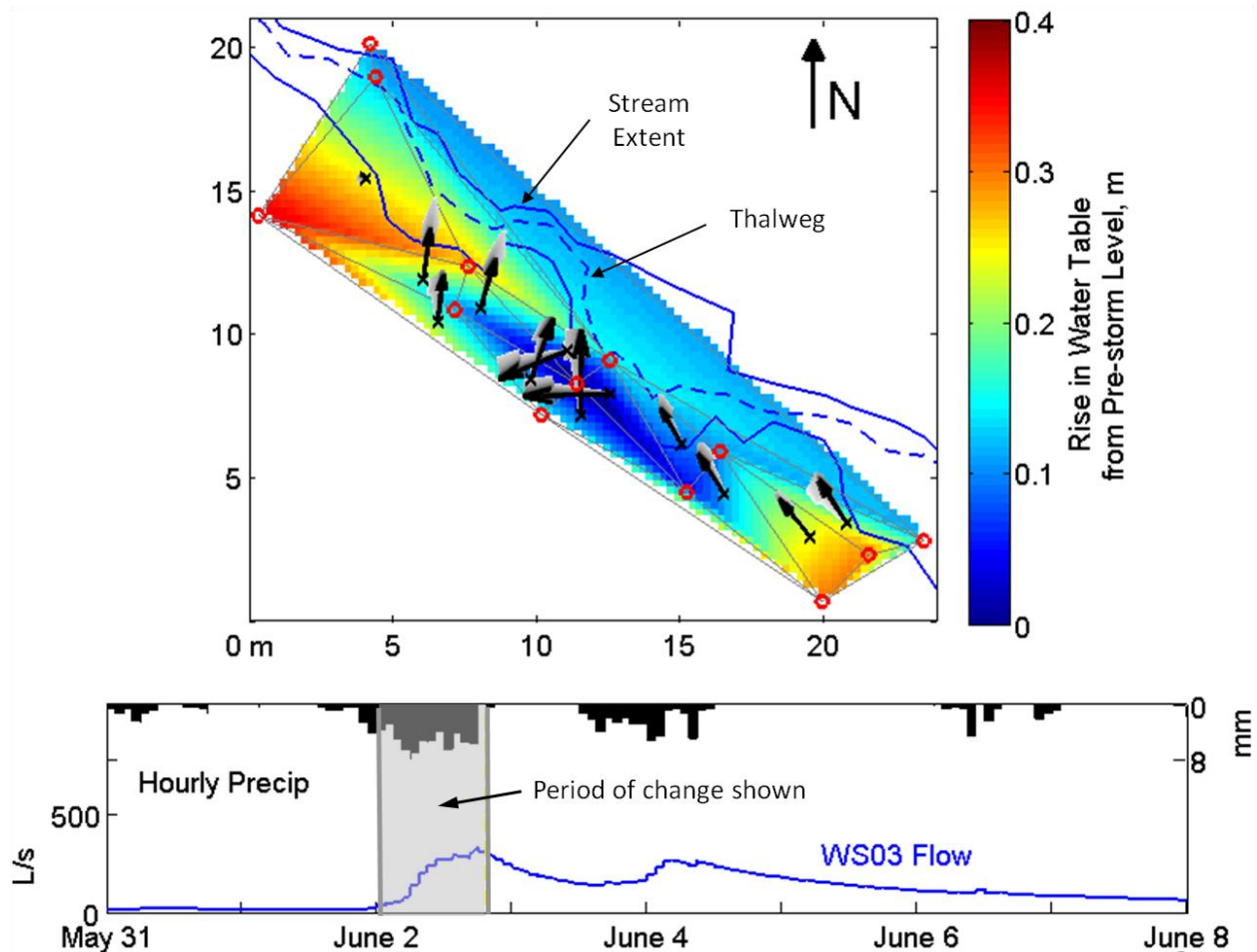


Figure 4-12. Time-lapsed image of the riparian gradient storm response in WS03. Gradient arrows are plotted such that the arrow color transitions from light grey to black as time progresses over the period displayed. The colored background indicates the rise in water level from the pre-storm level, to show how water levels rose to produce the observed gradient changes. Flow is from bottom right to top left.

the gradient responses (SA3 and NH6) imply that more stream water has the potential to enter the subsurface, and others (SA4) imply the opposite.

Overall, the monitored WS03 riparian area does not reflect conventional ideas about riparian water table response to a storm. While a few gradients (e.g. NH2, NH4, NH5, and SA4) showed an increased cross-valley gradient towards the stream, several showed a decrease (NH1, NH3, SA5, NH6), and two turned even further from the stream than prior to the storm

(SA1 and SA2). As the WS03 valley bottom is narrower than that of WS01 and was more recently subject to a major reordering of sediment and woody debris, it is difficult to draw broader conclusions about other headwater valley bottoms, but at the very least the data showcase the diverse nature of hydraulic gradient patterns in these types of systems, and the counter-intuitive responses they can show to rainfall events.

4.5 Gradient Dynamics over the Daily Time Scale

The final time scale considered in this analysis was that of a single day, as diurnal fluctuations were observed late in the dry season in groundwater levels, stream stage, and flow in the data from both study areas. The goal here is to assess whether these fluctuations seem to have appreciable effects on hydraulic gradient patterns on a daily basis, and whether those changes in patterns might affect the potential for stream-groundwater exchange. The observed fluctuations in WS01 were much more pronounced than in WS03, but the CDVR time series will be shown for both study areas. We chose a single week-long period from July 24 to 31, well into the period of observed diurnal fluctuations, over which to assess this potential impact.

4.5.1 WS01

The plots of CDVR shown in **Figure 4-13** give the impression that overall, the effect of the diurnal water table fluctuations on hydraulic gradients was relatively slight. However, most gradients do exhibit some noticeable diurnal fluctuation in CDVR, and three adjacent to wells E1 and E2 (MR1a, MR2, and MR3) showed a relatively strong response, owing to the very large-amplitude fluctuations there (especially at E2). Two of these gradient triangles angled towards the stream as the flow and groundwater levels fall during the afternoon, tending the other

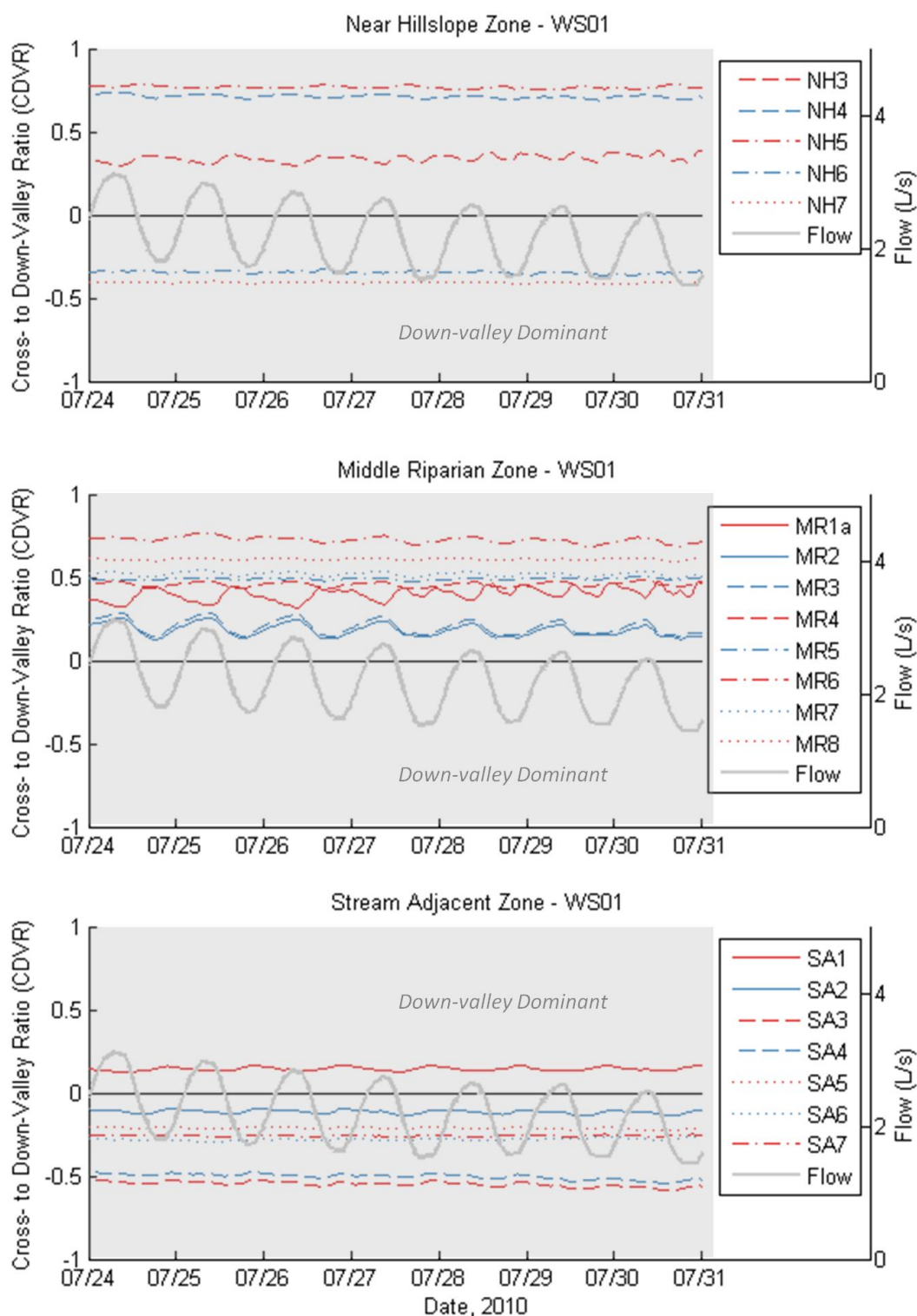


Figure 4-13. WS01 cross- to down-valley gradient ratio (CDVR) for the June 1-8 storm period, plotted according to the three zones labeled in **Figure 4-2**. Tick marks are displayed at 00:00 on the day labeled.

direction at night, and the other displayed the opposite behavior. Well E2 was also the only well outfitted with a capacitance-based TruTrack logger, which has a lower stated accuracy than the HOBO loggers used in other wells, so it is possible that the trends observed are exaggerated. Whatever the case may be, since these locations are further removed from the stream, they are less important to the question of whether diurnal fluctuations play a role in stream-groundwater exchange than those located nearer the stream. In the SA zone, most CDVRs do exhibit diurnal fluctuations, typically reaching the most positive CDVR value shortly after the minimum flow and water table level. This means that all gradients already angling towards the stream turn slightly more towards it, and those angling away turn slightly less away. Without physical evidence and more extensive analysis, it is difficult to say whether the magnitude of these fluctuations in CDVR lead to substantial changes in patterns of stream-groundwater exchange on a daily basis. However, the fact that these fluctuations were apparent during the last two injections begs the question of whether they had an impact on the observed increase in the extent of stream water intrusion into the WS01 riparian zone. On the basis of **Figure 4-13**, no fluctuations were great enough to cause a gradient to rotate across the down-valley axis (i.e. no CDVR changes sign throughout the course of a day, at least during the period presented), which would seem to be a necessary precursor to the potential for such exchange patterns. Tracer studies directed at this particular question on a sub-daily basis may yield more definitive answers, as would more in-depth analysis of water table fluctuations at the riparian-stream interface.

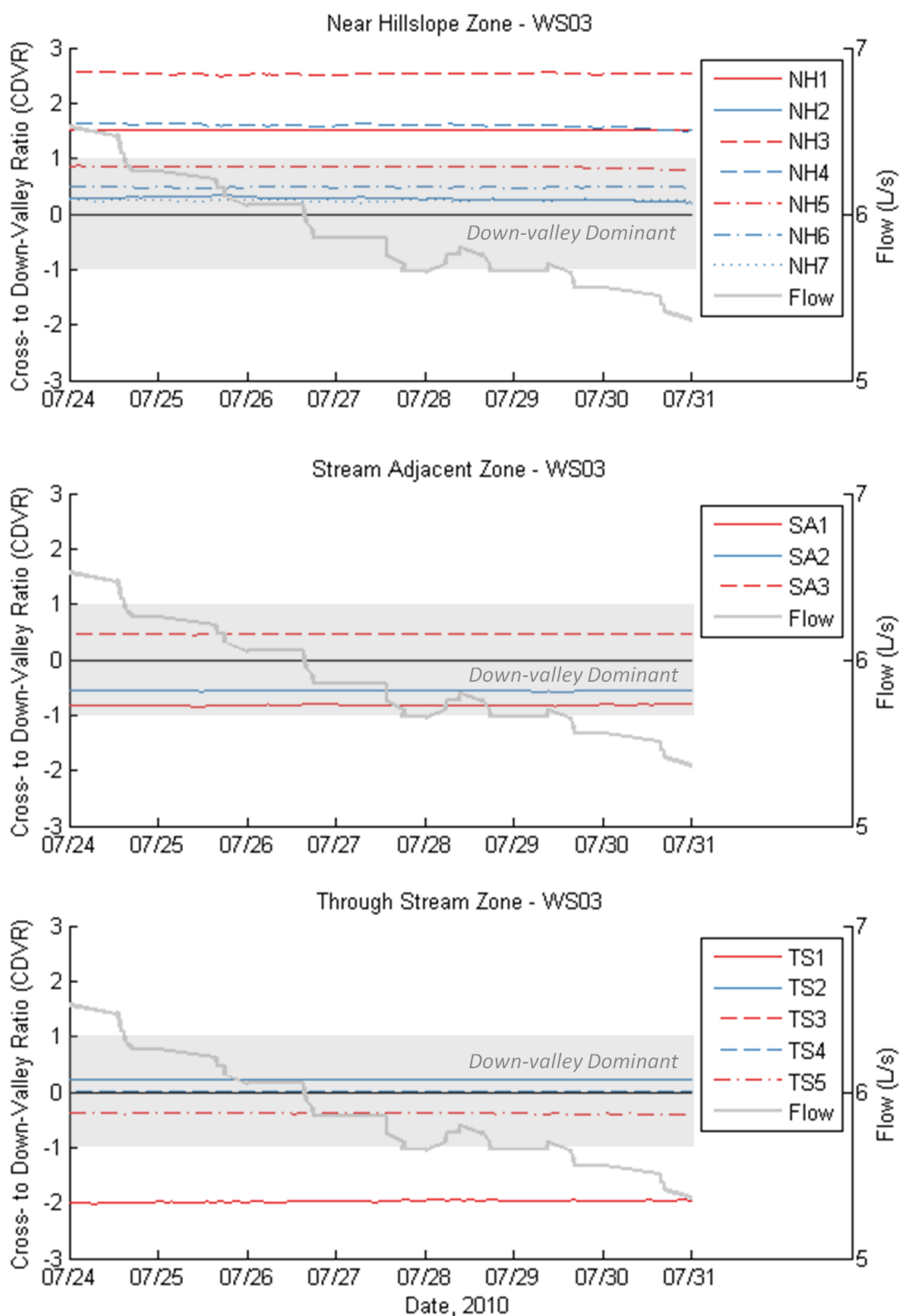


Figure 4-14. WS01 cross- to down-valley gradient ratio (CDVR) for the June 1-8 storm period, plotted according to the three zones labeled in **Figure 4-2**. Tick marks are displayed at 00:00 on the day labeled.

4.5.2 WS03

The WS03 riparian CDVR time series for the same week in July are shown below in **Figure 4-14**. Unlike the obvious fluctuations in flow seen in WS01, the flow in WS03 appears rather to be a gradually stepping down, which could be a consequence of lag in the float recorder that records stream stage at the WS03 gauge, a known issue with the device used. At the scale displayed, there do not seem to be any diurnal fluctuations in the CDVRs of WS03 riparian gradients that could significantly affect movement of water through the valley bottom.

4.6 Summary and Discussion

4.6.1 Seasonal Time Scale

Although less prevalent in WS03, both monitored riparian areas exhibited down-valley dominance in hydraulic gradients when considered over the entire season. Gradients throughout the WS01 riparian zone showed strong down-valley dominance, particularly in the stream-adjacent (SA) and middle-riparian (MR) zones. Seasonal trends of note observed in WS01 included the tendency of nearly all gradients in the SA zone – already angled generally away from the stream – to gradually turn even further from the stream. In addition, two gradients in the more distant near-hillslope (NH) zone began the season angling towards the stream, and ended it angling away. While it is difficult to speak absolutely, the changes observed in these gradients agree with the observed seasonal changes in the extent to which salt-labeled water increasingly intruded into the riparian zone, pointing to a link between gradient changes of this kind and increased stream-groundwater exchange. This is an important finding with implications for biogeochemical cycling, which may be affected by similar flow recessions in riparian areas of other watersheds.

The seasonal changes observed in WS03 tended to be less pronounced than those in WS01, with a general tendency for all gradients to 'straighten out' along the down-valley axis, showing cross- to down-valley gradient ratios (CDVRs) that grew closer to zero. However, in absolute terms of CDVR values, WS03 spans greater range of values, including several very strong cross-valley-dominant gradients in the downstream section of the riparian zone, where side slopes are very steep. There is also an interesting location centered around well G5, where gradients from the NH and SA zones appear to converge strongly on the riparian area downstream of the well, a convergence that grows stronger as the season progresses. In contrast to WS01, the WS03 valley bottom was subject to much more intrusion of salt-labeled water during the tracer injections, although a few locations indicated further intrusion as flow receded throughout the season. Examination of the seasonally varying gradient patterns did not shed much light on these changes in stream-groundwater exchange. However, the simple fact that nearly the entire valley bottom was heavily intruded by the salt tracer implies that the WS03 valley bottom riparian area is very well connected to its stream.

4.6.2 Storm Time Scale

Both study areas showed a variety of responses to the 1.25-year storm that took place in early June. The diversity of responses seen in both study areas underlines the heterogeneity inherent on even relatively small spatial scales, serving as a reminder that its effects will be seen in any study of this kind.

In the WS01 near-stream zone, gradients responded to the storm by turning even further away from the stream when the flow peaks passed, possibly pointing to a mechanism that drives more stream water into the subsurface. This occurred in spite of most of the more

distant gradients turning towards the stream, as a conventional conceptual model would imply. Despite these responses, only 1 of 23 gradients triangles ever ceased to remain down-valley dominant, and even then only for a brief time, which speaks to the dominant influence of the down-valley gradient in the WS01 valley bottom. If riparian zones subject to inflow of groundwater containing nitrate or other contaminants showed similar behavior, it would imply that riparian travel times can remain high even during a storm, allowing greater opportunity for biogeochemical reactions to take place and greater buffer capacity to be retained. It is also an interesting result that WS01 exhibited some of the same behavior in response to the storm as it did over the seasonal flow recession, with gradients near the stream turning further away from it, and a number of the more distant ones turning further towards it.

In WS03, the riparian gradients showed a wider variety of more extreme responses to the storm, few of which conformed to conventional ideas. Furthest downstream, two strongly cross-valley gradients showed a substantial decline in magnitude in response to the storm. Just as was observed on the seasonal scale, the converging gradients centered around well E5 converged more intensely during the storm. In the upstream part of the monitored area, some gradients responded by pointing more weakly towards the stream, while others adhered to conventional ideas by showing an enhanced cross-valley towards the stream.

4.6.3 Daily Time Scale

Only gradients in WS01 showed any noticeable changes in response to the diurnal rise and fall in groundwater levels and stream stage. The changes that were observed in the stream-adjacent zone of WS01 generally implied that at the minimum daily water table elevation, gradients angling towards the stream would turn slightly more towards it, and those

angled away would turn slightly less away. Wondzell et al. [2009] proposed a mechanism of lateral hyporheic exchange whereby daily ET-induced drawdown in the riparian water table would draw stream water into the subsurface, sending it back further downstream or later in the day when rising water tables again forced the water back into the stream. While the daily-scale CDVRs shown for the stream-adjacent zone in WS01 do not appear to directly support this, small-scale tracer studies designed to study this specific question would be needed to provide physical evidence in the affirmative or the negative. This question is complicated by the limitations imposed on the interpretation of data from one riparian area adjacent to a single 24-m stream reach, since the down-valley dominance of hydraulic gradients in WS01 make clear the importance of considering longitudinal flow as well. For example, if the reach studied exhibits near-stream gradients that would on a daily basis have the potential to drive more flow out of the stream at some time of day versus another (as seems to be the case for the WS01 study reach), it is conceivable that further downstream near-stream gradients exist that would return the water to the stream, at a rate contingent on the time of day and relative elevations of the stream and near-stream water table.

4.6.4 Discussion of Related Literature

The complex hydraulic gradient patterns observed throughout the study period for our two sites are similar in character to those observed in studies at other headwater sites. Before comparing to others, however, we have the benefit of comparing what we found to results of a groundwater modeling effort in the same study reaches of WS01 and WS03 [Kasahara and Wondzell, 2003]. Taken as a whole, the hydraulic gradient patterns in our study reflect the overall down-valley dominance seen in the other authors' modeled equipotential maps of both

study sites, but show some more detail on a small spatial scale not captured by the model, particularly in the strongly cross-valley gradients in the lower portion of the monitored WS03 riparian area. Kasahara and Wondzell [2003] developed only a steady state groundwater flow model, so the temporal dynamics of changing gradients throughout the riparian zone was not previously addressed at these sites. Studies at other headwater sites also showed similar down-valley dominance of riparian hydraulic gradients, as well as a variety of more complex gradient dynamics in localized areas within the riparian zones [Harvey and Bencala, 1993; Wroblicky et al., 1998]. Studies of this kind can be expanded upon and improved by employing methods used in the present study that span seasonal time scales and collect data at a high temporal resolution, showing how general gradient patterns calculated by models can change in response to short-term storm events and long-term seasonal flow recession. Knowledge of the potential that exists for spatial complexity of and variation over different time scales in patterns of headwater riparian hydraulic gradients can motivate future ecology- or biogeochemistry-based studies to undertake more extensive hydrologic monitoring, so that the ecological and biogeochemical patterns and changes observed can be placed in proper context of the dynamic flowing water system in which they occur.

The seasonal time scale over which we calculated gradients encompassed nearly the entire range of flows that these watersheds are likely to exhibit in a given year, from a 1.25-year storm flow (largest in WY2010) to the tiny flows remaining after two months of baseflow recession in the absence of precipitation. With that in mind, the overall seasonal changes exhibited by gradients in the two small riparian areas studied seem to be relatively small, and overall patterns relatively stable, compared to other systems. A field-based and two-

dimensional transient modeling study of riparian groundwater flow in New Mexico headwater streams during different flow conditions showed a much more dynamic response to changes in flow over a larger scale [Wroblicky et al., 1998]. In hillslope-constrained riparian areas of a stream with a catchment area only three times as large as WS01 and WS03, the authors observed and modeled stark changes in gradient direction, ranging from about 30 degrees away from the stream during low flow conditions to about 15 degrees towards or parallel to the stream during high spring-melt flow conditions (our interpretation) [Wroblicky et al., 1998]. Seasonal water table fluctuations were also as much as an order of magnitude greater than those observed in our study areas. In riparian zones draining much larger catchments, a wide variety of responses over different flow conditions, ranging from virtually no change to complete reversal of gradient direction has been observed [Vidon and Hill, 2004]. This same study found large seasonal fluctuations in water table, as large as one to two meters, while the largest seasonal fall in riparian water level (excluding the storm peaks) seen in WS01 or WS03 was 20 cm, with the average between 10 and 15 cm (see chapter 5). Nevertheless, the seasonal changes observed in hydraulic gradient patterns were sufficient to cause an increase in the extent of stream water intrusion into riparian zones, indicating that even apparently small changes in water table elevation can be associated with substantial changes in stream-groundwater exchange.

With regard to the extent of stream water intrusion into the riparian zones of WS01 and WS03, which is one indicator of the size of the hyporheic area, it is difficult to make substantive judgments about this area without a firm definition of where along the cross-valley axis to draw the line between the areas that are or are not connected to the stream. In the context of tracer

studies, one definition used in the literature [Triska et al., 1989; Valett et al., 1997] considers a location to be part of the active hyporheic zone (also termed the groundwater-surface water ecotone) if it shows greater than 10% of the tracer-labeled surface water. By this definition, both headwater riparian zones in this study are extraordinarily well connected to the stream, having a hyporheic area that spans essentially the entire valley bottom, up to where the very steep (> 50%), confining hillslopes begin, beyond which we have no information. Indeed, the only limitation to hyporheic area in these locations appears to be the width of the valley bottom, and more extensive field investigations would need to be undertaken to establish at which point on the lower hillslope the break occurs between pure groundwater and groundwater in connection with the surface stream water. Furthermore, the seasonal patterns evident in the changing extent of stream water intrusion into the riparian zone, particularly in WS01, are in agreement with other studies in the literature, which find that stream-groundwater exchange in the size of the roughly defined hyporheic zone are augmented when flows are lowest [Valett et al., 1997; Wroblicky et al., 1998], but disagreed with others [Fraser and Williams, 1998].

However, while the seasonal trend (especially in WS01) indicates a correlation between lower flows (and an overall drier catchment) and increased stream-groundwater exchange, it is important to draw attention to the observation that the response of near-stream riparian gradients to the storm mirrored to a considerable extent that of their response to the seasonal flow recession. Provided that there is a causal link between the seasonal patterns observed in near-stream gradients and the apparent increase in stream-groundwater interaction, it is logical to conclude that the (albeit relatively short-lived) gradient patterns during the storm would

elicit a similar change in the extent of stream-groundwater interaction. Intensive tracer or other studies conducted during large rainfall events in headwater streams would no doubt shed light on this question.

Chapter 5

Water Table Dynamics

5.1 Water Level Anomalies

Research objective 2a was aimed at assessing how the magnitudes of water table anomalies (recall, these are the deviations in water level from the mean over series of daily cycles) are organized spatially, and what general patterns of change they exhibit through time. In presenting the data, we group the plots of anomalies in an analogous fashion to the gradients in chapter 4, by zones divided along the down-valley axis, except that here the units are not triangular planes between wells, but rather the wells themselves. We took this approach because the strong down-valley dominance in riparian gradients may imply a greater connection among locations arranged parallel to the down-valley axis. Anomalies are plotted for the entire period in which fluctuations were apparent, from about June 20 to August 20, and then for three week-long sub-periods, to characterize the changes that occurred as the season progressed.

5.1.1 WS01 Anomalies

The anomalies for the WS01 water elevation records are given for the near-hillslope (NH) zone (**Figure 5-1**), the middle-riparian (MR) zone (**Figure 5-2**), the stream-adjacent (SA) zone (**Figure 5-3**), and for the in-stream loggers (**Figure 5-4**).

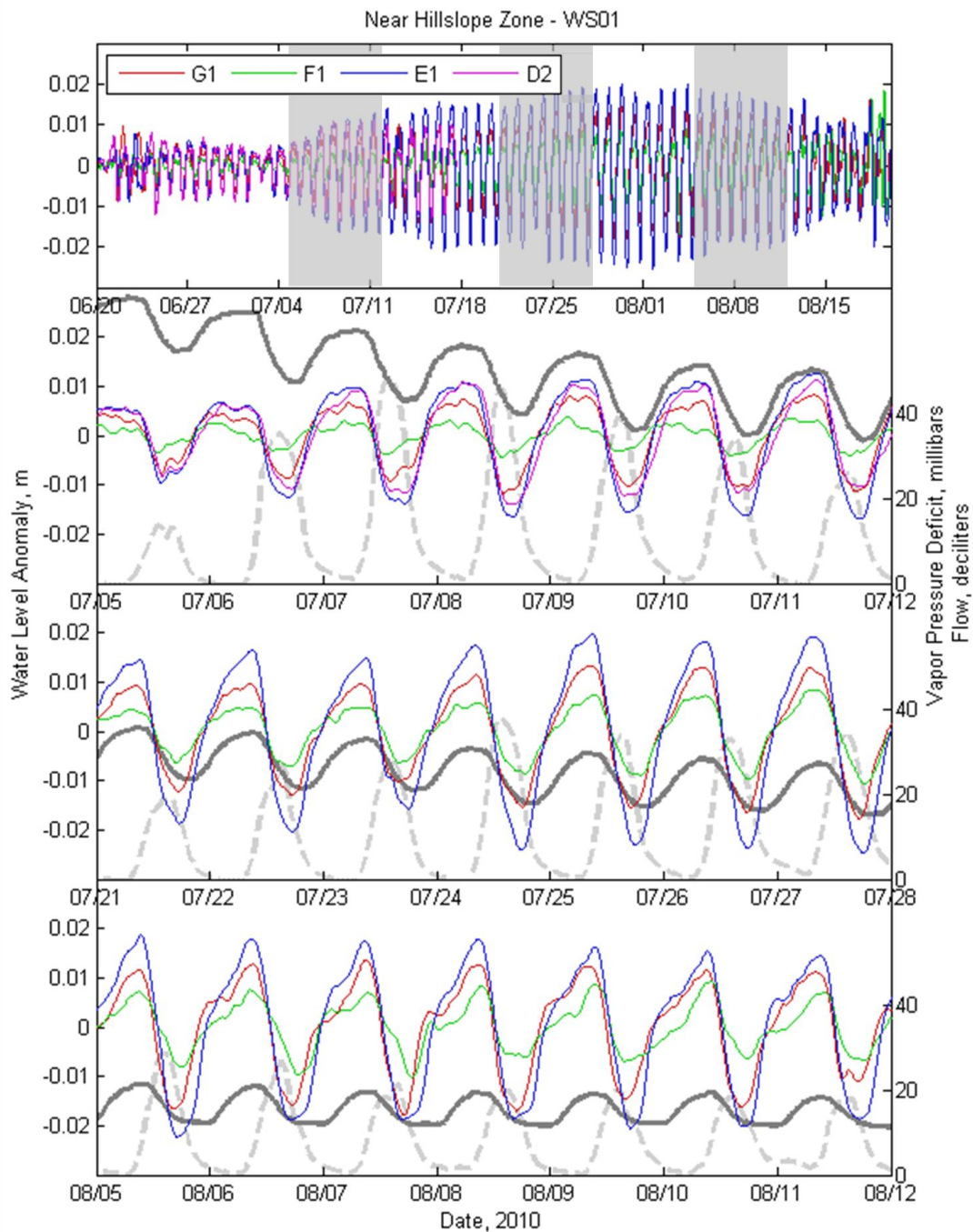


Figure 5-1. Water level anomalies in the WS01 riparian wells, near-hillslope (NH) zone. The dark grey line is flow at the weir 75 m downstream, and the light grey dashed line is vapor pressure deficit at 4.5 m above the ground, recorded at a meteorological station several hundred meters away. The grey rectangles in the top panel indicate when each of the week-long sub-periods occurs.

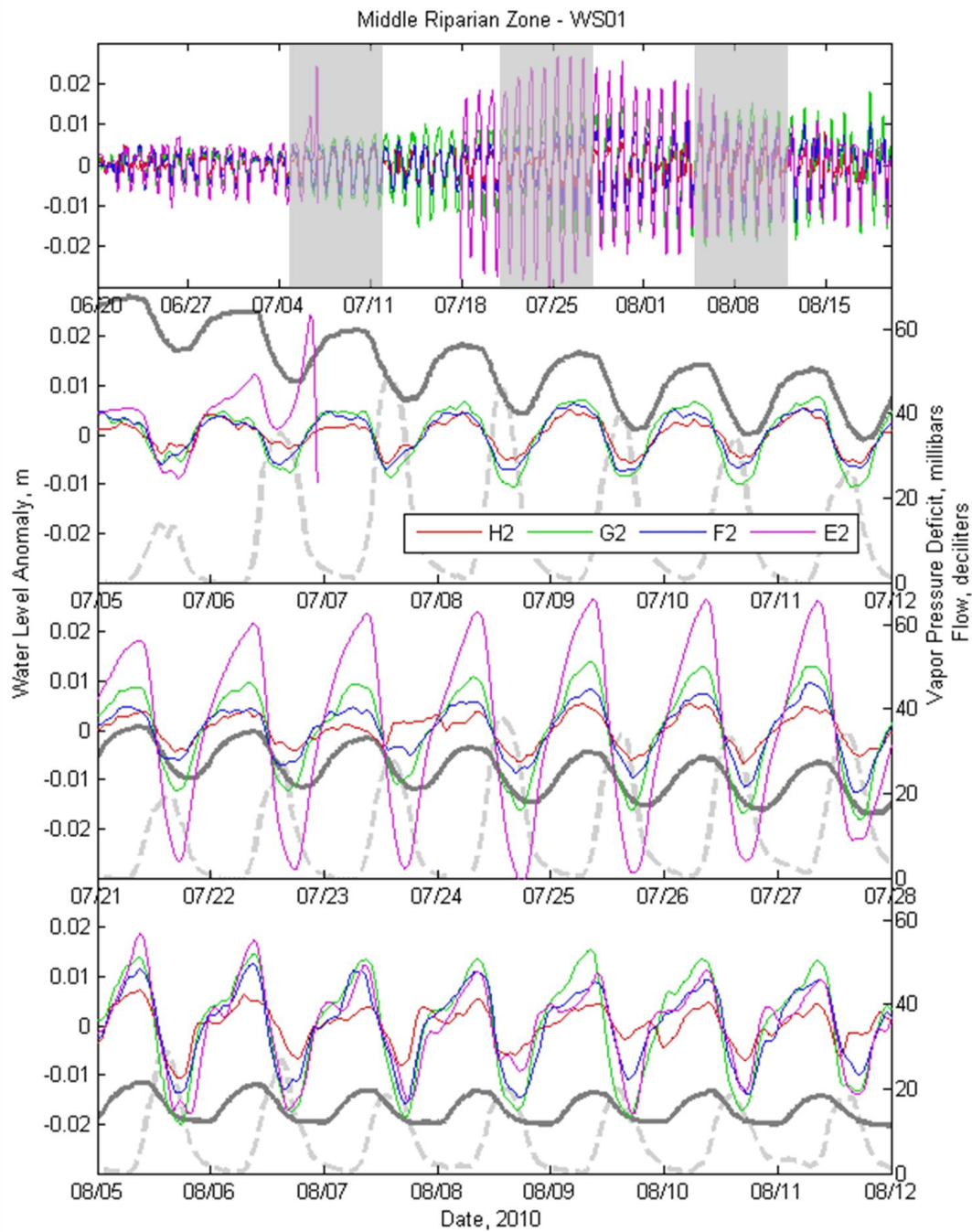


Figure 5-2. Water level anomalies in the WS01 riparian wells, middle-riparian (MR) zone. The dark grey line is flow at the weir 75 m downstream, and the light grey dashed line is vapor pressure deficit at 4.5 m above the ground, recorded at a meteorological station several hundred meters away. The grey rectangles in the top panel indicate when each of the week-long sub-periods occurs.

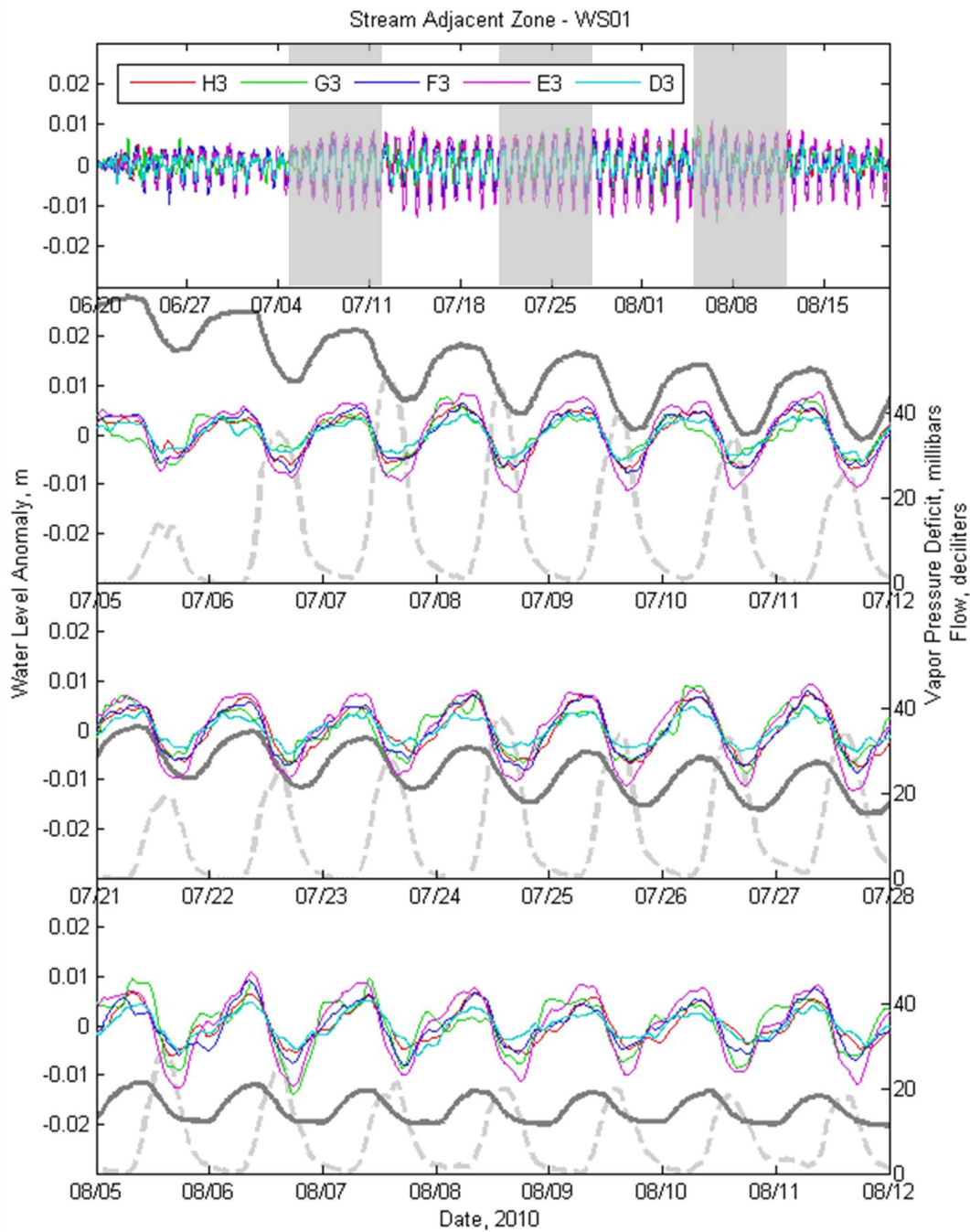


Figure 5-3. Water level anomalies in the WS01 riparian wells, stream-adjacent (SA) zone. The dark grey line is flow at the weir 75 m downstream, and the light grey dashed line is vapor pressure deficit at 4.5 m above the ground, recorded at a meteorological station several hundred meters away. The grey rectangles in the top panel indicate when each of the week-long sub-periods occurs.

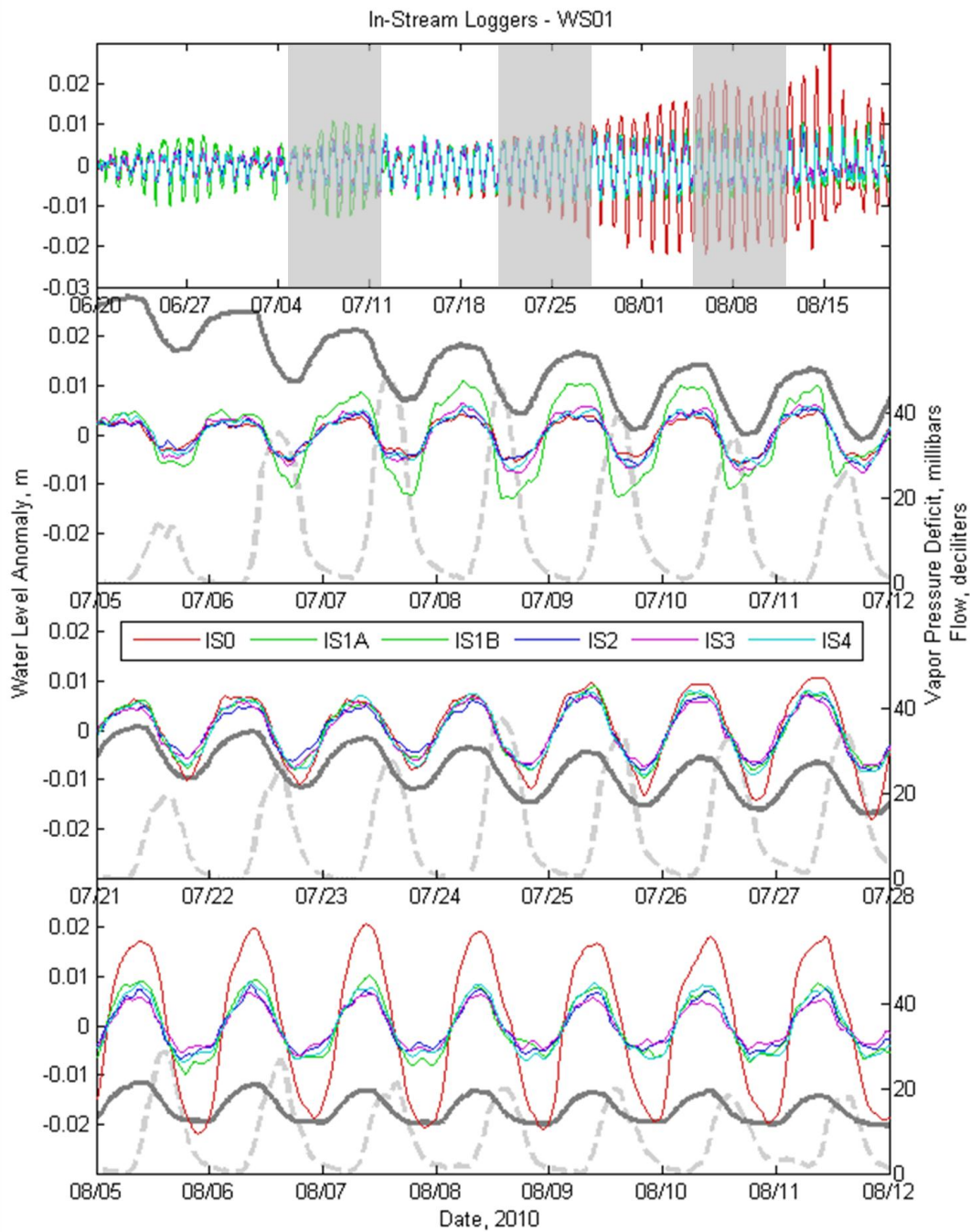


Figure 5-4. Water level anomalies for the WS01 in-stream loggers. The dark grey line is flow at the weir 75 m downstream, and the light grey dashed line is vapor pressure deficit at 4.5 m above the ground, recorded at a meteorological station several hundred meters away. The grey rectangles in the top panel indicate when each of the week-long sub-periods occurs.

There are a number of interesting patterns apparent in the various anomaly plots. One is the general tendency for the shape of the daily curves to change as the season progresses. In the NH zone (**Figure 5-1**) and MR zone (**Figure 5-2**), and more subtly in the SA zone (**Figure 5-3**), the curves have a more even, rounded shape in the first week-long period (July 5-12), and progressively become more irregularly shaped, increasing the time to peak and changing slope before reaching a peak, then dropping off sharply again. In contrast, the in-stream water level anomalies generally retain their symmetrical shape, but there is a noticeable tendency for the peaks to become sharper and more restricted in time as the season progresses. That is, the rise and fall of the stream stage occurs over a shorter period of time, and the minimum daily water level persists for a longer period of the day.

The most conspicuous attribute of these anomalies, however, is the diurnal amplitude (change from minimum to maximum daily level), which displays patterns in both space and time. Broadly speaking, the anomaly magnitudes both increase and show greater diversity of response with greater distance from the stream, with the NH zone (**Figure 5-1**) and MR zone (**Figure 5-2**) anomalies exhibiting larger fluctuations on average and a greater variety of anomaly magnitudes than the SA zone (**Figure 5-3**) and in-stream loggers (**Figure 5-4**). Within this spatial arrangement, there is also a general tendency for the anomaly magnitudes to increase as the season progresses, but only in proportion to increasing distance from the stream. The already larger anomalies in the NH zone seem on average to increase the most from the first week (July 5-12) to the last week (August 5-12), while the MR zone anomalies also increase, but to a lesser extent. In the SA zone and in the stream,

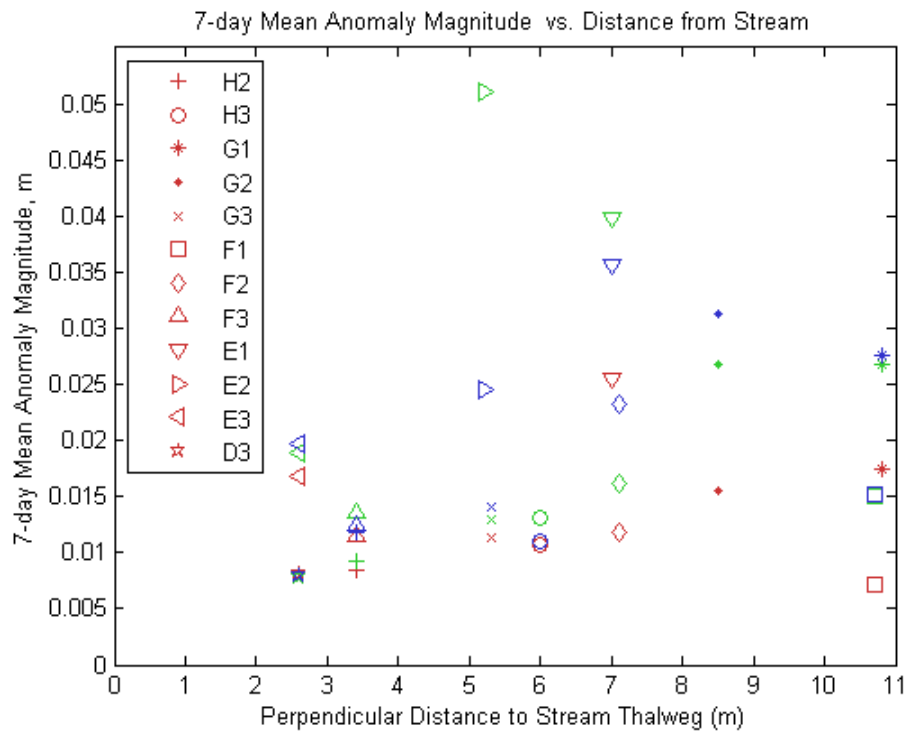


Figure 5-5. 7-day mean water level anomalies plotted against distance from the stream. The points represent the mean anomaly magnitudes for the weeks of July 5-12 (red), July 21-28 (green), and August 5-12 (blue). In-stream loggers not shown.

however, anomalies show very slight if any increases in magnitude. A summary plot of these patterns is shown in **Figure 5-5**, with mean anomaly magnitudes for each week plotted against perpendicular distance from the stream. Anomalies in the more distant wells show increases in magnitude ranging from about 8 mm (well F1) to about 17 mm (well G2) from the first to last week, while those closest to the stream show increases ranging from zero (well D3) to about 3 mm (well E3). Exceptions do exist, however, that serve as reminders of the heterogeneity at the site. Notably, in-stream logger ISO (**Figure 5-4**) shows a very large increase in anomaly magnitude beginning on about July 25 and gradually growing in size until about May 15, and

well E2 (**Figure 5-2**) shows very large fluctuations that begin on July 18 (immediately following a period of lost data) and become progressively smaller until the end of the period of record.

5.1.2 Patterns in WS01 Riparian Anomalies

These temporal and spatial patterns in how water level anomalies change are likely the product of multiple factors, all of which are subject to the hydrogeologic heterogeneity present in the riparian aquifer soils, and the riparian boundary conditions at the stream and hillslope. ET demand (which is direct proportion to the vapor pressure deficit) is an important driver of these diurnal patterns, being ultimately responsible for the occurrence of fluctuations in the first place. Certainly, there appears to be a direct causal link between daily changes in vapor pressure deficit (proxy for ET demand), as can be seen in the third panel (July 21-28) of **Figure 5-1**. The vapor pressure deficit slowly increases on July 21, 22, and 23, reaching greater peak daily values that occur for the rest of the week. Corresponding increases in anomaly magnitudes of the NH zone wells are apparent, with each fluctuation seeming to reflect the level of vapor pressure deficit preceding it. However, vapor pressure deficit decreases overall from the first week to the third, even as there is a general tendency (at least at locations more distant from the stream) for anomaly magnitudes to increase. One simple way to examine this potential relationship is shown in **Figure 5-6** below, which plots anomaly magnitudes in the NH zone against the magnitude of the vapor pressure deficit change for each day in the period. This plot (generally representative for the entire riparian area – other zones shown in **Appendix C**) reveals that many different magnitudes of vapor pressure deficit correspond to similar water table anomaly magnitudes, which undermines the explanatory power of changes in vapor pressure deficit with respect to changes in anomaly magnitudes. So, while the effect of vapor

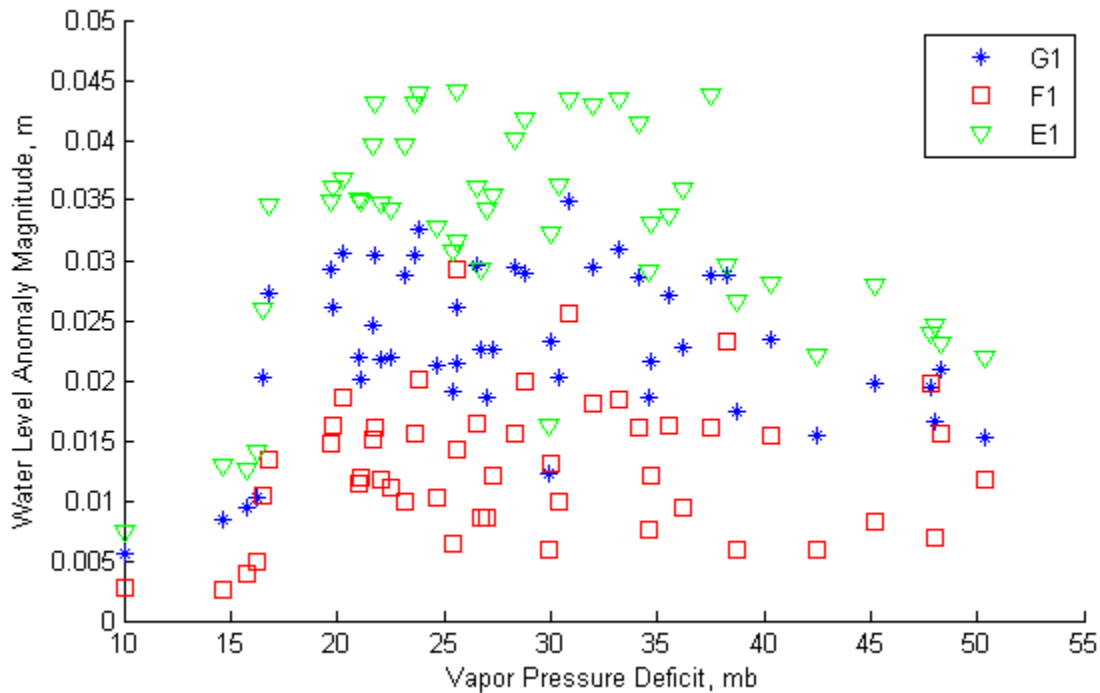


Figure 5-6. Water level anomaly magnitude plotted against change in vapor pressure deficit for the same daily periods in the near-hillslope (NH) zone of WS01.

pressure deficit can generally be seen in the daily water table response around the network, its magnitude cannot account for the increasing anomaly magnitude observed. Nor can it shed any light on the differing anomaly magnitudes that occurred around the riparian well network, or the tendency for stream-distant anomalies to be both larger in general and to increase as the catchment dries and flow recedes. It is possible that vegetation undergoes phenological changes during a season, increasing the rates of transpiration despite lower atmospheric ET demand [Gribovski et al., 2008], but sap flow measurements in WS01 have shown transpiration rates in riparian trees to be relatively steady throughout the summer dry season [Moore et al., 2004].

5.1.2.1 *Relation of Connectivity to Distance from Stream in WS01*

One possible explanation of the observations of increasing anomaly magnitude and greater tendency to increase over time at greater distance from the stream could be that the stream, which is not subject to the constraints of soil transmissivity, has a buffering effect on riparian water levels that diminishes with distance from the stream channel. This would account for the great similarity in anomaly magnitudes seen in the SA zone (**Figure 5-3**) as compared to the stream stage anomalies, and for the progressively larger and more varied anomaly patterns seen in the more distant MR and NH zones. This is similar to the conceptual model proposed in a study of hillslope and riparian groundwater dynamics in a Swedish till catchment [Seibert et al., 2003], which found a stronger and more coherent connection between the riparian groundwater responses to rainfall events and the groundwater responses observed in more distant wells (up to 100 m away from the stream). Here, the connection (or lack thereof) between the stream stage and riparian groundwater level fluctuations is in response to a different catchment stimulus, ET demand, but having monitored our study sites during a storm and subsequent seasonal drying, other water table dynamics can be related to distance from the stream, to determine whether a similar disconnection behavior occurs in the daily anomalies. The figures below show the relationships between the wells' perpendicular distance from the stream and the maximum rise in water level exhibited during the storm (**Figure 5-7**) and the total drop in water level observed from June 15 (after the storm had passed) to the end of the field season (**Figure 5-8**). The plot of maximum storm water level rise

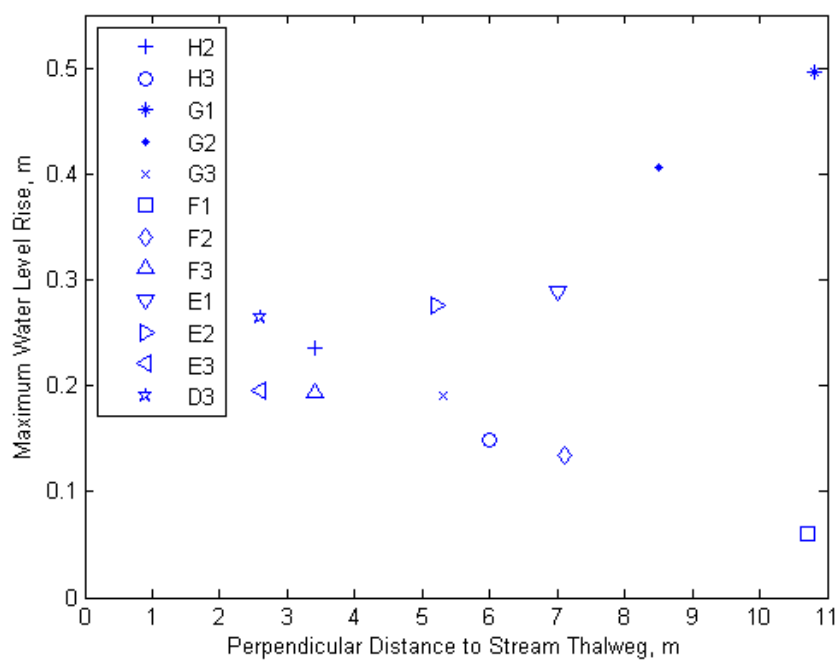


Figure 5-7. Maximum water level rise in WS01 riparian wells during the first peak of the storm on June 2 vs. perpendicular distance to the stream thalweg.

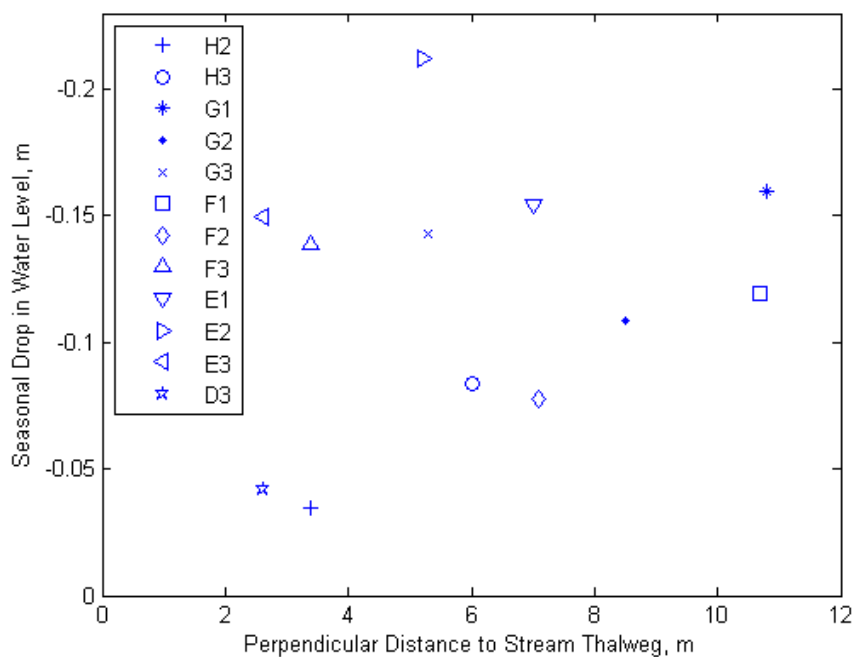


Figure 5-8. Seasonal drop in WS01 riparian water levels from June 15 to August 19 vs. perpendicular distance to the stream thalweg.

vs. distance reveals an apparent diverging trend, whereby locations most distant from the stream show the widest range of water level rises, ranging from 6 (well F1) to about 50 cm (well G1), with none in between. The relationship seems to support the idea of greater disconnection with distance. On the contrary, the seasonal drop in water level shows a somewhat converging trend, indicating a more subtle change in water level as a function of distance. This might support a view that more stream-distant water table dynamics are influenced by hillslope processes more than by the stream.

5.1.2.2 Consistency of Water Table Response in WS01

Another analysis may prove fruitful in characterizing the consistency of response exhibited by a particular riparian location. Rather than using distance as the basis of comparison, we can relate the mean anomaly magnitudes for the week-long periods displayed in **Figures 5-1** through **5-4** separately to the maximum water level rise in the storm (**Figure 5-9**), and the seasonal water level drop (**Figure 5-10**). Both plots imply a positive correlation between the magnitudes of the different water level changes represented. Not surprisingly, the mean anomaly magnitudes appear to be well correlated with the seasonal drop in water level, most likely because the seasonal drop is in a sense the accumulation of all of the repeated daily falls that a particular location is subject to. The storm rise also represents the wetting up of part of the soil column that has been dry before the diurnal fluctuations become apparent, and as such is subject to different soil transmissivities and may yield a different response. Nevertheless, the measure of relative consistency in the magnitude of water table responses observed in response to the seasonal, storm, and daily drivers is a sign that information gleaned

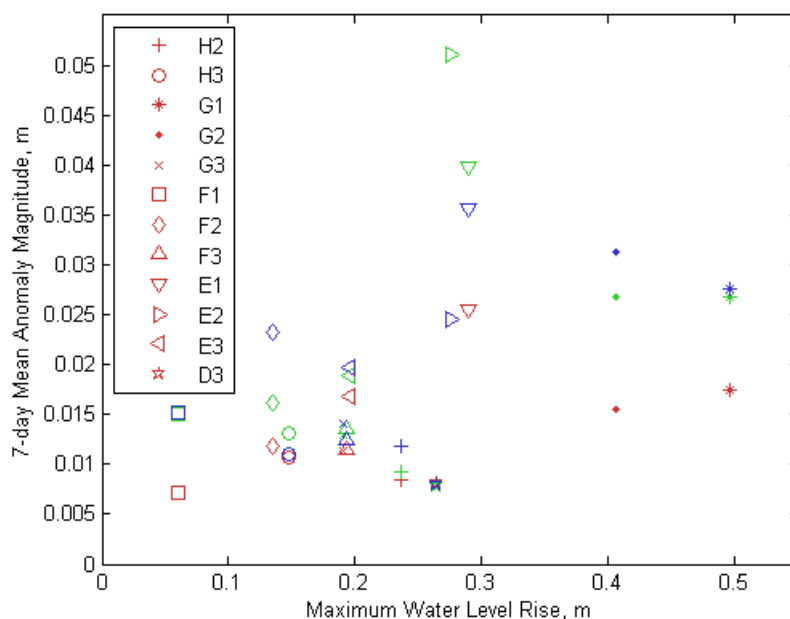


Figure 5-9. 7-day mean water level anomalies plotted against maximum water level rise during the storm. The points represent the mean anomaly magnitudes for the weeks of July 5-12 (red), July 21-28 (green), and August 5-12 (blue).

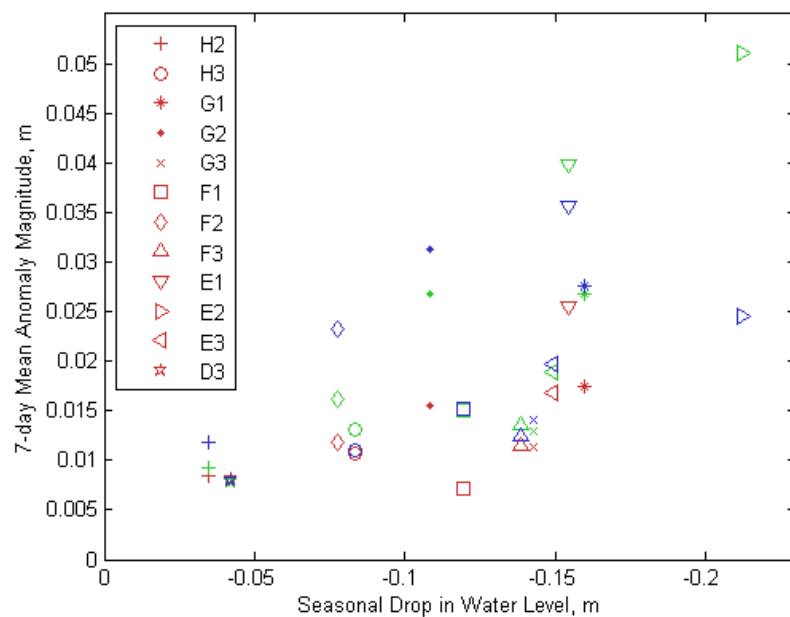


Figure 5-10. 7-day mean water level anomalies plotted against seasonal drop in water level from June 15 to August 19. The points represent the mean anomaly magnitudes for the weeks of July 5-12 (red), July 21-28 (green), and August 5-12 (blue).

from diurnal fluctuations could be used more broadly in the hydrogeologic and eco-hydrologic characterization of a site [Gribovski et al., 2010].

5.1.2.3 Possible Role of Tree Proximity in Anomaly Magnitude in WS01

Another line of evidence that could help account for the spatial diversity in anomaly magnitude is the proximity of the riparian wells to the riparian trees, which likely act as localized ET ‘pumps’, and may cause some cone of depression that would correlate with a larger anomaly magnitude in nearby wells. To investigate this possibility, we devised a basic index to describe a tree’s potential influence on a nearby well, defined as the tree’s breast-height diameter divided by the square of the distance from that tree to the well in question. This index was summed for each well relative to all trees in the WS01 riparian area, and against it was plotted the mean anomaly magnitude for the period from July 18 to August 20 (to obtain a longer-term average magnitude) (**Figure 5-11**). This plot does not indicate a clear correlation, implying that we can reject the simple notion that trees alone are responsible for the variety in anomaly magnitude observed throughout the WS01 riparian area. Most puzzling are the two wells E1 and E2 that both show very large fluctuations without the immediate presence of a large tree. This finding underlines the ubiquitous presence of hydrogeologic heterogeneity even at relatively small spatial scales and a spatially dense monitoring network, implying that no single factor considered alone can account for the diversity of water table responses observed in the riparian zone.

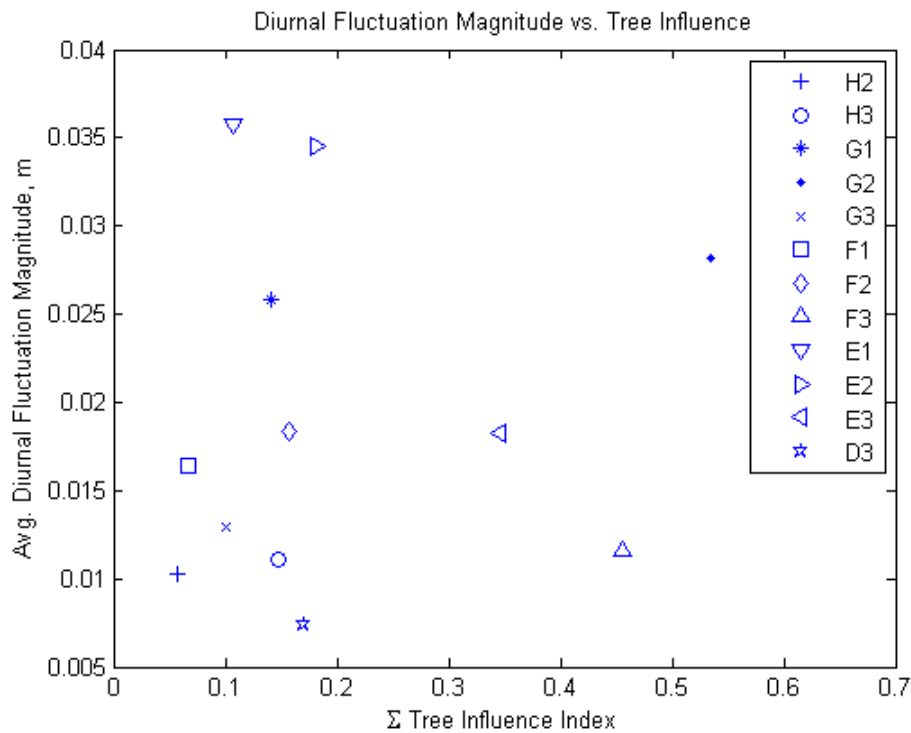


Figure 5-11. Mean water level anomalies over the period from July 18 to August 20 vs. the sum of the tree influence index (diameter/distance²) for each well.

5.1.3 WS03 Anomalies (or Lack Thereof)

Although WS01 and WS03 are very similar with respect to size, stream network lengths, geologic history, and soil distribution, when all catchment processes are integrated at the outlet where flow is recorded, no diurnal fluctuations were evident in WS03 during the 2010 summer baseflow recession. To try to explain this first without examining the riparian water level data, we draw from the findings of Wondzell et al. [2007] that considered ET to be a signal generated over an entire catchment (and therefore stream network), showing conceptually that at high flows ET-induced signals will arrive together and in phase at the outlet, but at low flow the reduced stream velocity will produce destructive interference of down-network traveling signals, masking some or all of the signals arriving from upstream. This might be a plausible

explanation for why no diurnal fluctuations were evident in the low flow part of the record at the WS03 gauge (see **Figure 4-1**) during the 2010 flow recession. However, the riparian water level data collected during this study affords an opportunity to test this idea, in part. At a few locations in the riparian zone of WS03 water levels demonstrate a very weak diurnal signal. In only a few cases (wells D3, D6, H6, I5) do the anomaly amplitudes exceed the 3-mm tolerance of the loggers used, although it never occurs on a regular basis, and in some cases appears to be a consequence of human disturbance or noise. **Figure 5-12** shows the anomalies in the NH zone of WS03 for the same periods shown for

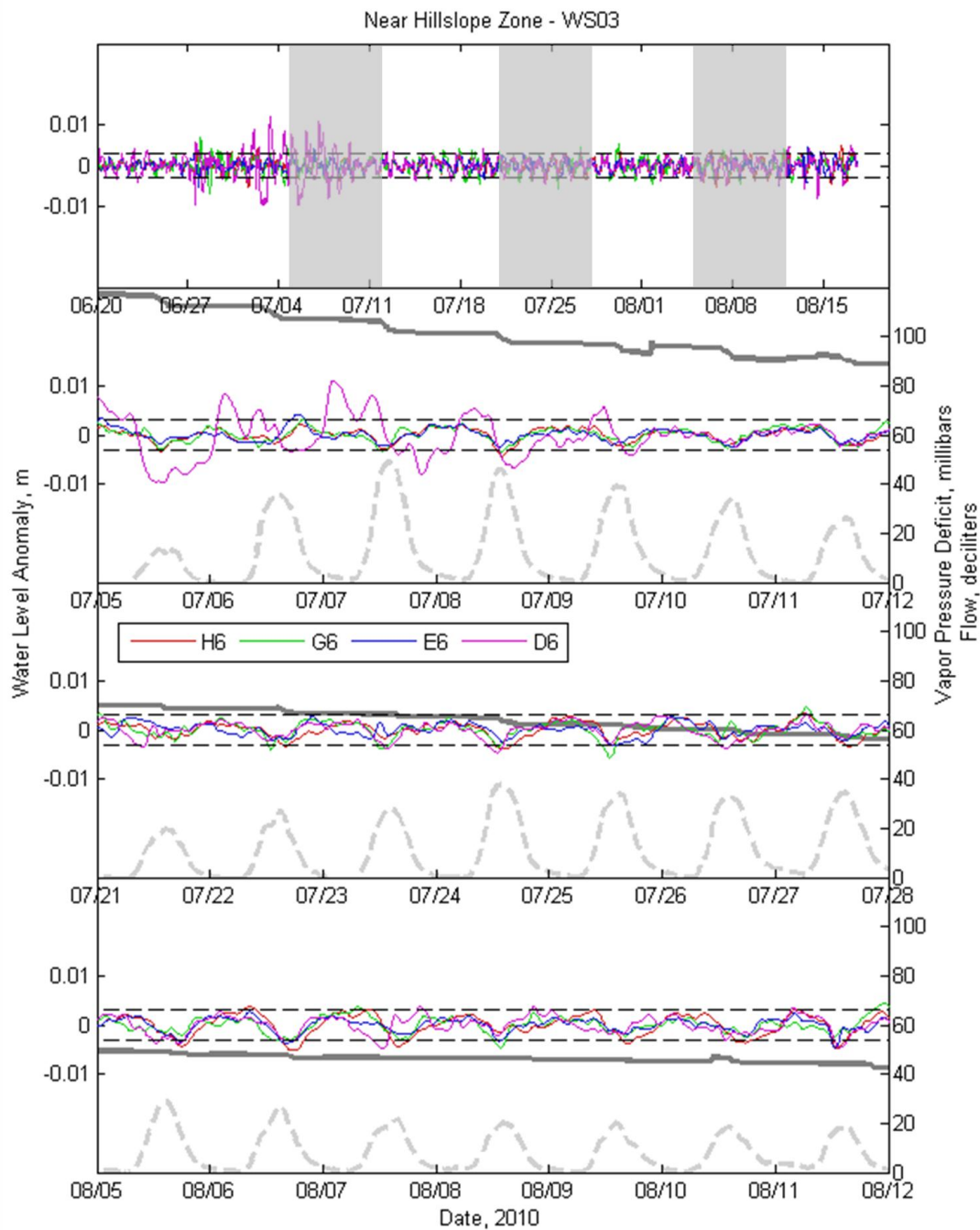


Figure 5-12. Water level anomalies in the WS03 riparian wells, near-hillslope (NH) zone. The dark grey line is flow at the weir 75 m downstream, and the light grey dashed line is vapor pressure deficit at 4.5 m above the ground, recorded at a meteorological station several hundred meters away. The grey rectangles in the top panel indicate when each of the week-long sub-periods occurs. 3-mm data logger tolerance is shown as black dashed lines.

WS01. This plot contains the strongest diurnal fluctuations that occurred in WS03; the plots of the weaker anomalies in the SA zone and the in-stream loggers are given in **Appendix D**. Since there is a known potential for pressure-based water level loggers to report artificial diurnal fluctuations, as discussed in chapter 3 [Cuevas et al., 2010], and the data are especially noisy, no further water level anomaly analysis was undertaken for WS03. Of course, an identical artificial diurnal fluctuation could be present in all of the WS01 data, but since no additional data collection was done with the intention of isolating that effect in order to remove it, we cannot mathematically account for this probable effect and must simply acknowledge that it likely exists in the background of the data series presented and analyzed above.

5.1.4 Accounting for the Difference between WS01 and WS03

Although the water level data collected in our WS03 study area represent a small fraction of the overall riparian area throughout the stream network, the effective lack of diurnal fluctuations exhibited by the data suggests that there may in fact be no diurnal signal in water elevations that is translated to the stream, or else it is so small that it does not survive the journey to the outlet or is otherwise below the level of detection of the flow gauge. The most compelling explanation may lie in the valley-bottom conditions created by the 1996 flood which scoured much of the upper stream reaches in WS03, and eliminated nearly all mature valley-bottom vegetation. In the warm summer conditions that prevail in the H.J. Andrews Experimental Forest (HJA), diurnal fluctuations are unequivocally caused by ET of the groundwater, either directly or indirectly, by vegetation with roots close enough to reach it. Several studies of diurnal stream flow and groundwater level fluctuations found that removal of riparian vegetation results in the elimination or near-elimination of diurnal fluctuations in

stream flow [Dunford and Fletcher, 1947; O'Loughlin et al., 1982; Lawrence, 1990], and one concluded that only the riparian vegetation was responsible for diurnal fluctuations by removing all other vegetation in the catchment [Bren, 1997]. Dunford and Fletcher [1947] found only a near-elimination of fluctuations in a small catchment within the Coweeta Experimental Forest, having topography not as steep as that of WS01 and WS03 in the HJA. Hence, it is possible that the Coweeta catchment may not have been steep enough to sever the lower hillslope vegetation's connection to near-stream groundwater (and the valley-bottom groundwater system). Since there is a threshold groundwater 'extinction' depth, below which the soil moisture gradients caused by vegetative ET are not large enough to overcome gravity [Baird et al., 2005; Shah et al., 2007], a steep hillslope that rises at a greater angle than the groundwater table will quickly bring the surface vegetation out of reach of the groundwater. A modeled estimate of this extinction, based on forested land with loamy soils, is 4.5 m, but a 50% reduction in groundwater ET occurs when the water table is as shallow as 1 m below the land surface [Shah et al., 2007]. Although we have no direct observations of hillslope groundwater depth, the apparent groundwater slope based on riparian measurements indicates that the water table would very abruptly fall below this extinction depth in the hillslopes of both WS01 and WS03. Therefore, the relative lack of diurnal fluctuations in either water levels or stream flow in WS03 may be a consequence of the absence of mature trees in the riparian zone and particularly steep hillslopes. Only young red alder were growing in our WS03 study reach, and due to their relatively small total leaf area may not exert enough ET demand to substantially alter the riparian groundwater levels on a daily basis, at least within the confident range of detection of our instruments.

5.1.5 Timing of Daily Peak and Trough Water Levels

One other aspect of the WS01 water level anomalies that is evident upon inspection of the plots in **Figures 5-1** through **5-4** is the seasonal and spatial variation in timing among the peaks and troughs of the various riparian and in-stream anomaly records, vapor pressure deficit, and stream flow record. In examining these timings in the context of diurnal fluctuations, the benchmark timing is that of vapor pressure deficit, since it is a proxy for ET demand and the ultimate reason for the occurrence of diurnal fluctuations, although not always for the specific physical and temporal characteristics manifest in the actual fluctuations observed around the monitored area and through the season. Vapor pressure deficit reached a peak at essentially the same time every day, between 14:00 and 15:00, about 1-2 hours past solar noon. The minimum vapor pressure deficit generally occurred between 04:00 and 07:00, although when not reaching zero, it seldom reached a well-defined minimum. The timings of the peaks and troughs in water level anomalies are shown below, grouped according to the NH zone (**Figure 5-13**), MR zone (**Figure 5-14**), SA zone (**Figure 5-15**), and in-stream loggers (**Figure 5-16**). The timing of the peaks and troughs in stream flow at the weir is included on every plot for comparison. Also shown are the average times of maximum and minimum vapor pressure deficit. Many of the outliers that produce jagged protrusions in the time series are artifacts of the noise in the data. In order to ease comprehension of the time series, which have a rough appearance, Theil linear regression lines are plotted to show the overall trend in each time series. Theil regression finds the slope equal to the median slope of all possible slopes between all points in the time series, making it robust against outliers, and a regression line is plotted

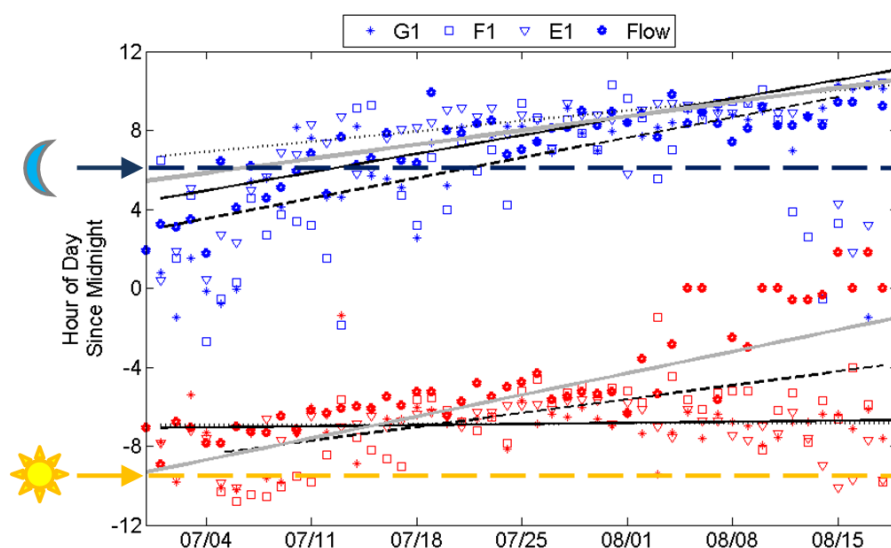


Figure 5-13. WS01 near-hillslope (NH) zone. Timing of peak (blue) and trough (red) water levels through the baseflow recession period. The y-axis is shown with midnight at the center (hour 0). Their best-fit lines are black for wells (G1 = solid; F1 = dash; E1 = dot) and thick grey for stream flow. Timing of peak and trough stream flow values at the gauge weir are shown for context. Time of maximum vapor pressure deficit indicated by the sun symbol and dashed yellow line, minimum by the moon symbol and dashed dark blue line.

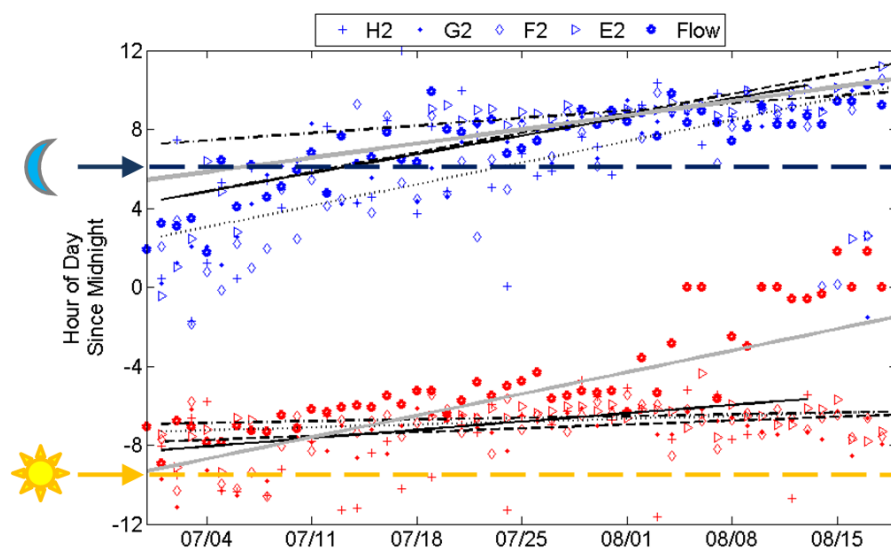


Figure 5-14. WS01 middle-riparian (MR) zone. Timing of peak (blue) and trough (red) water levels through the baseflow recession period. Their best-fit lines for wells are shown in black (H2 = solid; G2 = dash; F2 = dot; E2 = dot-dash) and in thick grey for flow. See **Figure 5-13** caption for more details.

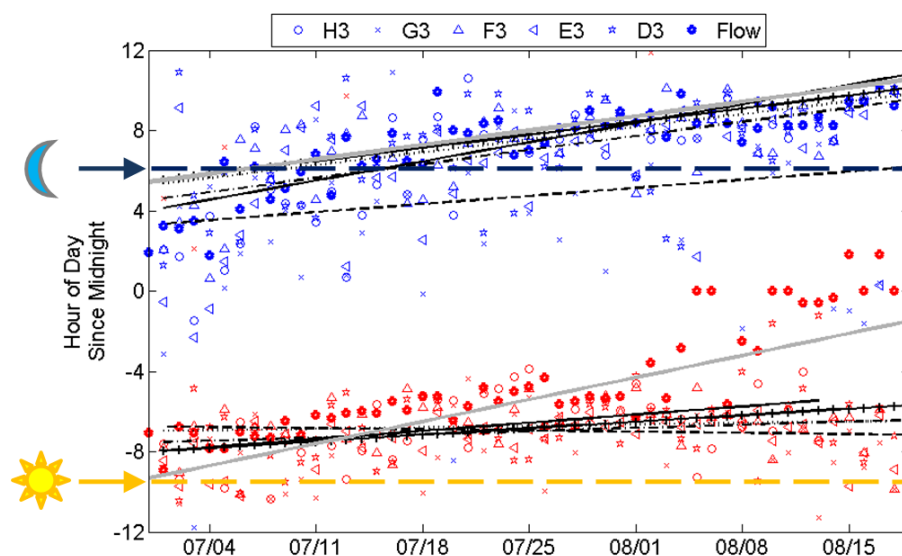


Figure 5-15. WS01 stream-adjacent (SA) zone. Timing of peak (blue) and trough (red) water levels through the baseflow recession period. Their best-fit lines for wells are shown in black (H3 = solid; G3 = dash; F3 = dot; E3 = dot-dash; D3 = solid crossed) and in thick grey for flow. See **Figure 5-13** caption for more details.

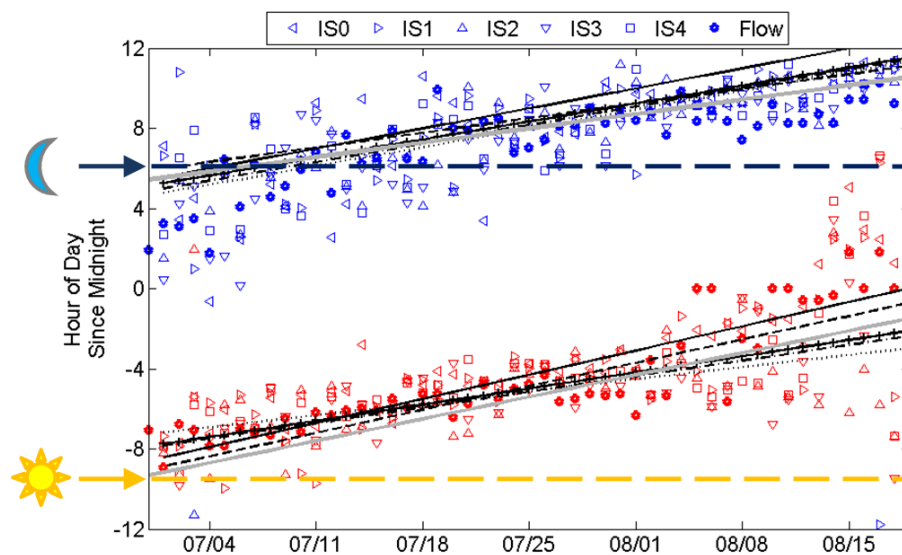


Figure 5-16. WS01 in-stream loggers. Timing of peak (blue) and trough (red) water levels through the baseflow recession period. Their best-fit lines for in-stream loggers are shown in black (IS0 = solid; IS1 = dash; IS2 = dot; IS3 = dot-dash; IS4 = solid crossed) and thick grey for flow. See **Figure 5-13** caption for more details.

such that the line passes through the median of the data set. The deviation in the peak timing time series (or best-fit lines) from the time of maximum vapor pressure deficit (sun symbol) indicates the lag time between maximum ET demand and the response to it.

The most obvious feature common to all of the seasonal water level trends is that the daily timing of both the peak and trough water levels and stream flow moves forward in the day as the season progresses and the WS01 catchment dries out. This simply indicates that time lag between maximum and minimum ET demand and the responding water levels increased as the season went on. Comparing plots of the riparian wells (**Figure 5-13, Figure 5-14, and Figure 5-15**) to that of the in-stream loggers (**Figure 5-16**) also shows that the time series for the wells are generally much noisier, and exhibit a much greater variety of best-fit slopes than the in-stream logger records, which are very tightly grouped. The more intriguing differences between the riparian well plots and the in-stream plot, however, are the best-fit slopes of the trough timing time series (red). While the two groups of peak and trough best-fit slopes for the in-stream loggers (along with the stream flow at the downstream weir) are generally parallel, the trough timing best-fit slopes are consistently lower than the those of the peaks, occurring later in the day at a relatively slower rate but also indicating less time lag between maximum vapor pressure deficit and the occurrence of a water level trough. A graphical summary of this relative difference in the slopes of the best-fit lines is given in **Figure 5-17**. There do not appear to be any patterns in these best-fit slopes values relative to the zone in which they occur.

The physical reason for the increase in time of day at which peak and trough water levels occur, as well as the reason for different best-fit slopes between the peak and trough timings, are not completely understood. One explanation for the increasing lag between peak

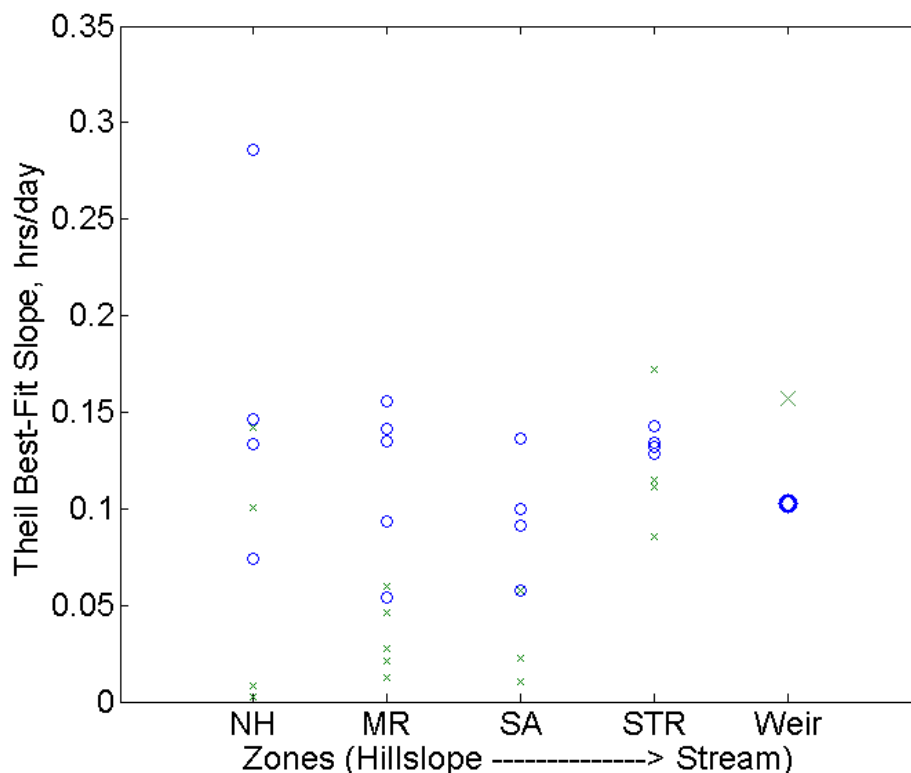


Figure 5-17. Theil regression slopes for the timing of peaks (blue circles) and troughs (green x's) in riparian, in-stream, and down-stream flow at the weir.

vapor pressure deficit and the minimum daily water level could be that the seasonal drawdown in riparian water levels brings the water table slightly lower and lower in or just below the root zone of riparian vegetation, increasing the time necessary for water to be drawn from the soil column. Reasons that the peak water levels also occur later and later in the season may be twofold. First, the peak water level reflects the rebound of the water table following the daily perturbation and water loss to ET, so any increase in time lag occurring with the daily drawdown will likely be translated into a later rebound. Second, as the catchment dries out, hillslope water tables may fall lower and lower, reducing the hydraulic gradients towards the riparian zone that cause water to flow back into the soil spaces that are voided on a daily basis

by ET from riparian vegetation. That the rates at which peaks and troughs occur later in the day are substantially different for the riparian wells may simply reflect a difference in the rate of change in one of the mechanisms described above, such as the water table falling in the riparian zone or in the hillslopes. This explanation would generally hold for the mechanisms suggested above, since the hillslope water table (likely being at a steeper angle) is likely to fall at a greater rate than that in the riparian zone, causing the lag time for peak water level to increase at a faster rate, as water travels more slowly to refill the emptied soil spaces. Evidence of the relatively minor fall in the riparian water table (10-15 cm) can be seen in **Figure 5-8** and **Figure 5-10**, but lack of water table data from the hillslopes prevents further validation of this possible explanation.

5.2 Discussion of WS01 Conceptual Models

Much work has already been done to try to address the question of exactly how diurnal fluctuations in both stream stage, flow, and groundwater level are generated in WS01, and how the patterns in space and time can be interpreted to inform a more complete conceptual model of the interaction of hydrology and ecology in this small headwater catchment as a whole. Comparison of the results presented here with these previous conceptual models is useful for further challenging and refining them.

Bond et al. [2002] made a first effort to explain the WS01 diurnal fluctuations in streamflow during the summer, linking ecology to hydrology by comparing sapflow-based estimates of transpiration in riparian tree species to the amount of stream flow “lost” on a daily basis to ET. They propose a conceptual model of the vegetation-hydrology coupling in the valley bottom of WS01, describing the what they envision as the likely interplay of hydrologic

flowpaths, transpiring plant roots, and seasonal water table dynamics. We can address some of the proposed elements of their conceptual model with the data collected and discussed in this study, assessing their credibility based on our interpretation of the data and field observations.

In their conceptual model, Bond et al. [2002] propose that the water table will eventually drop enough so that more and more flow paths into and out of the stream bypass the roots and are not subject to ET loss, effectively de-coupling the vegetation from stream flow. This model accounts for the eventually disappearing stream flow fluctuations observed at the weir at the very end of the flow recession season. However, the persistence of and general increase in the size of riparian water table fluctuations observed during this field season (see **Figures 5-1** through **5-4**) indicate that the water table at no point loses the hydraulic connection to the vegetation responsible for ET loss. It is possible that other mechanisms are at work to cause the absence of diurnal fluctuations in the stream flow at the outlet, such as the down-catchment transport of ET signals out of phase with each other as proposed by Wondzell et al. [2007], which could result in destructive interference that eliminates the signal. This is an important consideration, since Bond et al. [2002] do not seem to take into account the ET that would be generated in upstream riparian areas along the entire length of the stream network.

Bond et al. [2002] also make predictions about near-stream hyporheic flowpaths, anticipating that a fall in water table will cause less hyporheic exchange along short-scale flow paths. Wondzell et al. [2009] address this point with evidence from tracer studies suggesting that there is not an appreciable change in relative dominance of short- versus long-scale hyporheic flow paths as flow recedes. The results of our tracer injections in WS01 reveal that

more stream-groundwater exchange seems to occur as flow recedes and the catchment dries (see **Figure 4-6**), thus supporting this notion.

The network-scale transport model developed by Wondzell et al. [2007] (mentioned above) would ideally be an improvement for its ability to incorporate multiple basin-wide factors that contribute to diurnal stream flow fluctuations at the outlet. A couple of observations from this study can be brought in to explore the validity of this model. First, since the magnitude of the diurnal stream flow fluctuation at the weir of WS01 steadily decreases as the season progresses, even as the magnitude of diurnal riparian water table fluctuations generally tend to increase (see **Figure 5-10**), it is possible that the declining stream flow fluctuation magnitude is caused by some destructive interference process as signals are transported down the stream network under low-flow, low-velocity conditions [Wondzell et al., 2007]. However, the timing of peak and trough water stages in the stream almost exactly mirrors that of the stream flow at the weir downstream (see **Figure 5-16**), whereas one might expect to find a time lag between the in-stream loggers' timing and the flow fluctuation timing occurring about 75 m downstream. One obvious time lag is in the timing of minimum water level in the riparian zone wells versus that of both the in-stream loggers and the downstream weir, which towards the end of the season occur about 4-6 hours later, on average. Lag between dynamics in the riparian zone and those that are felt in the stream could affect the arrival of an ET signal at the downstream weir, but it would be necessary for them to occur sufficiently far up the stream network, so the travel time in the stream itself was great enough to spread the signals apart and produce destructive interference. Whatever the case may be, the approximately 75 m of stream reach separating our WS01 study area and the weir do not

seem sufficient to produce destructive interference even at the lowest flows observed during this field season, given the inconsequential lag time between the in-stream loggers reaching a peak or trough and the stream flow showing the same response shortly thereafter. However, a clear conclusion cannot be reached, since the entire WS01 stream network is about 1.4-km long and estimated travel times range from 7 to 24 hours by the end of summer [Wondzell et al., 2007]. Yet the synchrony of water level peak and trough timing along the stream network are similar to the findings in the Santa Ana River by Troxell [1936], who concluded (unfortunately without a well-developed body of supporting reasoning) that diurnal stream flow fluctuations are *not* transmitted down the river channel, and that instead the river could be thought of as a long, narrow, pulsating body of water that moved in unison in response to the ET-induced fluctuations.

Wondzell et al. [2009] sought to further refine their thinking about this subject by testing the possibility of making predictions about characteristics of riparian diurnal fluctuations. They found that fluctuation behavior proved much more complex than is implied by a conceptual that considers ET losses from vegetation as the sole cause of all fluctuations. Instead, they conjectured that it is necessary to also consider 1) the transmission of ET-induced signals via groundwater flow paths from up-gradient locations in the aquifer, and 2) the possible interaction of the stream and the adjacent aquifer. While consideration of the former would require a more complex analysis, there is evidence from the water level dynamics observed in this study to indicate that the stream might have a buffering influence on nearby wells. In particular, the discussion in section 5.1.2.1 above addresses this question, drawing on observations from **Figures 5-1** through **5-5** to show that there is a correlation between

increasing distance from the stream and the likelihood of a well to exhibit a much more varied, and larger daily water table response. **Figure 5-7** supports this view, showing that the response in wells to the June 2 storm became progressively less uniform and buffered with distance away from the stream. As discussed by Wondzell et al. [2009], the diversity of responses in both anomaly magnitude and timing seems to suggest that groundwater flow paths need to be considered in a more practical way, perhaps as part of a 3-d transient groundwater model informed by a detailed set of parameters from the field.

5.3 Summary of Findings

In view of the work done on the subject, and in light of some of the most recent observations from the 2010 field season, the question remains of what causes diurnal fluctuations to manifest themselves in the way they do in WS01 and catchments in general, and how a proper conceptual model ought to be constructed to establish a proper framework in which to seek answers to these questions. The preceding discussion and synthesis of field data from the latest season indicates that some ideas proposed in the past are not supported by field observation, and that others are brought into question, pending further study. Putting aside the conceptual frameworks, some of the noteworthy results from this portion of the work, which aid in understanding and characterizing WS01 and other similar headwater systems, can be summarized as follows.

Evidence from riparian and in-stream water level anomalies and the changes they show over a season support the view that the stream plays some kind of buffering role in regulating water level responses of wells in the adjacent riparian aquifer. The general tendency found was for spatial organization, in which water level anomaly magnitudes vary more widely and tend to

be greater with increasing distance from the stream. Temporally, there is a pattern in which the wells further from the stream are more likely to increase anomaly magnitude, whereas in-stream and near-stream locations showed very little change over the recorded field season.

Simple evaluations of the diversity of water table response found a measure of consistency, whereby wells exhibiting larger water table responses on a daily basis also tended to show a larger response to the June 2 storm and to the season-long drying of the catchment and riparian zone. Attempts to link well proximity to ET-causing trees to anomaly magnitude proved unfruitful.

Evaluation of the available data from WS03 supports the idea that no (or very slight, below the limit of detection) diurnal fluctuations occur there, likely due to the lack of mature, transpiring vegetation in the valley bottom riparian zone. The hillslope trees are most likely too far above the groundwater to exert an ET demand on the saturated zone, and so no such diurnal fluctuations are generated.

The diurnal timing of the peak and trough water level in all WS01 loggers advanced forward in the day as the season progressed, by as much as 6 hours. While in-stream loggers (and the stream flow measured at the downstream weir) showed tightly grouped, nearly parallel slopes for the timings of peaks and troughs, all riparian wells showed a more diverse response in which the slope of increase in peak water level timing almost always exceeded that of the troughs. This could be due to the different rates at which physical mechanisms occur to remove water from the soil column via ET and replenish it from elsewhere at a later time.

Chapter 6

Conclusions

The primary objectives of this work were to investigate 1) how the relative dominance of down-valley and cross-valley hydraulic gradients in headwater riparian zones changes over various time scales, and how that might impact stream-groundwater interaction, and 2) how patterns of water table dynamics, particularly on a daily scale but also in response to rainfall and catchment drying, are organized in space, how these patterns change through time, whether correlation exists among different dynamics, and whether these findings corroborate elements of conceptual models developed at our study site. Our analysis of the data supports the following conclusions:

With respect to patterns in hydraulic gradients and potential for stream-groundwater exchange:

- [*Objective 1a*] Although less pronounced in WS03, both WS01 and WS03 exhibited down-valley dominance in riparian hydraulics over the entire field season. In WS01, near-stream gradients gradually turned away from the stream, while most other gradients gradually turned towards the stream. In WS03, there was a general tendency for gradients turn towards the down-valley axis, pointing more dominantly downstream as the season progressed. Relative to other studies in headwater systems, the seasonal responses observed in both watersheds are relatively stable, but dominated by an overall down-valley gradient.

- [Objective 1b] Both watersheds exhibited increased intrusion of salt-labeled stream water into the riparian zones in response to the constant-rate tracer injections as the season progressed and flows receded. In WS01, there was a relatively steady increase over the season in the penetration of salt-labeled stream water into the riparian aquifer (the least-affected well had 40% stream water by the last injection), as would in general be predicted by the near-stream hydraulic gradients' seasonal tendency to turn away from the stream. In WS03, seasonal increases in stream water intrusion were slight and restricted to a few isolated locations, since nearly the entire valley bottom aquifer was penetrated by about 80% stream water for all injections. No clear links could be made between changes in hydraulic gradients and observed changes in stream water intrusion. These changes are in agreement with other studies that find increasing hyporheic area with decreasing flows.
- [Objective 1a] In response to a 1.25-year storm event, WS01 riparian gradients exhibited similar behavior to that observed across the entire season, pointing to the potential for storms to drive increased stream-groundwater exchange. With a minor exception, all gradients in WS01 were down-valley dominant, even at the peak of the storm, implying that subsurface travel times of stream water could remain long, even during a storm. WS03 riparian gradients showed a more diverse set of responses, few of which reflected conventional ideas about cross-valley-dominated flow during storms. For example, one area exhibited a sharp decline in total gradient magnitude, while another area showed a strong potential for convergence of flow on one riparian location.

- [*Objective 1a*] Daily water table fluctuations produced diurnally varying cross- to down-valley gradient ratios in WS01, while no response was observed in WS03. The response observed in WS01 may play a role in enhancing stream-groundwater exchange on a daily basis, but further study is required.

Overall, the complex and time-varying hydraulic gradient responses observed in both watersheds underline the need to consider the critical role played by hydrology in biogeochemical processes, and such studies should be conducted so that they take the hydrological context into account by undertaking basic monitoring of water table levels through time.

With respect to patterns in water table dynamics:

- [*Objective 2a,d*] Examination of patterns in water level anomalies (deviation in water level about the mean) support the view that water table responses exhibit increasing disconnection with distance from the stream, which seems to have a buffering effect on the anomalies in the near-stream area. This is akin to the results of Seibert et al. [2003], albeit on a much shorter cross-valley scale. Spatially, anomaly magnitude tends to increase with distance from the stream, or otherwise display a wider variety of magnitudes. Temporally, there is a tendency for anomalies further from the stream to increase in magnitude as the season progresses and the catchment dries, but this tendency diminishes with proximity to the stream, and the in-stream loggers recorded only very slight changes in anomaly magnitude as the season advanced.

- [Objective 2e] Water level dynamics exhibit a measure of internal consistency, in that locations exhibiting large daily anomalies also tend to show a greater response to other hydrologic stimuli, such as the June 2 storm and the seasonal fall in water level.
- [Objective 2c] An attempt to explain some of the spatial diversity in water level anomaly magnitude by calculating the influence of riparian trees proved led to a rejection of this simple hypothesis, as there was no correlation evident between anomaly magnitude and the proximity of a well to riparian trees.
- WS03 exhibited no diurnal fluctuations in stream flow at the outlet gauge, and only very slight (possibly artificial) fluctuations in the riparian study area and stream. We conclude that this is most likely due to steep hillslopes that prevent a connection between hillslope trees and groundwater, and the lack of mature riparian vegetation to cause groundwater ET loss, a consequence of a 1996 flood which scoured much of the upstream channel network and removed nearly all living vegetation.
- [Objective 2b] In all cases, the daily timing of the peak and trough water levels in the WS01 riparian wells and in-stream logger locations grew later in the day as the season progressed. However, the timing of trough water levels in the riparian in-stream logger locations vs wells in WS01 grew later in the day at a much faster rate, possibly indicative of a distortion in timing caused by ET signals arriving from upstream [Wondzell et al., 2007].
- Consideration of the above observations in WS01 found points of disagreement with features of conceptual models proposed by Bond et al. [2002] and Wondzell et al. [2007], but support of several of the ideas proposed by Wondzell et al. [2009].

References

- Alexander, R.B., E.W. Boyer, R.A. Smith, G.E. Schwarz, and R.B. Moore (2007), The role of headwater streams in downstream water quality, *J. Am. Water Res. Assoc.*, *43*(1), 41-59, DOI: 10.1111/j.1752-1688.2007.00005.x.
- Altman, S.J., and Parizek, R.R. (1995), Dilution of Nonpoint-Source Nitrate in Groundwater, *Journal of Environmental Quality*, *24*, 707-718.
- Baird, K.J., J.C. Stromberg, and T. Maddock III (2005), Linking Riparian Dynamics and Groundwater: An Ecohydrologic Approach to Modeling Groundwater and Riparian Vegetation, *Environmental Management*, *36* (4), 551-564, doi: 10.1007/s00267-004-0181-z.
- Barnard, H.R., C.B. Graham, W.J. Van Verseveld, J.R. Brooks, B.J. Bond, J.J. McDonnell (2010), Mechanistic assessment of hillslope transpiration controls of diel subsurface flow: a steady-state irrigation approach, *Ecohydrology*, *3*, 133-142, doi:10.1002/Eco.114.
- Bond, B. J., J. A. Jones, G. Moore, N. Phillips, D. Post, and J. J. McDonnell (2002), The zone of vegetation influence on baseflow revealed by diel patterns of streamflow and vegetation water use in a headwater basin, *Hydrol. Processes*, *16*, 1671–1677.
- Bren, L.J. (1997), Effects of slope vegetation removal on the diurnal variations of a small mountain stream, *Water Resources Research*, *33*, 321-331.
- Burt, T.P. (1979), Diurnal variations in stream discharge and throughflow during a period of low flow, *J. Hydrol.*, *41*, 291--301.
- Burt, T.P., L.S. Matchett, K.W.T. Goulding, C.P. Webster, and N.E. Haycock (1999), Denitrification in riparian buffer zones: the role of floodplain hydrology, *Hydrological Processes*, *13*, 1451-1463.
- Butler Jr., J.J., G.J. Kluitenberg, D.O. Whittemore, S.P. Loheide II, W. Jin, M.A. Billinger, X. Zhan (2007), A field investigation of preatophyte-induced fluctuations in the water table, *Water Resources Research*, *43*, doi:10.1029/2005WR004627.
- Cuevas, J.G., M. Calvo, C. Little, M. Pino, and P. Dassori (2010), ARE DIURNAL FLUCTUATIONS IN STREAMFLOW REAL?, *J. Hydrol. Hydromech.*, *58*, 149-162, doi: 10.2478/v10098-010-0014-0.
- Curt, T., E. Lucot, and M. Bouchaud (2001), Douglas-fir root biomass and rooting profile in relation to soils in a mid-elevation area (Beaujolais Mounts, France), *Plant and Soil*, *233*, 109-125.

Dahm, C.N., N.B. Grimm, P. Marmonier, H.M. Valett, and P. Vervier (1998), Nutrient dynamics at the interface between surface waters and groundwaters, *Freshwater Biology*, 40, 427-451.

Delaunay, B. (1934), Sur la sphère vide, *Bulletin of the Academy of Science of USSR VII: Class. Sci. Mat. Nat.*, 793-800.

Dieterich, M., and N.H. Anderson (1998), Dynamics of abiotic parameters, solute removal and sediment retention in summer-dry headwater streams of western Oregon, *Hydrobiologia*, 379, 1-15.

Dunford, A.R., and P.W. Fletcher (1947), Effect of removal of streambank vegetation upon water yield, *Transactions, American Geophysical Union*, 28, 105–110.

Dyrness, C. T. (1969), Hydrologic properties of soils on three small watersheds in the western Cascades of Oregon, *Res. Note PNW-111*, Pac. Northwest For. and Range Exp. Stn., For. Serv., U.S. Dep. of Agric., Portland, Oreg.

Fraser, B.G., and D.D. Williams (1998), Seasonal Boundary Dynamics of a Groundwater/Surface-Water Ecotone, *Ecology*, 79 (6), 2019-2031.

Federer, C.A. (1973), Forest Transpiration Greatly Speeds Streamflow Recession, *Water Resources Research*, 9 (6), 1599-1604.

Gooseff, M.N., S.M. Wondzell, and B.L. McGlynn (2008), On the relationship among temporal patterns of evapotranspiration, streamflow, and riparian water levels in headwater catchments during baseflow, paper presented at 36th IAH Congress, Toyama, Japan.

Gribovski, Z., J. Szilágyi, and P. Kalicz (2010), Diurnal fluctuations in shallow groundwater levels and streamflow rates and their interpretation – A review, *Journal of Hydrology*, 385, 371-383.

Gribovski, Z., P. Kalicz, J. Szilágyi, M. Kucsara (2008), Riparian zone evapotranspiration estimation from diurnal groundwater level fluctuations. *Journal of Hydrology* 349 (1–2), 6–17.

Harbaugh, A.W. and R.T. Getzen (1977), Stream simulation in an analog model of the groundwater system on Long Island, New York, *U.S. Geol. Surv. Water. Resour. Invest.* 77-58, 15 pp.

Harvey, J.W. and K.E. Bencala (1993), The Effect of Streambed Topography on Surface-Subsurface Water Exchange in Mountain Catchments, *Water Resources Research*, 29 (1), 89-98.

Haycock, N.E., G. Pinay, and C. Walker (1993), Nitrogen retention in river corridors: European perspectives, *Ambio*, 22, 340-346.

- Heilman, P.E. (1990), Growth of Douglas Fir and Red Alder on Coal Spoils in Western Washington, *Soil Science Society of America Journal*, 54, 522-527.
- Hill, A.R. (1996), Nitrate Removal in Stream Riparian Zones, *J. Environ. Qual.*, 25, 743-755.
- Horton, R.E (1945), Erosional Development of Streams and Their Drainage Basins: Hydrophysical Approach to Quantitative Morphology, *Bulletin of the Geological Society of America*, 56, 275-370.
- Jacobs, T.C., and J.W. Gilliam, Headwater Stream Losses of Nitrogen from Two Coastal Plain Watersheds, *J. Environ. Qual.*, 14(4), 467-472.
- Jones, J.B., and L.A. Smock (1991), Transport and Retention of Particulate Organic Matter in Two Low-Gradient Headwater Streams, *J. N. Am. Benthol. Soc.*, 10(2), 115-126.
- Jones, J.B., and R.M. Holmes (1996), Surface-subsurface interactions in stream ecosystems, *TREE*, 11 (6), 239-242.
- Kasahara, T., and S. M. Wondzell (2003), Geomorphic controls on hyporheic exchange flow in mountain streams, *Water Resour. Res.*, 39 (1), 1005, doi:10.1029/2002WR001386.
- Larkin, R.G. and J.M. Sharp, Jr. (1992), On the relationship between river-basin geomorphology, aquifer hydraulics, and ground-water flow direction in alluvial aquifers, *GSA Bulletin*, 104, 1608-1620.
- Lautz, L.K. (2008), Estimating groundwater evapotranspiration rates using diurnal water-table fluctuations in semi-arid riparian zone, *Hydrogeology Journal*, 16, 483-497.
- Lawrence, R. E. (1990), The interaction between the environment, land use, and hydrology of the Bogong High Plains area from 1850 to 1985, Ph.D. thesis, 798 pp., Univ. of Melbourne, Parkville, Australia.
- Lee, D.T., and B.J. Schachter (1980), Two Algorithms for Constructing a Delaunay Triangulation, *International Journal of Computer and Information Sciences*, 9 (3), 219-242.
- Leopold L.B., M.G. Wolman, and J.P. Miller (1964), *Fluvial Processes in Geomorphology*, W. H. Freeman, San Francisco, Calif.
- Loheide, S.P. II (2008), A method for estimating subdaily evapotranspiration of shallow groundwater using diurnal water table fluctuations, *Ecohydrology*, 1, 59-66, doi:10.1002/eco.7.

Loheide, S.P. II, J. J. Butler, Jr., and S. M. Gorelick (2005), Use of diurnal water table fluctuations to estimate groundwater consumption by phreatophytes: A saturated-unsaturated flow assessment, *Water Resour. Res.*, *41*, W07030, doi: 10.1029/2005WR003942.

Lowe, W.H., and G.E. Likens (2005), Moving Headwater Streams to the Head of the Class, *Bioscience*, *55*(3), 196-197.

Lutz, J.A., and C.B. Halpern (2006), Tree Mortality during Early Forest Development: A Long-Term Study of Rates, Causes, and Consequences, *Ecological Monographs*, *76* (2), 257-275.

McClain, M.E., E.W. Boyer, C.L. Dent, S.E. Gergel, N.B. Grimm, P.M. Groffman, S.C. Hart, J.W. Harvey, C.A. Johnston, E. Mayorga, W.H. McDowell, and G. Pinay, 2003. Biogeochemical Hot Spots and Hot Moments at the Interface of Terrestrial and Aquatic Ecosystems, *Ecosystems*, *6*, 301-312.

McDowell, W.H. (1985), Kinetics and Mechanisms of Dissolved Organic Carbon Retention in a Headwater Stream, *Biogeochemistry*, *1*(4), 329-352.

Meyboom, P. (1965), Three observations on streamflow depletion by phreatophytes, *Journal of Hydrology*, *2* (3), 248–261.

Meyboom, P. (1967), Groundwater studies in the Assiniboine River drainage basin—Part II: Hydrologic characteristics of phreatophytic vegetation in south-central Saskatchewan, *Geol. Surv. Can. Bull.*, 139.

Meyer, J.L., L.A. Kaplan, D.N. Newbold, D.L. Strayer, C.J. Woltemade, J.B. Zedler, R. Beilfuss, Q. Carpenter, R. Semlitsch, M.C. Watzin, and P.H. Zedler (2007), Where Rivers are Born: The Scientific Imperative for Defending Small Streams and Wetlands, *Sierra Club, American Rivers, Turner Foundation*, Washington D.C.

Millard, C.J., P.F. Kazyak, and D.M. Boward (1999). Lower Susquehanna Basin: Environmental Assessment of Stream Conditions, in *Chesapeake Bay and Watershed Programs: Monitoring and Non-Tidal Assessment (CBWP-MANTA), Report EA-99-10*, Maryland Department of Natural Resources, Annapolis, Maryland.

Moore, G.W., B.J. Bond, J.A. Jones, N. Phillips, and F.C. Meinzer, (2004), Structural and compositional controls on transpiration between 40- and 450-yr-old forests in Western Oregon, USA, *Tree Physiology*, *24*, 481–491.

Morrice, J.A., H.M. Valett, C.N. Dahm, and M.E. Campana (1997), Alluvial characteristics, groundwater-surface water exchange and hydrological retention in headwater streams, *Hydrological Processes*, *11*, 253-267.

Murray, R.E., Y.S. Feig, and J.M. Tiedje (1995), Spatial heterogeneity in the distribution of denitrifying bacteria associated with denitrification activity zones, *Applied Environmental Microbiology*, 61, 2791-2793.

Ogata, G., L.A. Richards, and W.R. Gardner (1960), Transpiration of alfalfa determined from soil water content changes, *Soil Science*, 89 (4), 179-182.

O'Loughlin, E. M., N. P. Cheney, and J. Burns (1982), The Bushrangers Experiment: Hydrological response of a eucalypt catchment to fire, in *The First National Symposium on Forest Hydrology, 1982, Natl. Conf. Publ. 82/6*, edited by E. M. O'Loughlin and L. J. Bren, pp. 132-139, Inst. of Eng. of Aust., Canberra, Australia.

Parkin, T.B. (1987), Soil microsites as a source of denitrification variability, *Soil Science Society of America Journal*, 51, 1194-1199.

Peterson, B.J., W.M. Wollheim, P.J. Mulholland, J.R. Webster, J.L. Meyer, J.L. Tank, E. Marti, W.B. Bowden, H.M. Valett, A.E. Hershey, W.H. McDowell, W.K. Dodds, S.K. Hamilton, S. Gregory, D.D. Morrall (2001), Control of Nitrogen Export from Watersheds by Headwater Streams, *Science*, 292(5514), 86-90.

Prince, K.R. (1980), Preliminary investigation of a shallow groundwater flow system associated with Connetquot Brook, Long Island, New York, *U.S. Geol. Surv. Water-Resour. Invest. 80-47*, p. 37

Reigner, I.C. (1966), A method for estimating streamflow loss by evapotranspiration from the riparian zone, *Forest Science* 12, (2), 130-139.

Robinson, T.W. (1958), PHREATOPHYTES, *United States Geological Survey Water-Supply Paper 1423*, 84 pp., Washington.

Rothacher, J., C. T. Dyrness, and R. L. Fredriksen (1967), Hydrologic and related characteristics of three small watersheds in the Oregon Cascades, report, Pac. Northwest For. and Range Exp. Stn., For. Serv., U.S. Dept. of Agric., Portland, Oregon.

Running, S.W., R.H. Waring, and R.A. Rydell (1975), Physiological control of water flux in conifers: a computer simulation model, *Oecologia*, 18, 1-18.

Santantonio, D. (1979), Seasonal dynamics of fine roots in mature stands of Douglas-fir of different water regimes - a preliminary report, paper presented at Symposium on root physiology and symbiosis, Comptes Rendus Reunions du Groupe d'Etude des Racines, Champenoux, France, pp. 190-203.

Santantonio, D., R.K. Herman, and W.S. Overton (1977), Root biomass studies in forest ecosystems, *Pedobiologia*, 17, 1-31.

Seibert, J, K. Bishop, A. Rodhe and J. McDonnell (2003), Groundwater dynamics along a hillslope: A test of the steady-state hypothesis, *Water Resources Research*, 39 (1), 1014, doi:10.1029/2002WR001404.

Shah, N., M. Nachabe, and M. Ross (2007), Extinction Depth and Evapotranspiration from Ground Water under Selected Land Covers, *Ground Water*, 45 (3), 329-338.

Sollins, P., C.C. Grier, F.M. McCorison, K. Cromack Jr., R. Fogel, R.L. Fredriksen (1980), The Internal Element Cycles of an Old-Growth Douglas-Fir Ecosystem in Western Oregon, *Ecological Monographs*, 50 (3), 261-285.

Strahler, A.N (1957), Quantitative Analysis of Watershed Geomorphology, *Transactions of the American Geophysical Union*, 38, 913-920.

Swanson, F.J. and J.A. Jones (2002), Geomorphology and Hydrology of the H.J. Andrews Experimental Forest, Blue River, Oregon, *Field Guide to Geologic Processes in Cascadia: Oregon Department of Geology and Mineral Industries Special Paper 36*, 289-314.

Swanson, F. J., and M. E. James (1975), Geology and geomorphology of the H.J. Andrews Experimental Forest, western Cascades, Oregon, *Res. Pap. PNW-188*, Pac. Northwest For. and Range Exp. Stn., For. Serv., U.S. Dep. of Agric., Portland, Oreg.

Thomas, S.A., H.M. Valett, P.J. Mulholland, C.S. Fellows, J.R. Webster, C.N. Dahm, and C.G. Peterson (2001), Nitrogen Retention in Headwater Streams: The Influence of Groundwater-Surface Water Exchange, *TheScientificWorld*, 1(S2), 623-631, DOI 10.1100/tsw.2001.272.

Triska, F.J., V.C. Kennedy, R. J. Avanzino, G.W. Zellweger, and K.E. Bencala (1989), Retention and Transport of Nutrients in a Third-Order Stream in Northwestern California: Hyporheic Processes, *Ecology*, 70(6), 1893-1905.

Troxell, H.C. (1936), The diurnal fluctuation in the ground-water and flow of the Santa Anna River and its meaning, *Transactions, American Geophysical Union*, 17 (4), 496-504.

Tschinkel, H.M. (1963), Short-term fluctuation in streamflow as related to evaporation and transpiration, *Journal of Geophysical Research* 68 (24), 6459-6469.

Valett, H.C., J.A. Morrice, C.N. Dahm, and M.E. Campana (1996), Parent Lithology, Surface-Groundwater Exchange, and Nitrate Retention in Headwater Streams, *Limnology and Oceanography*, 41(2), 333-345.

Valett, H.C., C.N. Dahm, M.E. Campana, J.A. Morrice, M.A. Baker, C.S. Fellows (1997), Hydrologic Influences on Groundwater-Surface Water Ecotones: Heterogeneity in Nutrient Composition and Retention, *J. N. Am. Benthol. Soc.*, 16 (1), 239-247.

Vidon, P.G.F., and A.R. Hill (2004), Landscape controls on the hydrology of stream riparian zones, *Journal of Hydrology*, 292, 210-228.

Vidon, P.G.F., C. Allan, D. Burns, T.P. Duval, N. Gurwick, S. Inamdar, R. Lowrance, J. Okay, D. Scott, and S. Sebestyn (2010), Hot spots and hot moments in Riparian zones: potential for improved water quality management, *JAWRA*, 1-21, DOI: 10.1111 /j.1752-1688.2010.00420.x.

Waring, R.H., and J.F. Franklin (1979), Evergreen Coniferous Forests of the Pacific Northwest, *Science*, 204, 1380-1386.

Waring, R.H., and S.W. Running (1976), Water Uptake, Storage and Transpiration by Conifers: A Physiological Model, in *Ecological Studies: Analysis and Synthesis*, vol. 19 (E), edited by O.L. Lange et al., 189-202, Springer-Verlag, Heidelberg and Berlin, Germany.

Webster, J.R., A.P. Covitch, J.L. Tank, T.V. Crockett (1994), Retention of Coarse Organic Particles in Streams in the Southern Appalachian Mountains, *J. N. Am. Benthol. Soc.*, 13(2), 140-150.

Weisman, R.N. (1977), The effect of evapotranspiration on streamflow recession, *Hydrological Science – Bulletin*, XXII (3), 371-377.

White, W. N. (1932), A method of estimating ground-water supplies based on discharge by plants and evaporation from soil—Results of investigations in Escalante Valley, Utah, *U. S. Geol. Surv. Water Supply Pap.*, 659-A, 105 pp.

Winter, T.C., J.W. Harvey, O.L. Franke, and W.M. Alley (1998), Groundwater and Surface Water: A Single Resource, *U.S. Geological Survey Circular 1139*, Denver, Colorado.

Woessner, W.W. (2000), Stream and Fluvial Plain Ground Water Interactions: Rescaling Hydrogeologic Thought, *Ground Water*, 38 (3), 423-429.

Wondzell, S. M. (2006), Effect of morphology and discharge on hyporheic exchange flows in two small streams in the Cascade Mountains of Oregon, USA, *Hydrol. Processes*, 20, 267–287.

Wondzell, S.M., M.N. Gooseff, and B.L. McGlynn (2007), Flow velocity and the hydrologic behavior of streams during baseflow, *Geophysical Research Letters*, 34, L24404, doi:10.1029/2007GL031256.

Wondzell, S.M., M.N. Gooseff, and B.L. McGlynn (2009), An analysis of alternative conceptual models relating hyporheic exchange flow to diel fluctuations in discharge during baseflow recession, *Hydrological Processes*, 24, 686-694, doi:10.1002/hyp.7507.

Woods, F.W., and D. O'Neal (1965), Tritiated Water as a Tool for Ecological Field Studies, *Science*, 147 (3654), 148-149.

Wroblicky, G.J., M.E. Campana, H.M. Valett, and C.N. Dahm (1998), Seasonal variation in surface-subsurface water exchange and lateral hyporheic area of two stream-aquifer systems, *Water Resources Research*, 34 (3), 317-328.

Appendix A

Water Level Plots

A-1. WS01 - Uncorrected, Corrected, Smoothed, Mean, and Manual Readings

Notes:

- 1) On all plots, the stepped black line at the bottom represents the timing of the constant-rate tracer injections. When the line is stepped up, that indicates that frequent measurements of electrical conductivity (EC) were underway, and artificial errors in the record are most likely to appear.
- 2) Effort was taken to use the manual depth sounder measurements as the guide during the correction process, but there were instances when it was concluded that the depth sounder reading must have been in error, particularly during the storm, when a false positive may have occurred if the circuit was completed prematurely.
- 3) For the in-stream loggers, the appearance of the raw level record is sometimes misleading. Some of the manual measurements (used to reference the raw levels to a datum) taken for the in-stream loggers were taken using a stick ruler and were much less accurate than the elevations measured using a total station, which was ultimately used to connect the record to the datum.

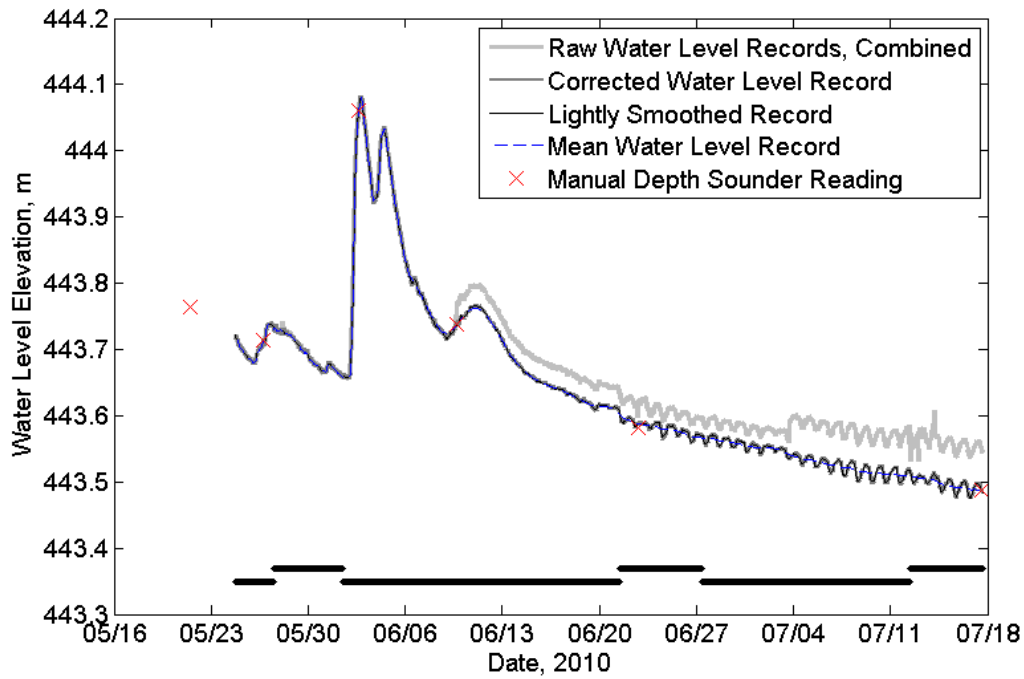


Figure A-1-1. Evolution of the water elevation record in well D2, WS01.

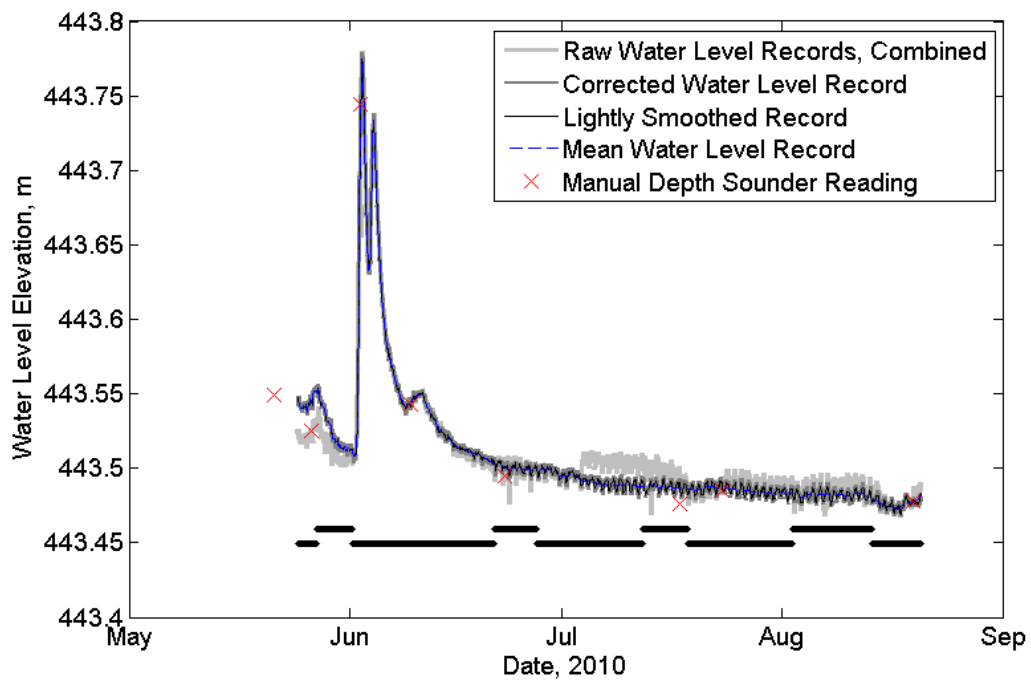


Figure A-1-2. Evolution of the water elevation record in well D3, WS01.

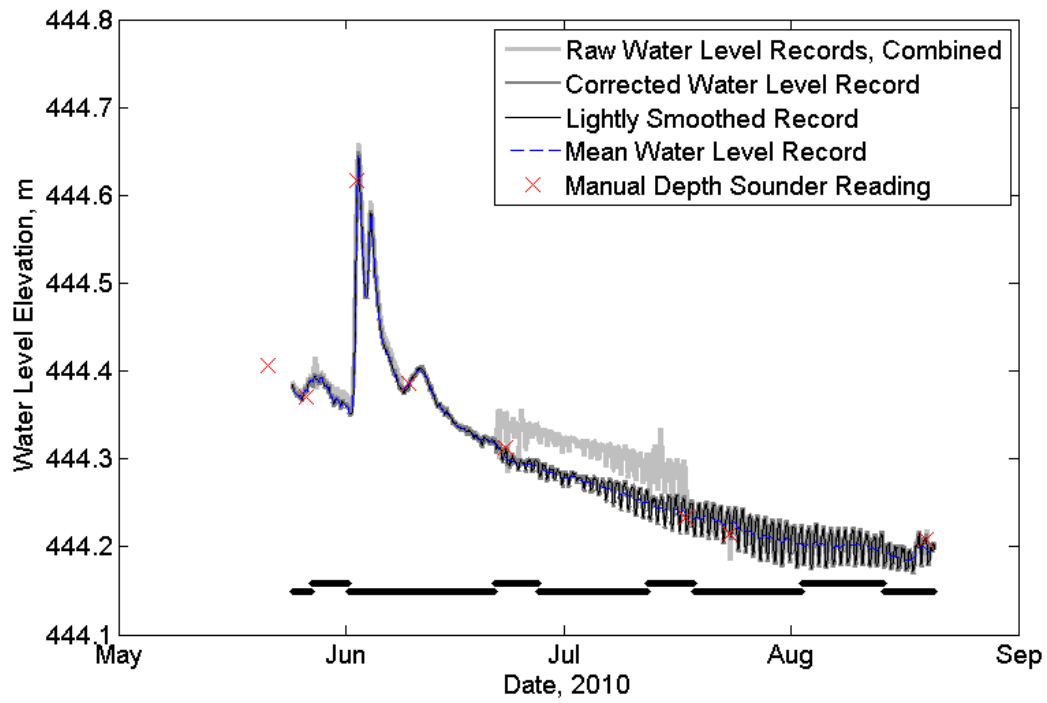


Figure A-1-3. Evolution of the water elevation record in well E1, WS01.

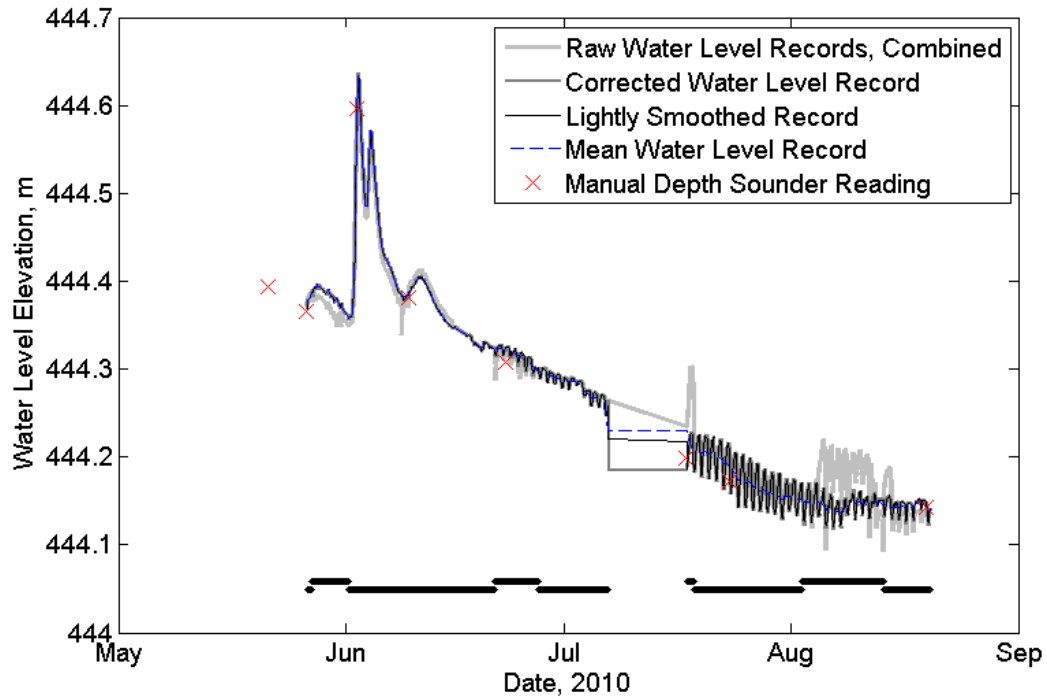


Figure A-1-4. Evolution of the water elevation record in well E2, WS01.

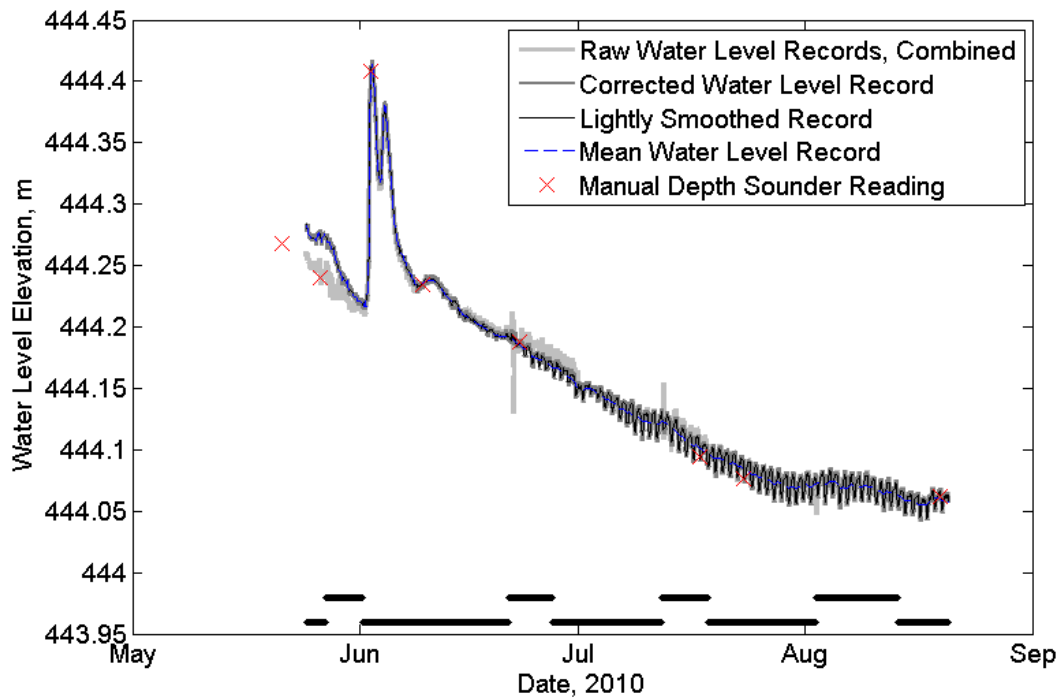


Figure A-1-5. Evolution of the water elevation record in well E3, WS01.

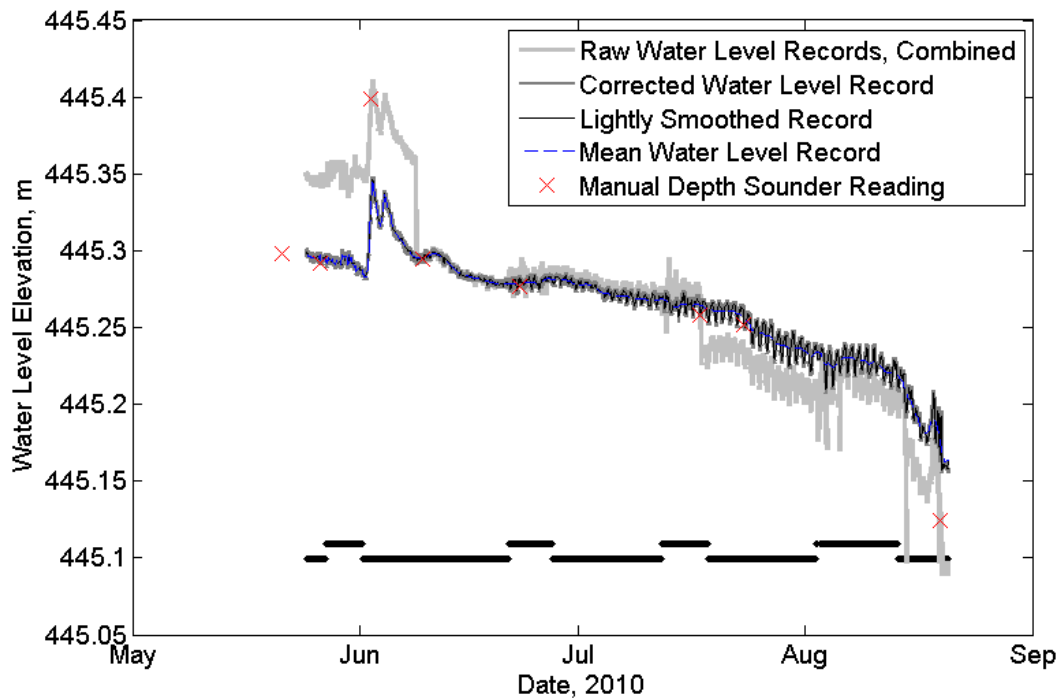


Figure A-1-6. Evolution of the water elevation record in well F1, WS01.

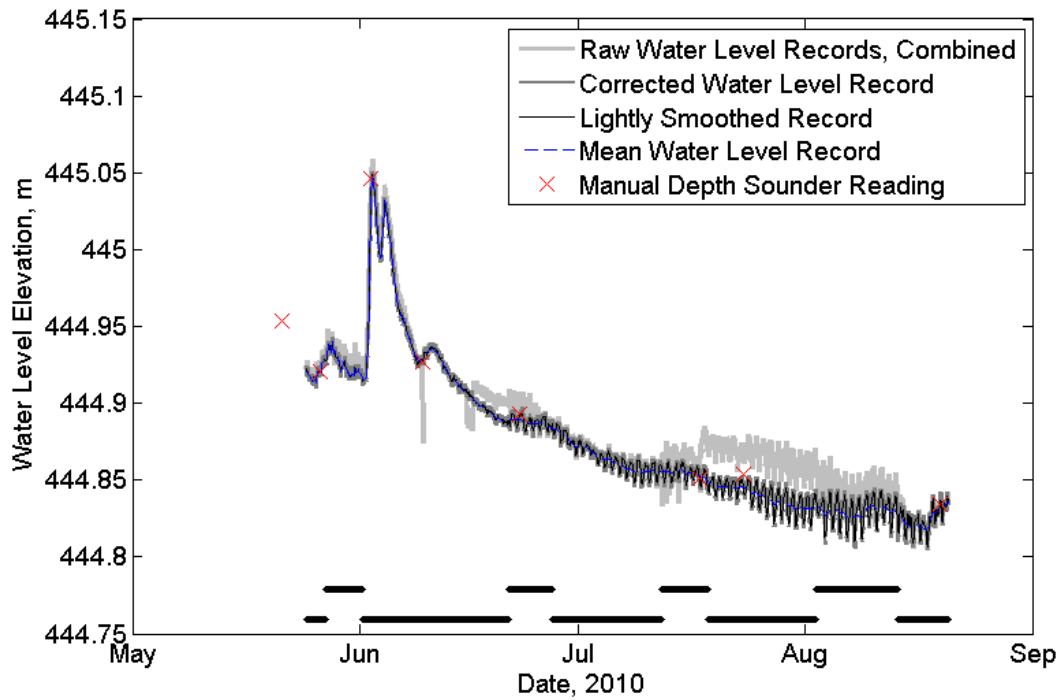


Figure A-1-7. Evolution of the water elevation record in well F2, WS01.

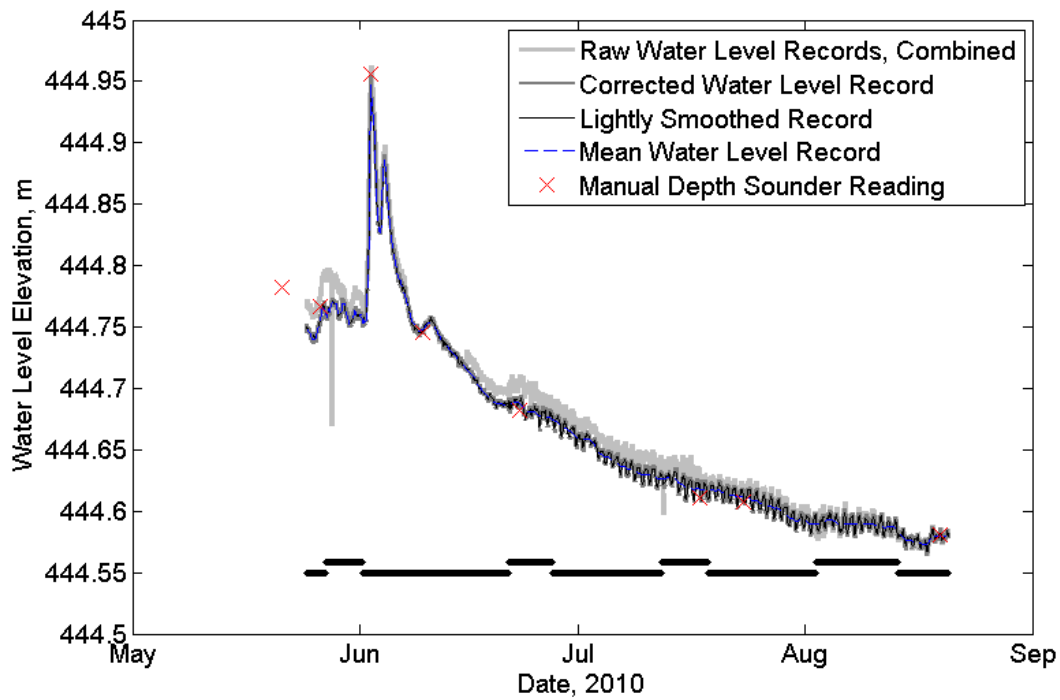


Figure A-1-8. Evolution of the water elevation record in well F3, WS01.

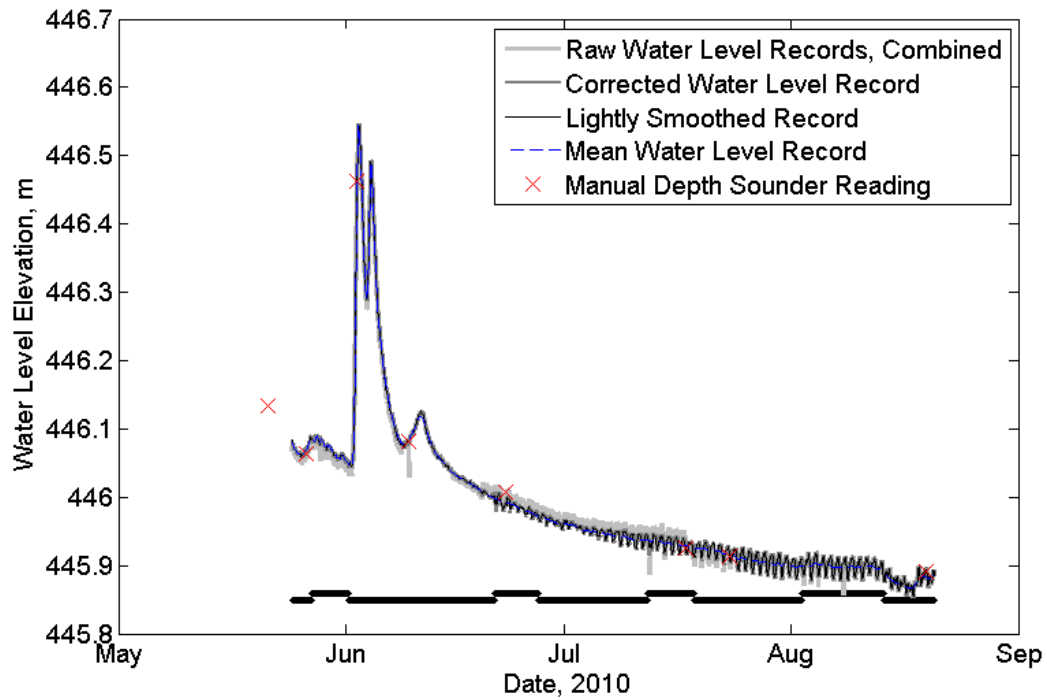


Figure A-1-9. Evolution of the water elevation record in well G1, WS01.

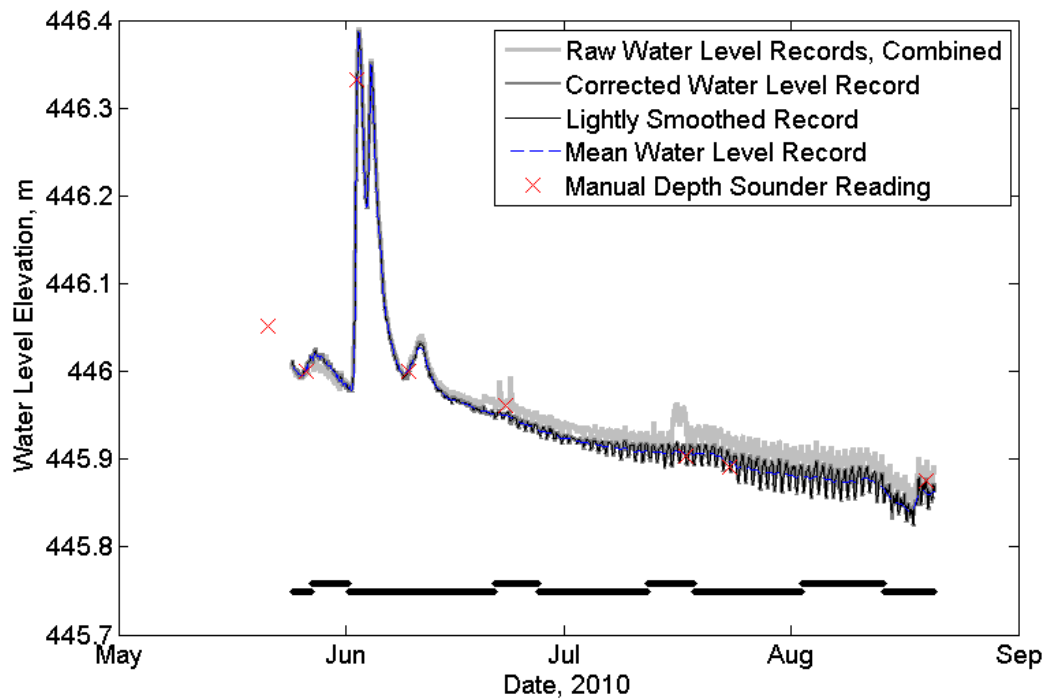


Figure A-1-10. Evolution of the water elevation record in well G2, WS01.

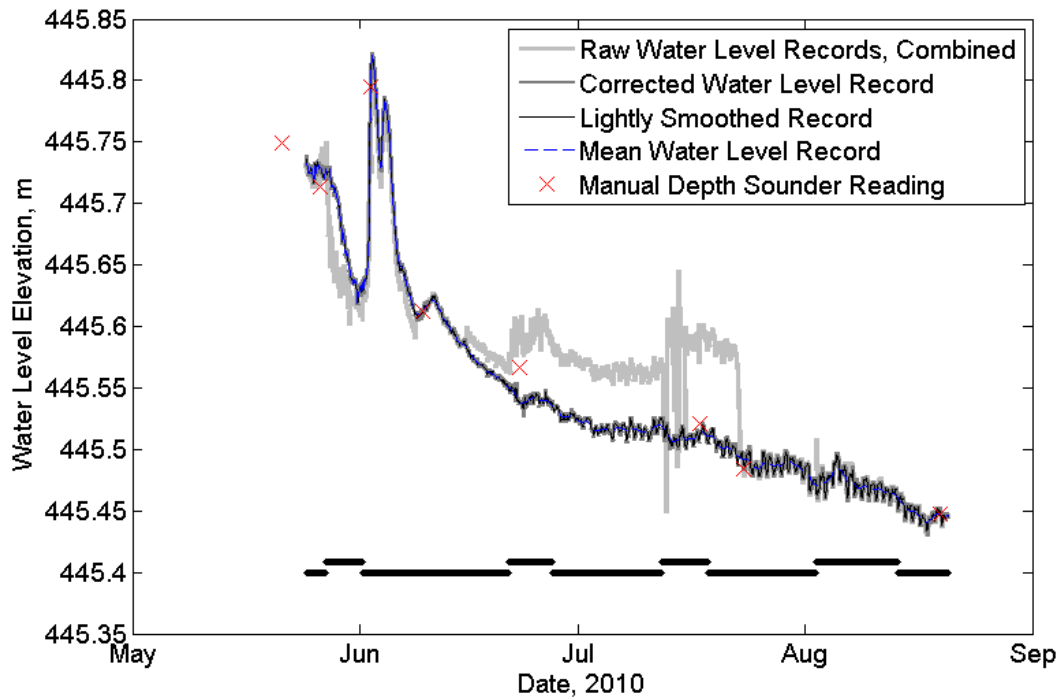


Figure A-1-11. Evolution of the water elevation record in well G3, WS01.

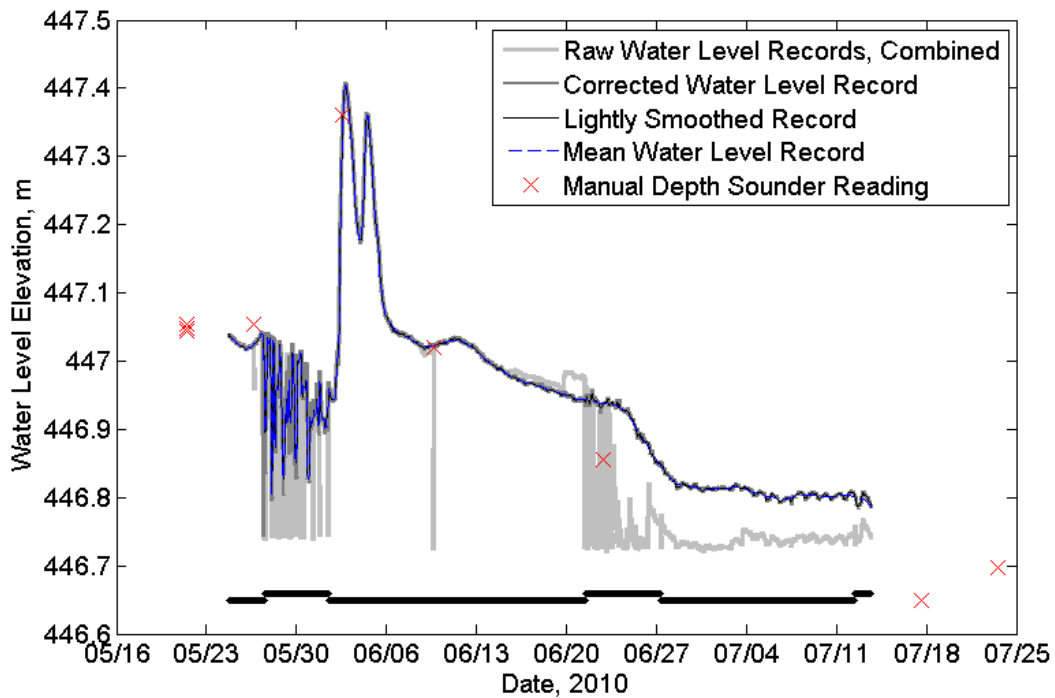


Figure A-1-12. Evolution of the water elevation record in well H1, WS01.

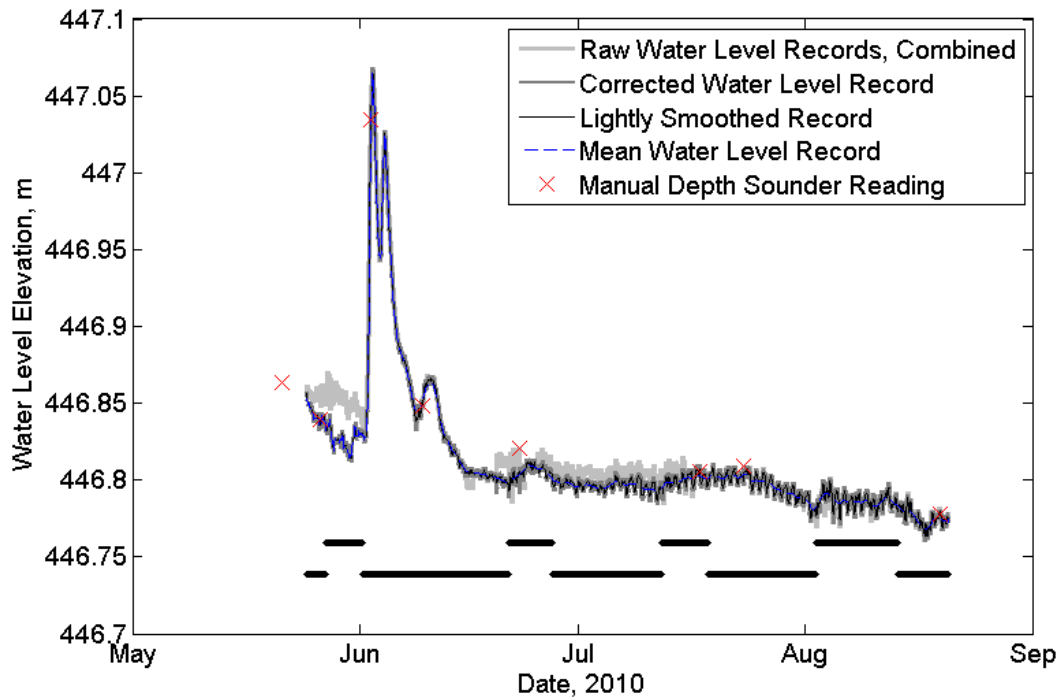


Figure A-1-13. Evolution of the water elevation record in well H2, WS01.

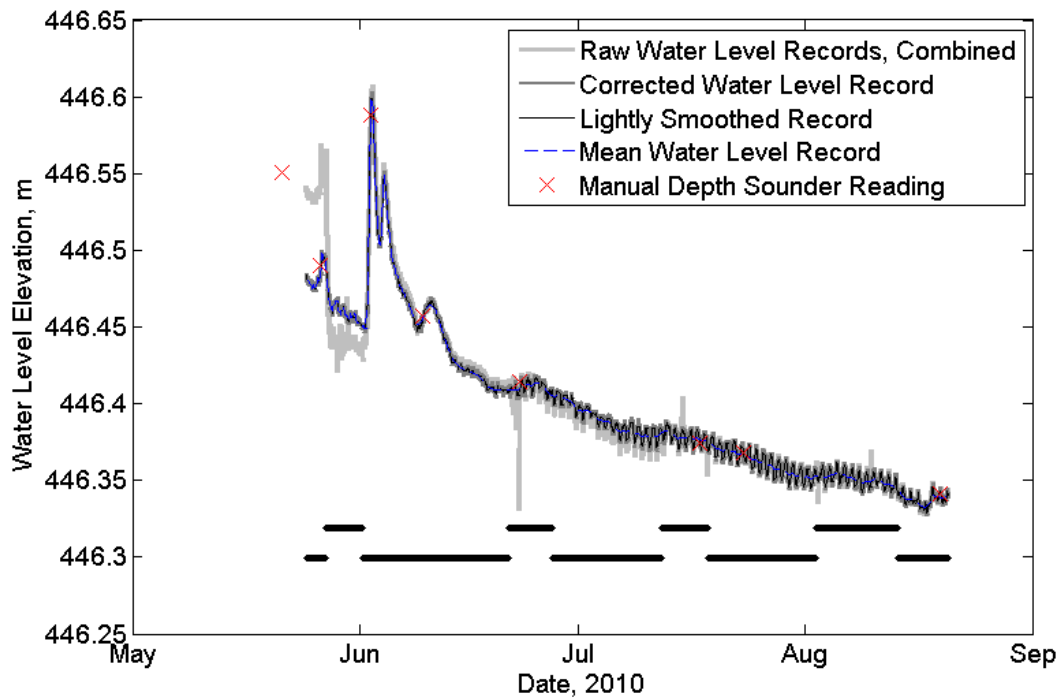


Figure A-1-14. Evolution of the water elevation record in well H3, WS01.

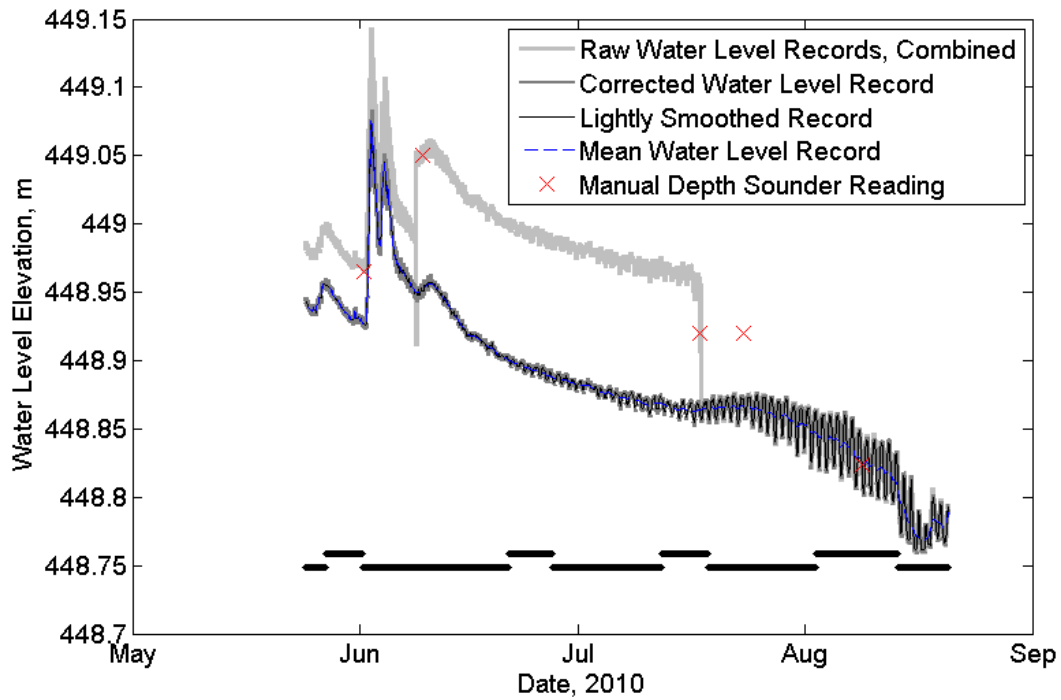


Figure A-1-15. Evolution of the water elevation record of in-stream logger IS0, WS01.

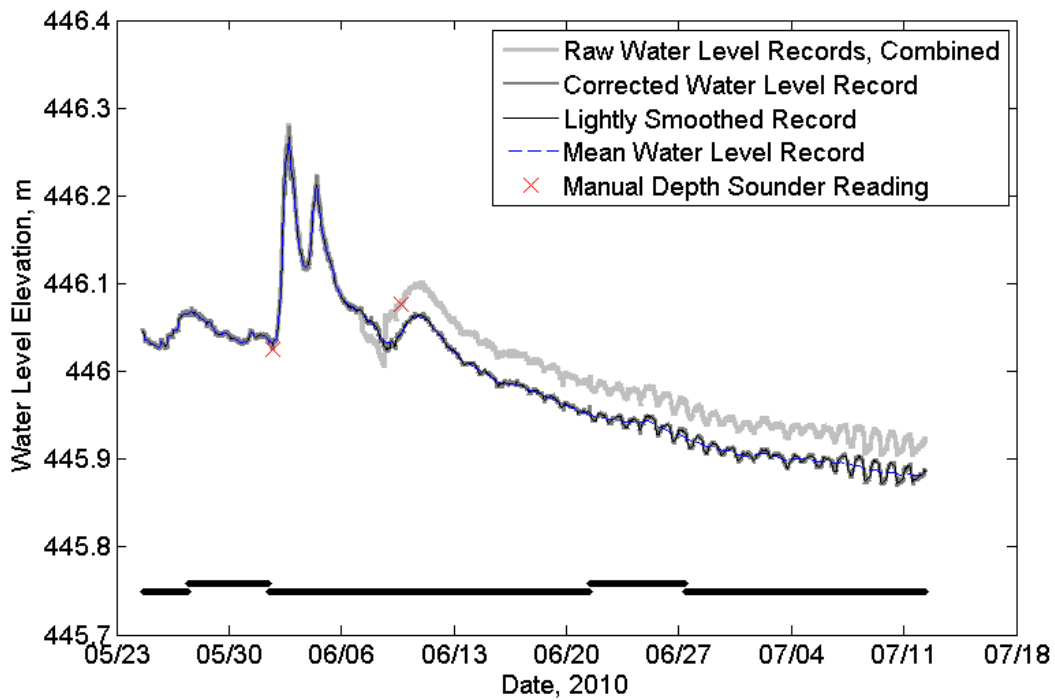


Figure A-1-16. Evolution of the water elevation record of in-stream logger IS1A, WS01.

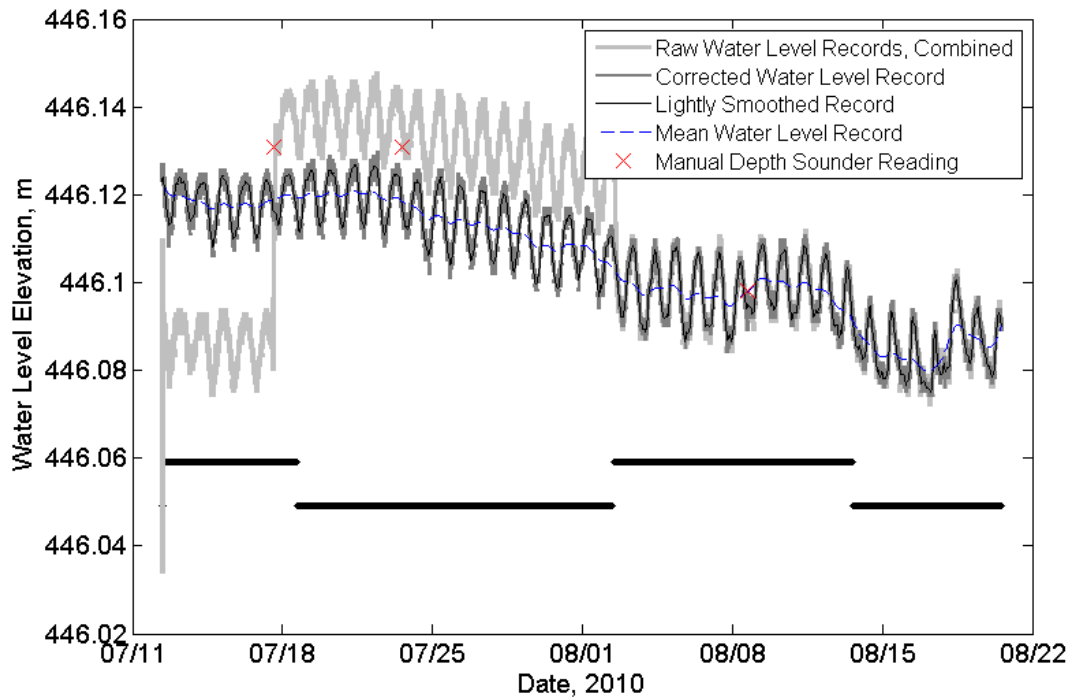


Figure A-1-17. Evolution of the water elevation record of in-stream logger IS1B, WS01.

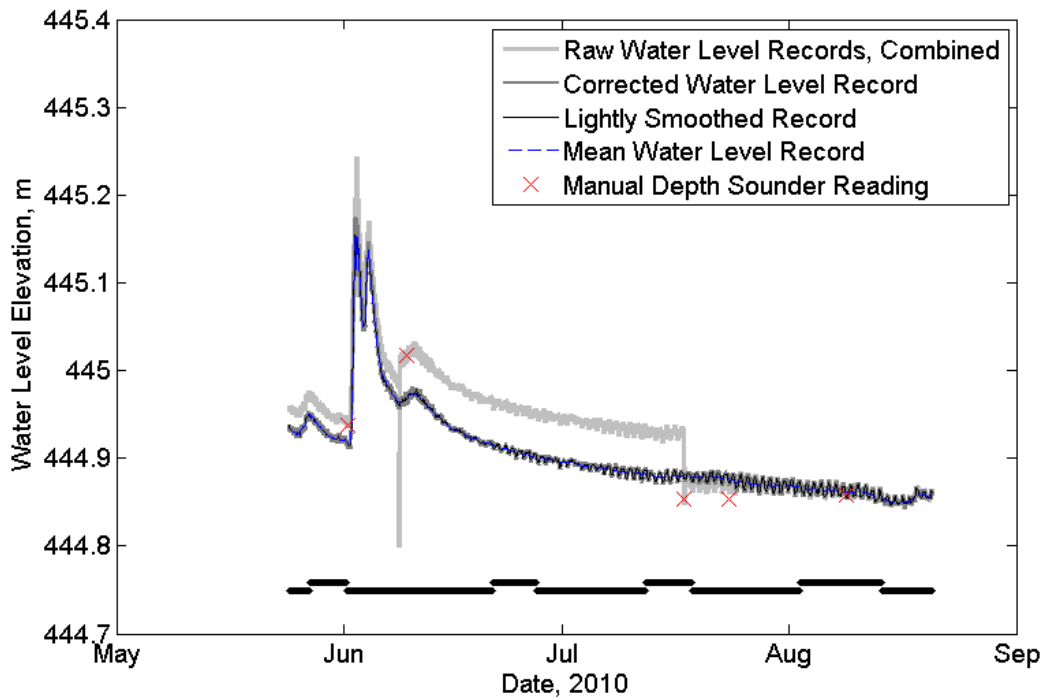


Figure A-1-18. Evolution of the water elevation record of in-stream logger IS2, WS01.

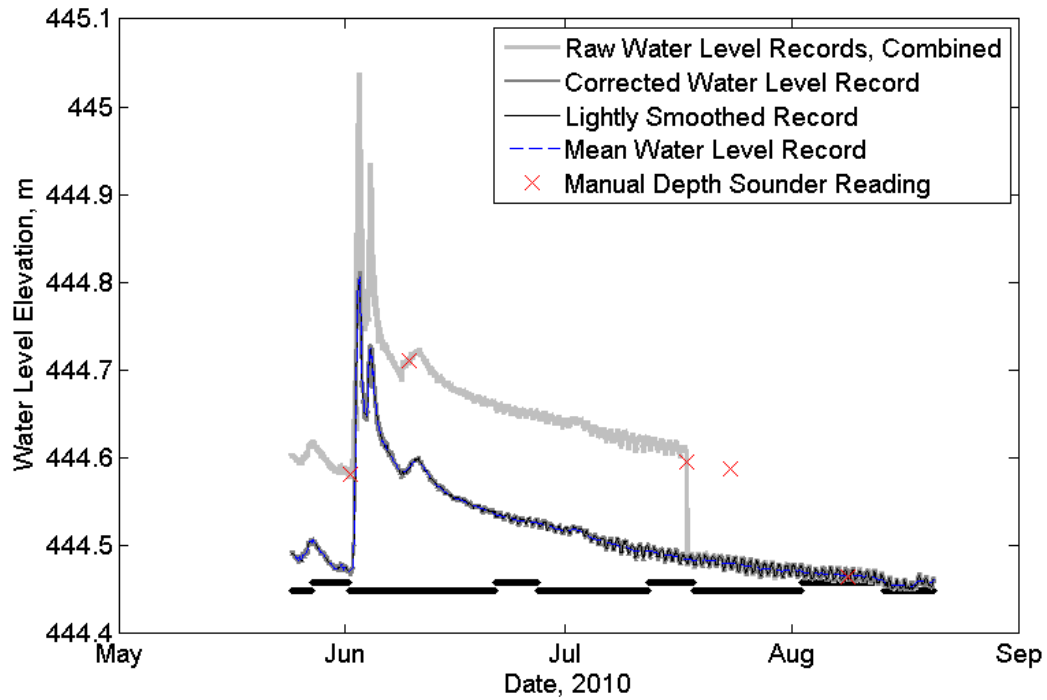


Figure A-1-19. Evolution of the water elevation record of in-stream logger IS3, WS01.

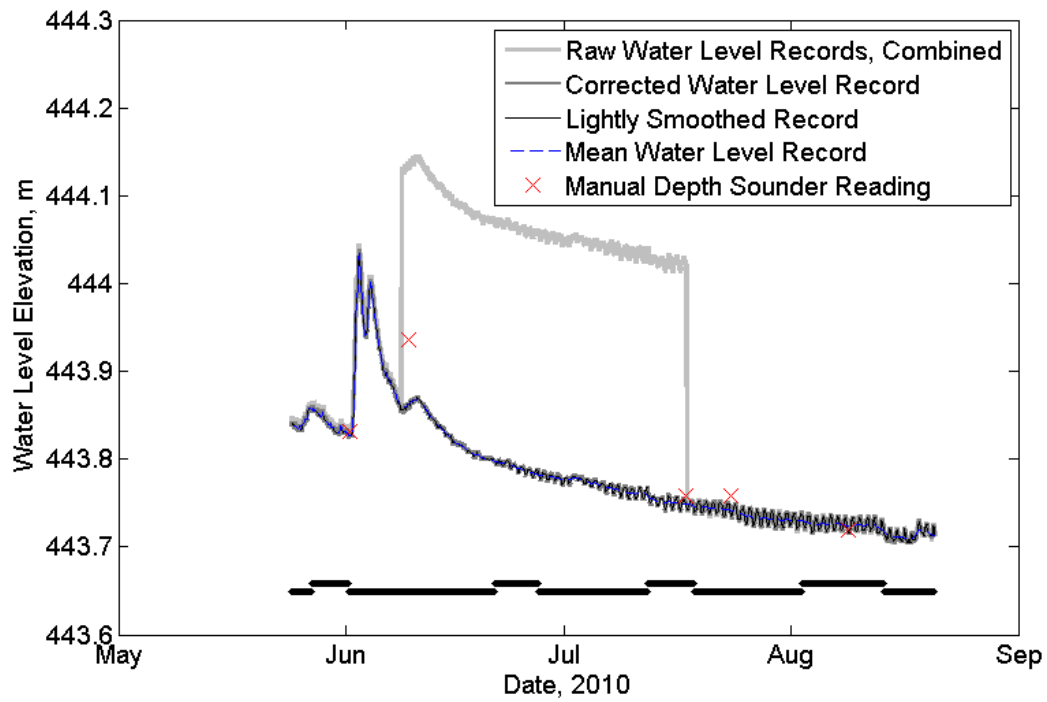


Figure A-1-20. Evolution of the water elevation record of in-stream logger IS4, WS01.

A-2. WS03 - Uncorrected, Corrected, Smoothed, Mean, and Manual Readings

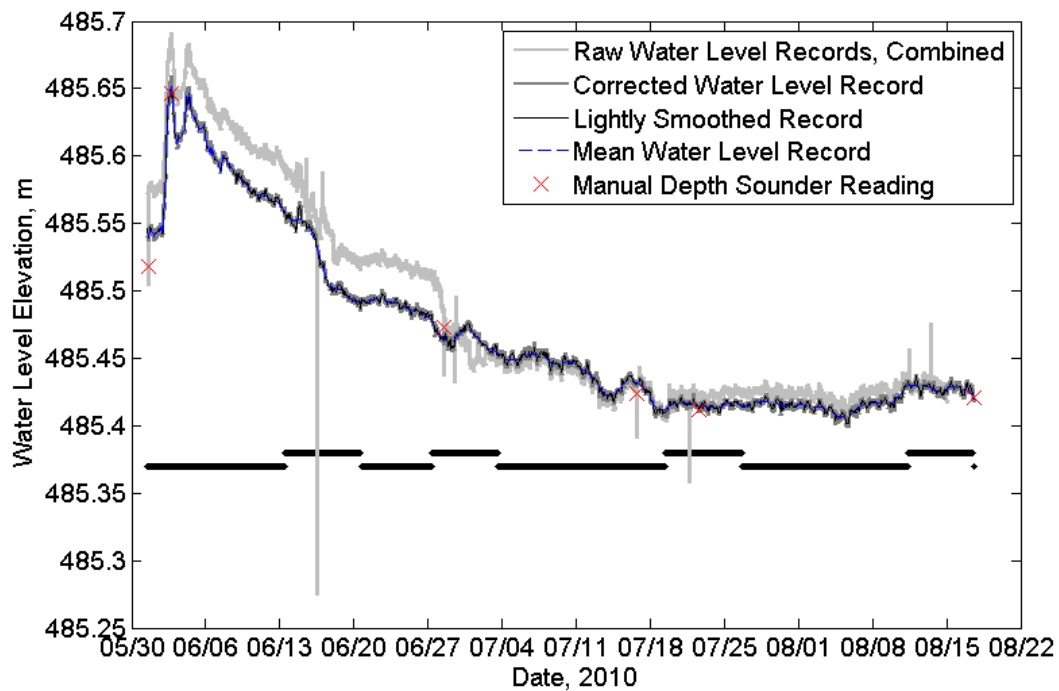


Figure A-2-1. Evolution of the water elevation record of well D3, WS03.

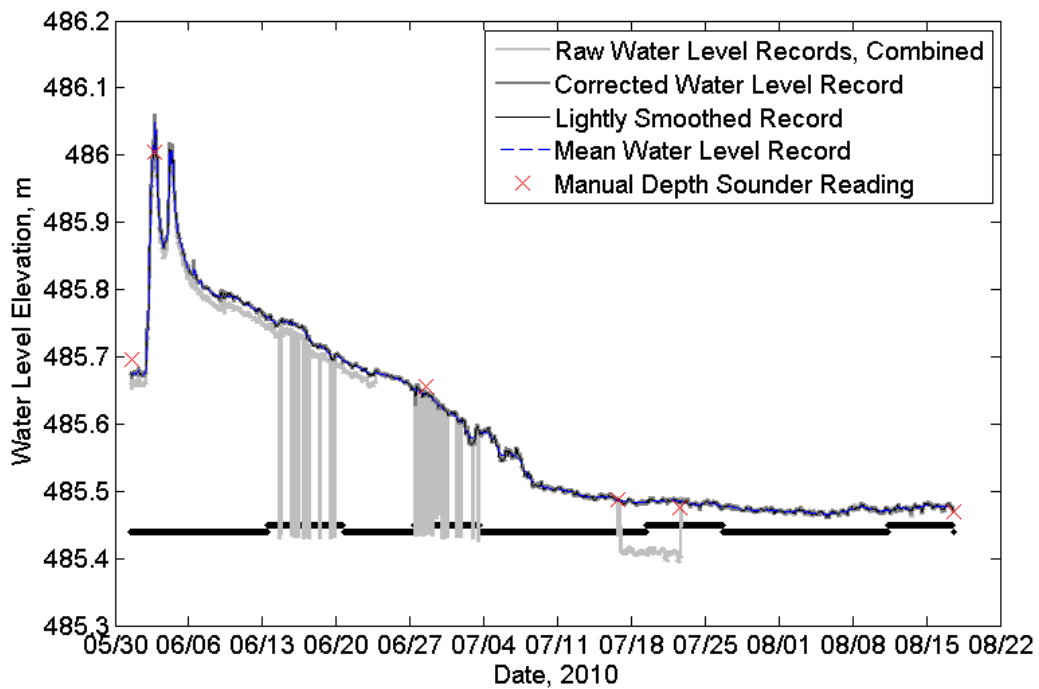


Figure A-2-2. Evolution of the water elevation record of well D6, WS03.

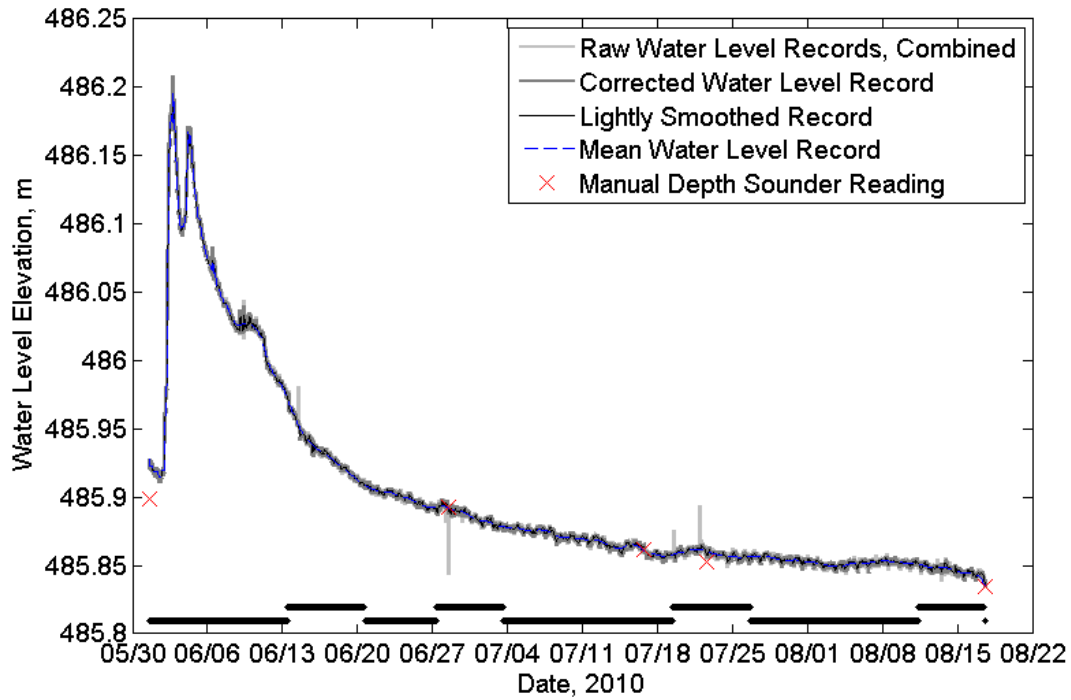


Figure A-2-3. Evolution of the water elevation record of well E5, WS03.

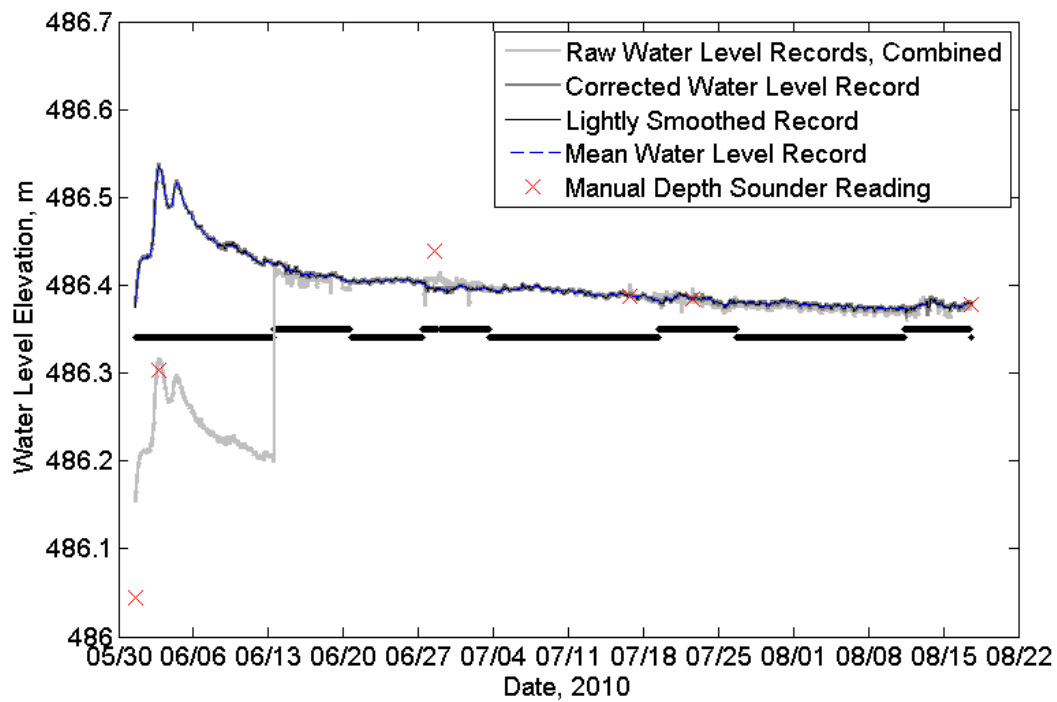


Figure A-2-4. Evolution of the water elevation record of well E6, WS03.

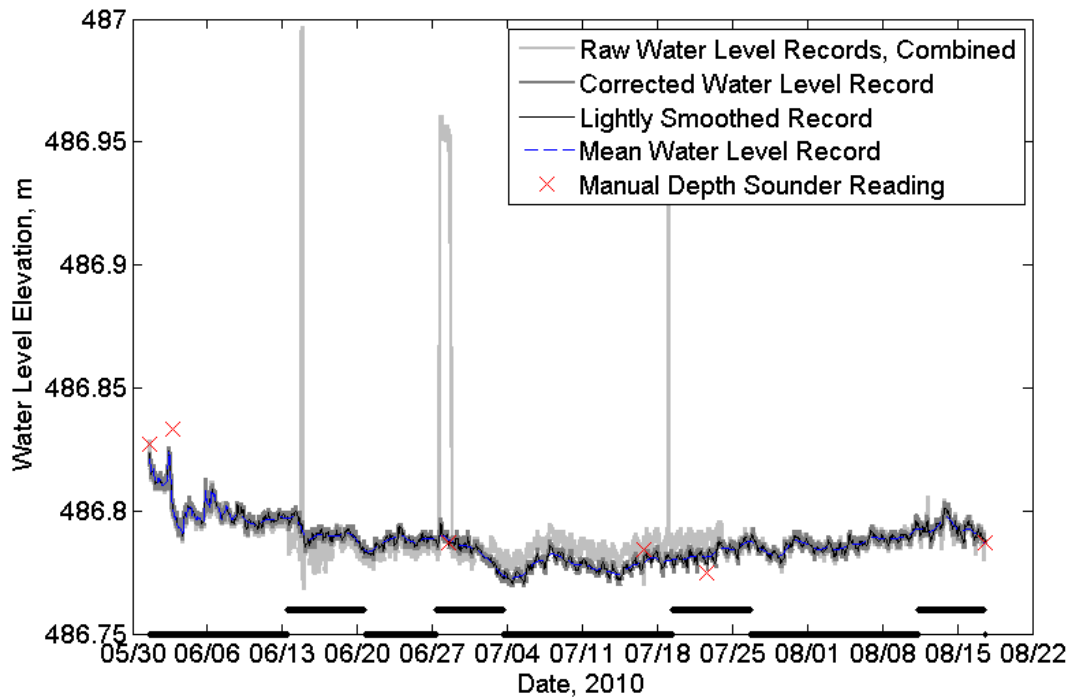


Figure A-2-5. Evolution of the water elevation record of well G5, WS03.

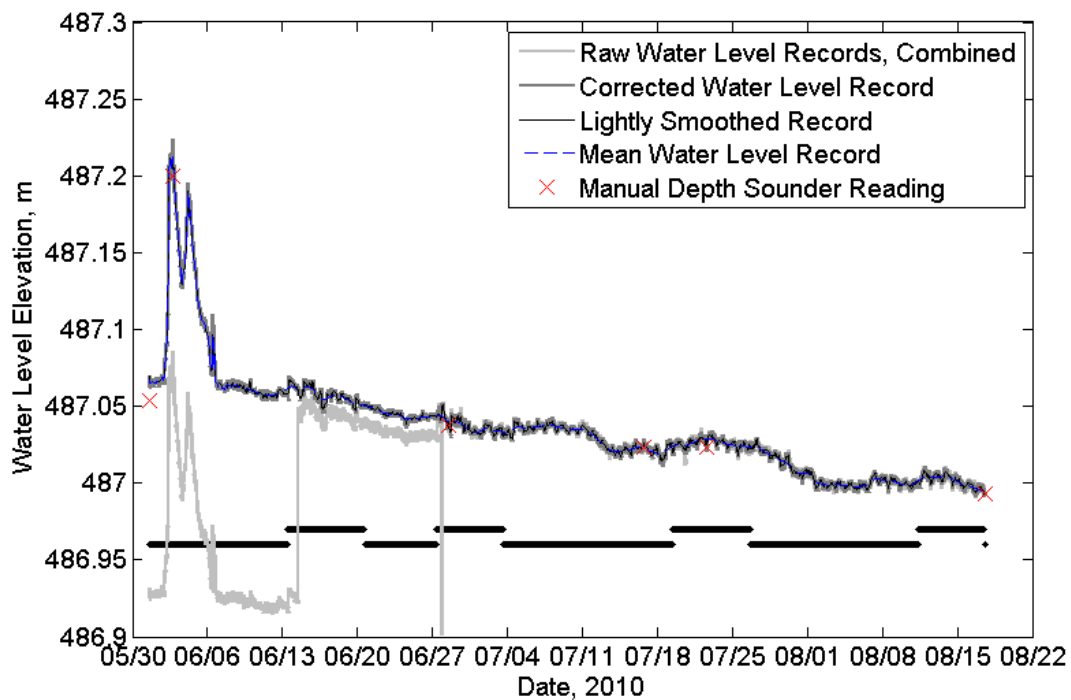


Figure A-2-6. Evolution of the water elevation record of well G6, WS03.

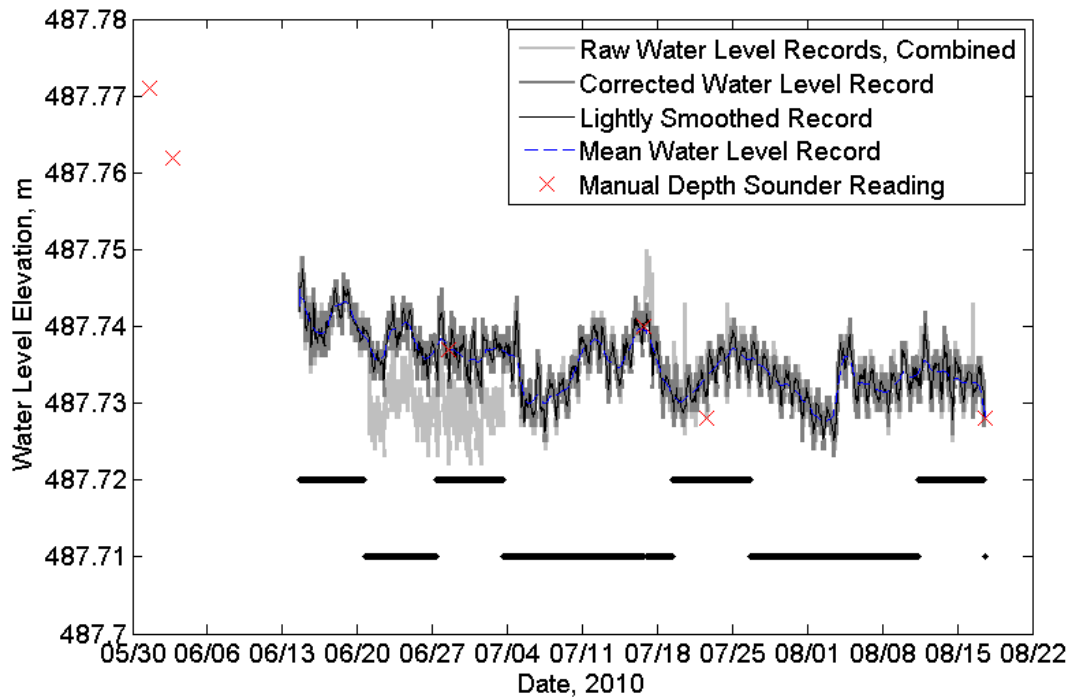


Figure A-2-7. Evolution of the water elevation record of well H3, WS03.

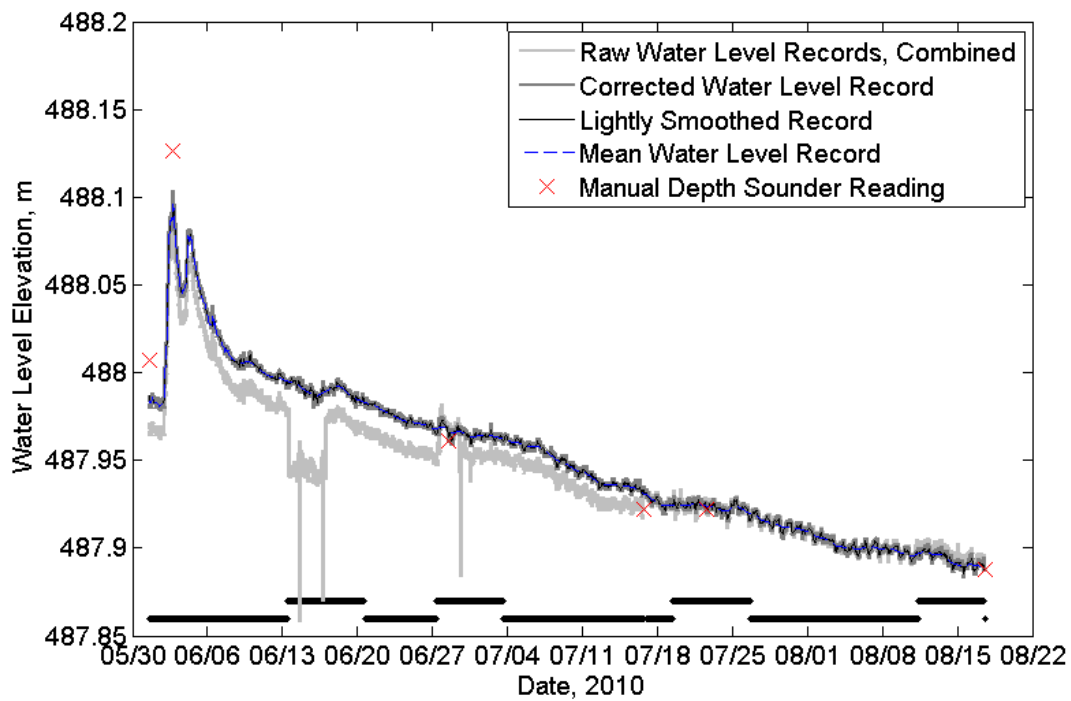


Figure A-2-8. Evolution of the water elevation record of well H5, WS03.

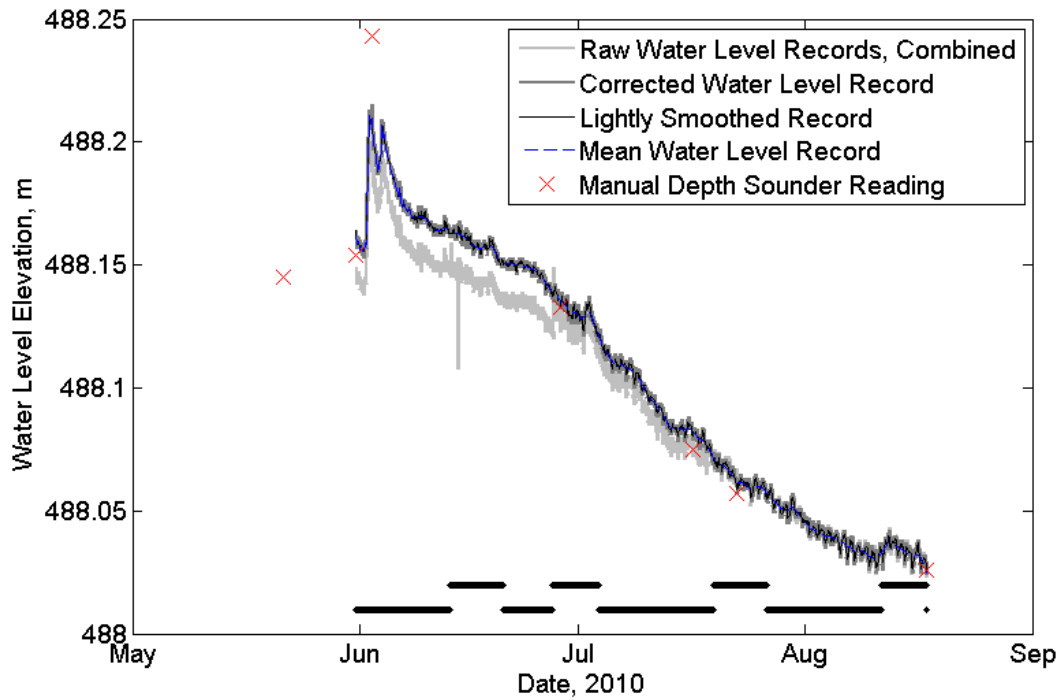


Figure A-2-9. Evolution of the water elevation record of well H6, WS03.

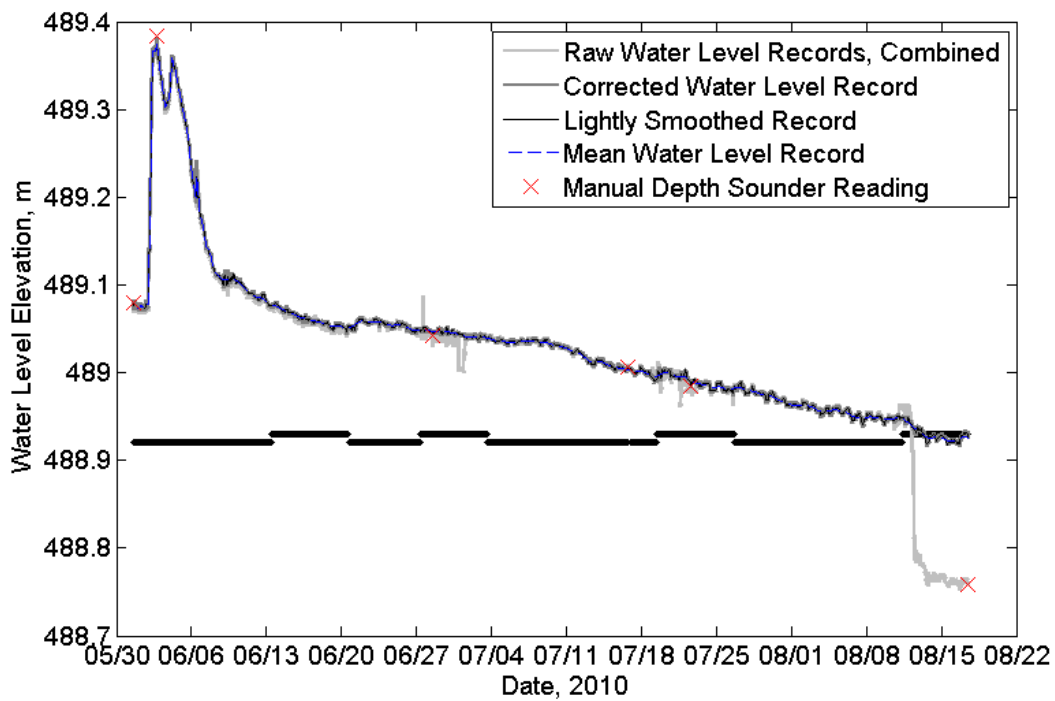


Figure A-2-10. Evolution of the water elevation record of well I5, WS03.

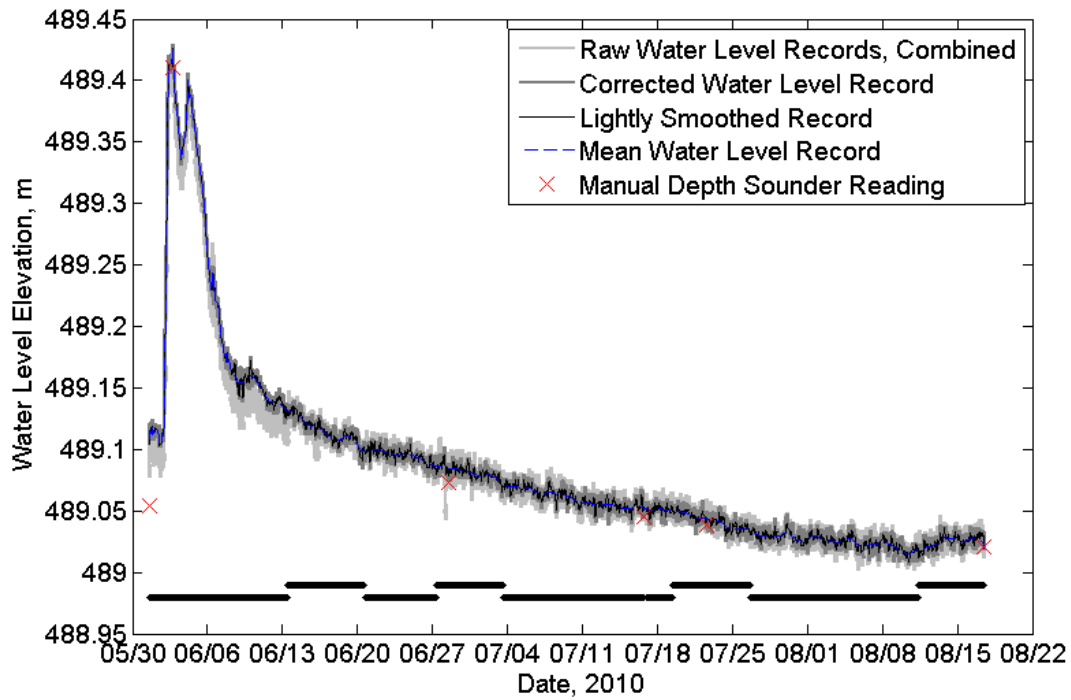


Figure A-2-11. Evolution of the water elevation record of well I6, WS03.

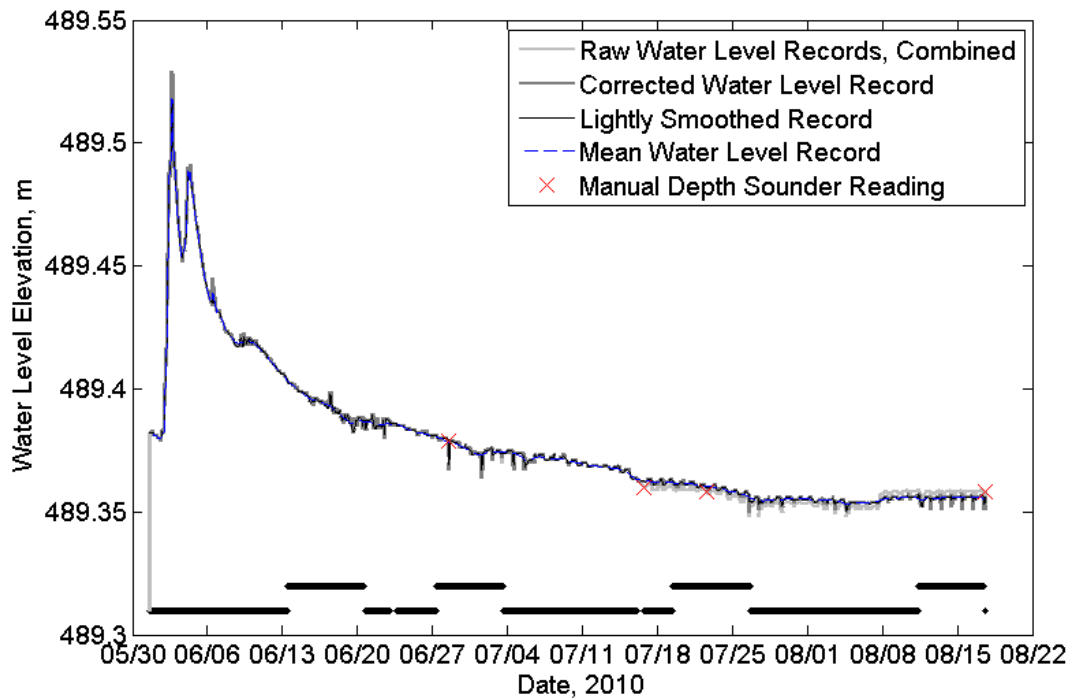


Figure A-2-12. Evolution of the water elevation record of in-stream logger IS0, WS03.

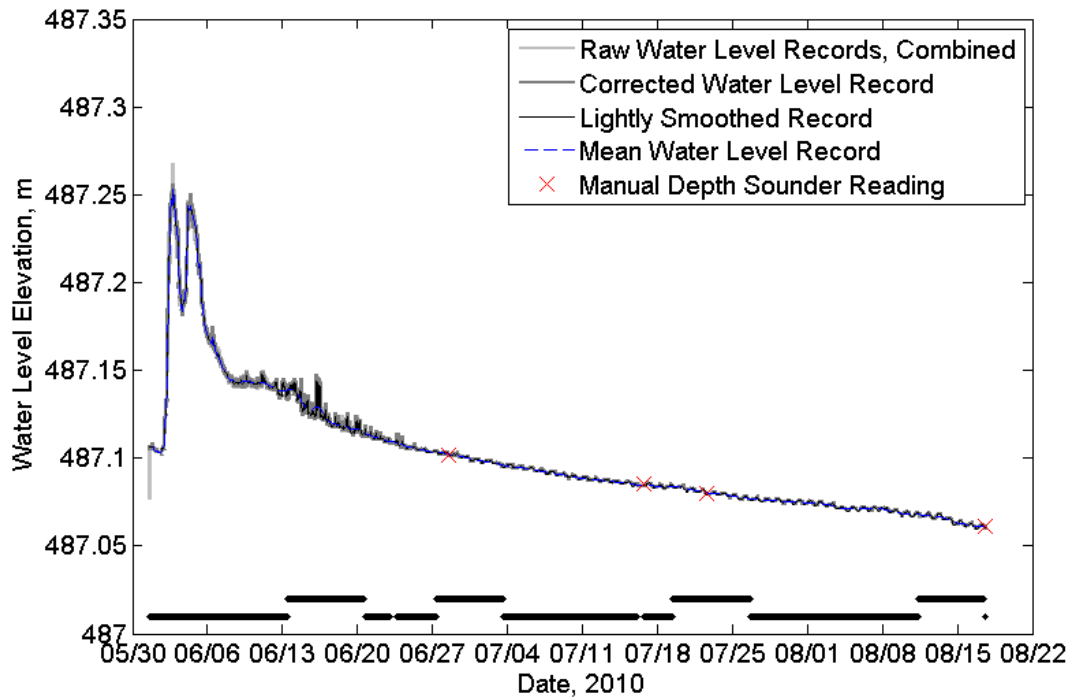


Figure A-2-13. Evolution of the water elevation record of in-stream logger IS2, WS03.

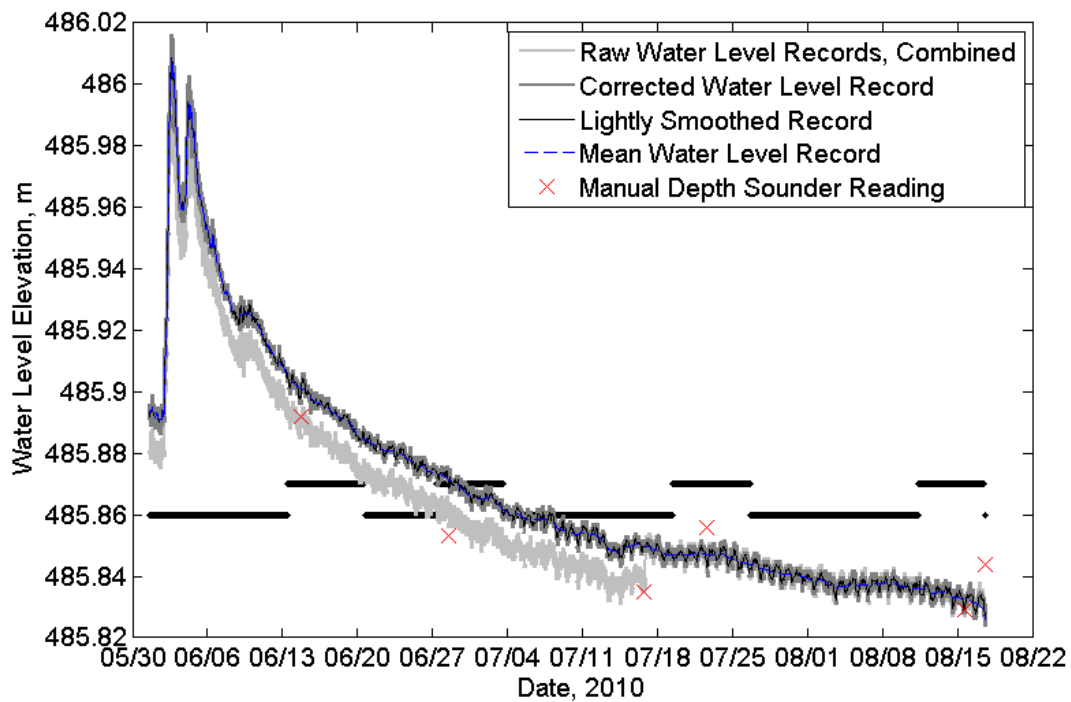


Figure A-2-14. Evolution of the water elevation record of in-stream logger IS3, WS03.

Appendix B

Down- and Cross-valley Gradient Magnitude Plots

B-1. WS01 – Down-valley Gradient Magnitudes

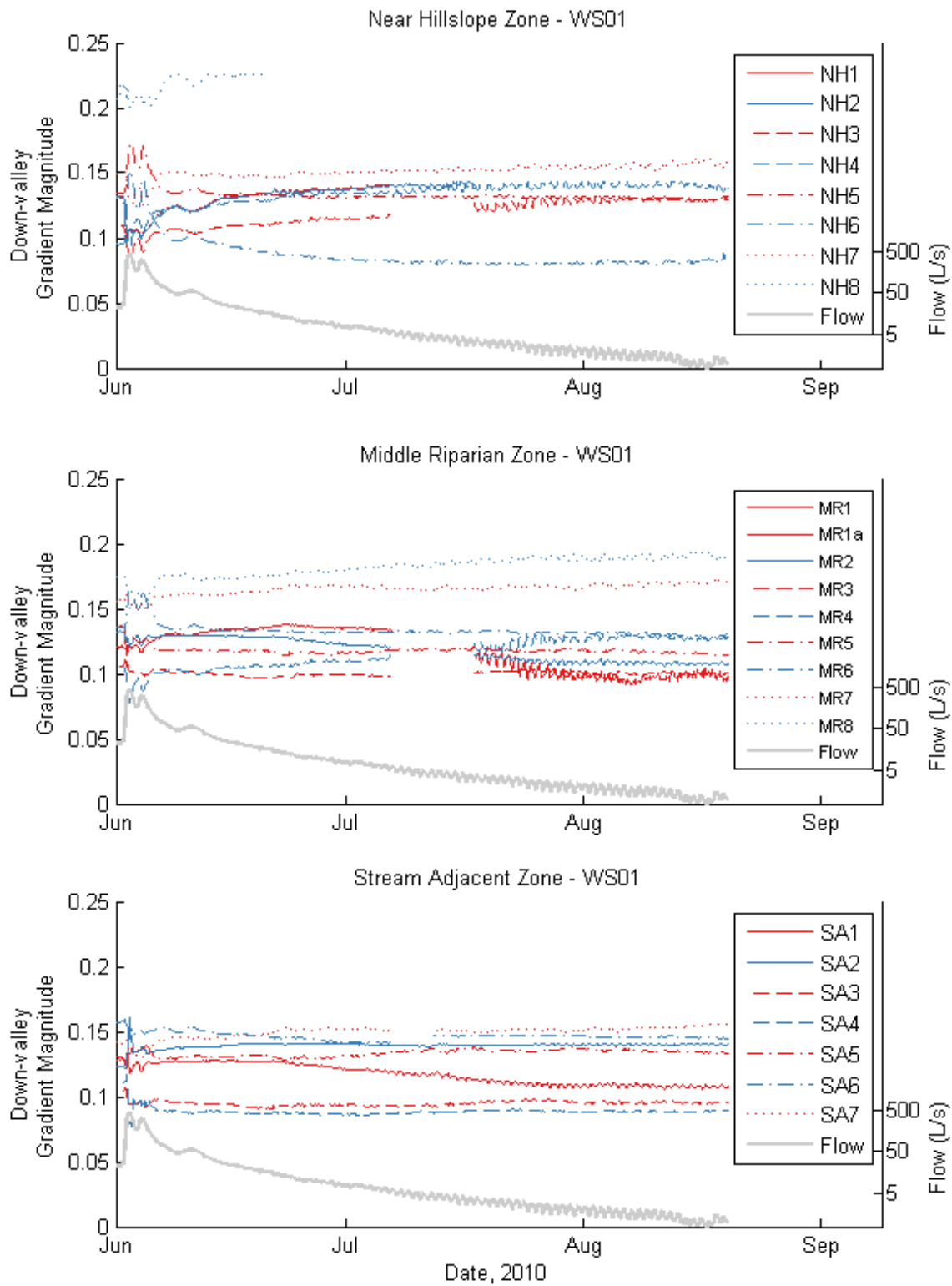


Figure B-1-1. WSD1 down-valley gradient magnitude for the entire field season, plotted according to the three zones labeled in **Figure 4-2**.

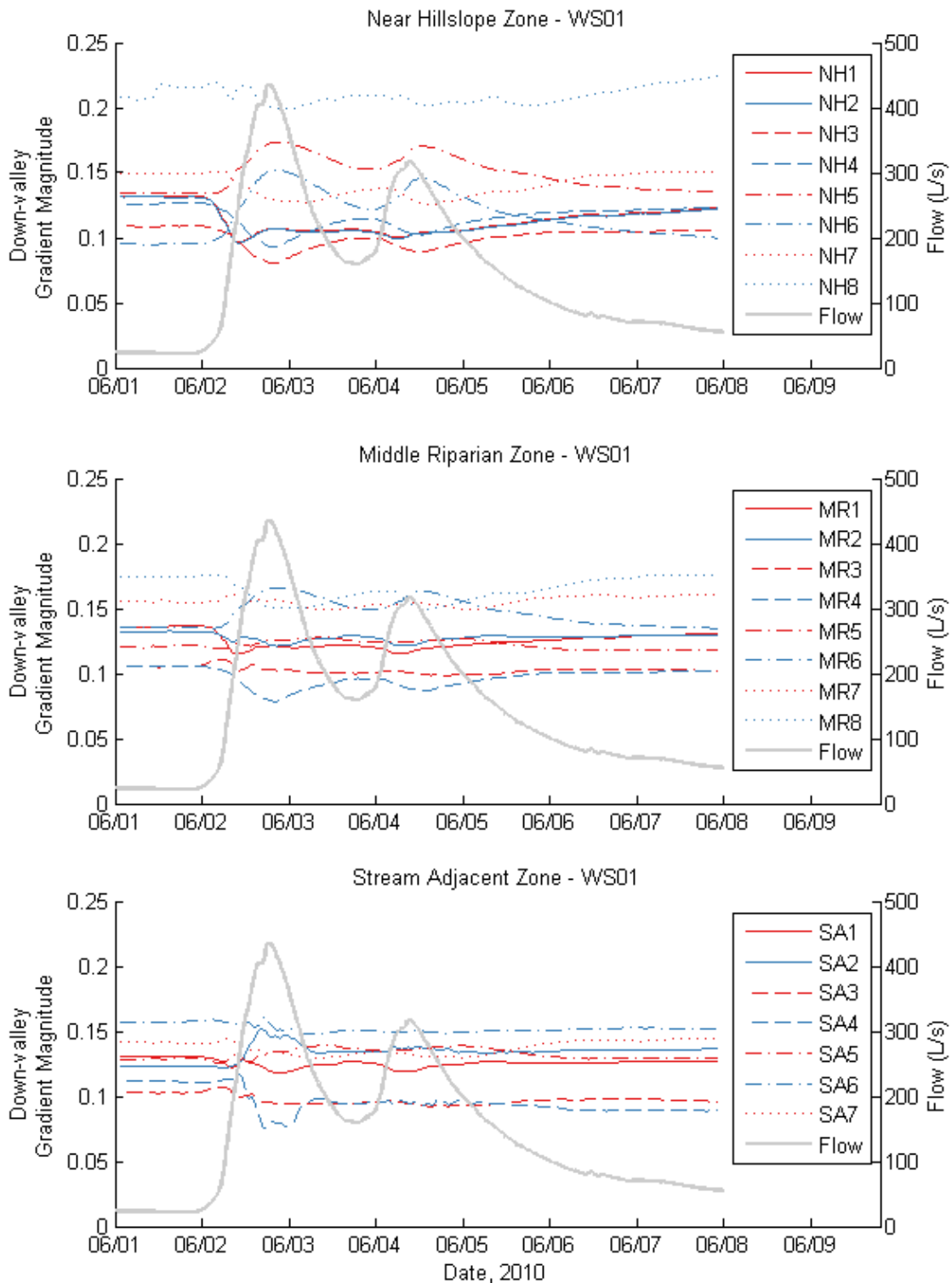


Figure B-1-2. WS01 down-valley gradient magnitude for the storm period, plotted according to the three zones labeled in **Figure 4-2**.

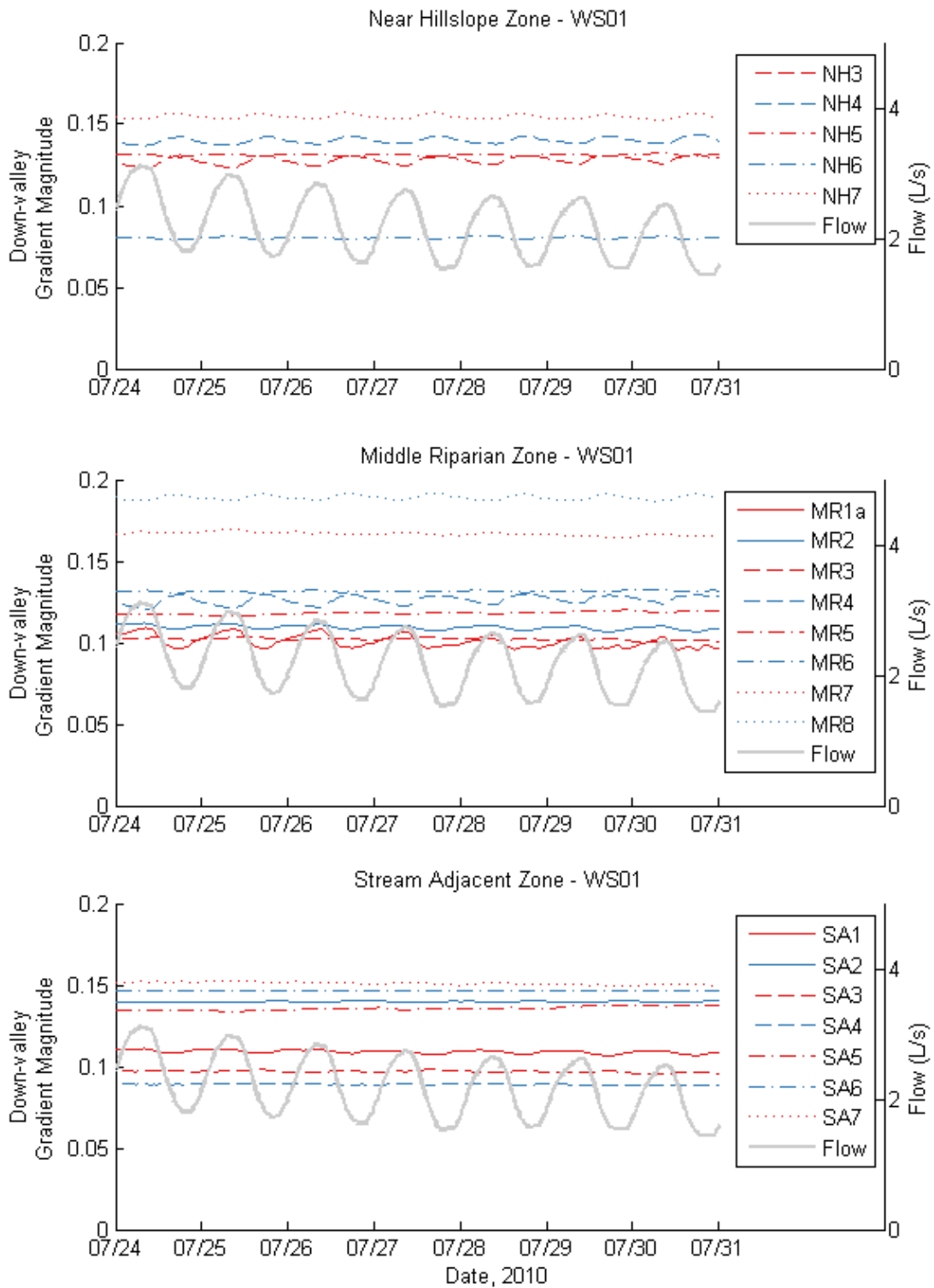


Figure B-1-3. WS01 down-valley gradient magnitude for the week of July 24-31, plotted according to the three zones labeled in **Figure 4-2**.

B-2. WS01 – Cross-valley Gradient Magnitudes

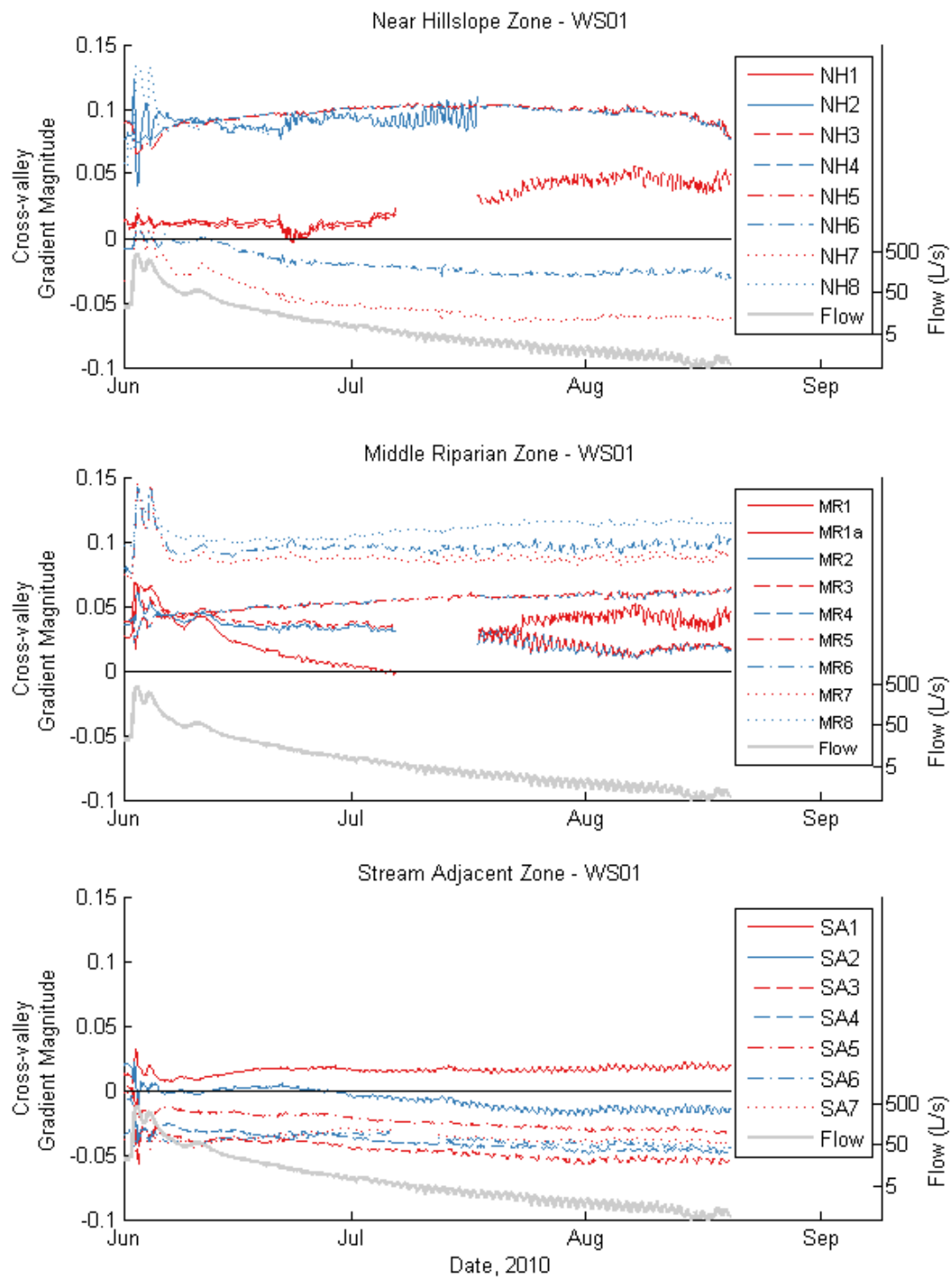


Figure B-2-1. WS01 cross-valley gradient magnitude for the entire field season, plotted according to the three zones labeled in **Figure 4-2**.

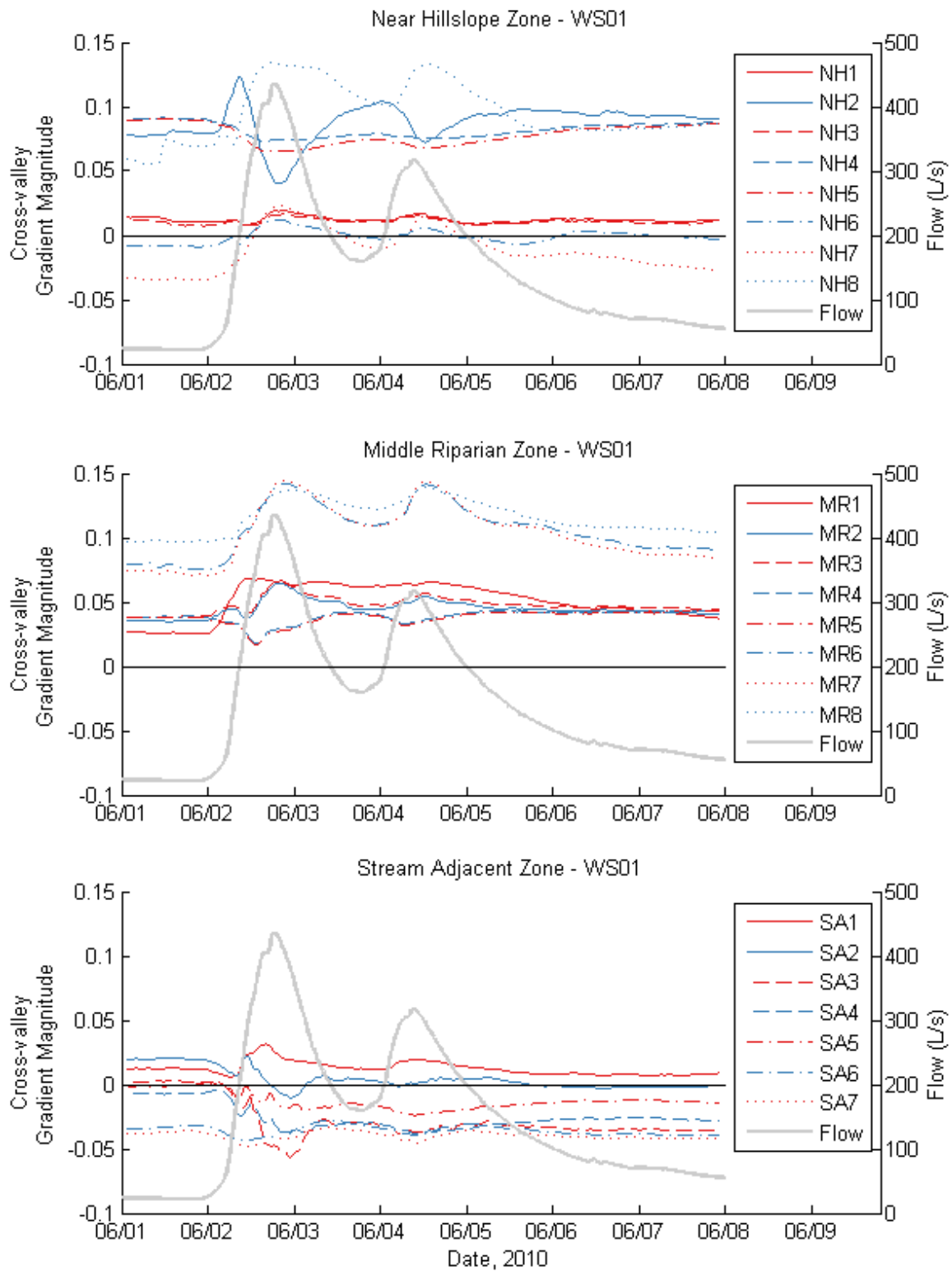


Figure B-2-2. WS01 cross-valley gradient magnitude for the storm period, plotted according to the three zones labeled in **Figure 4-2**.

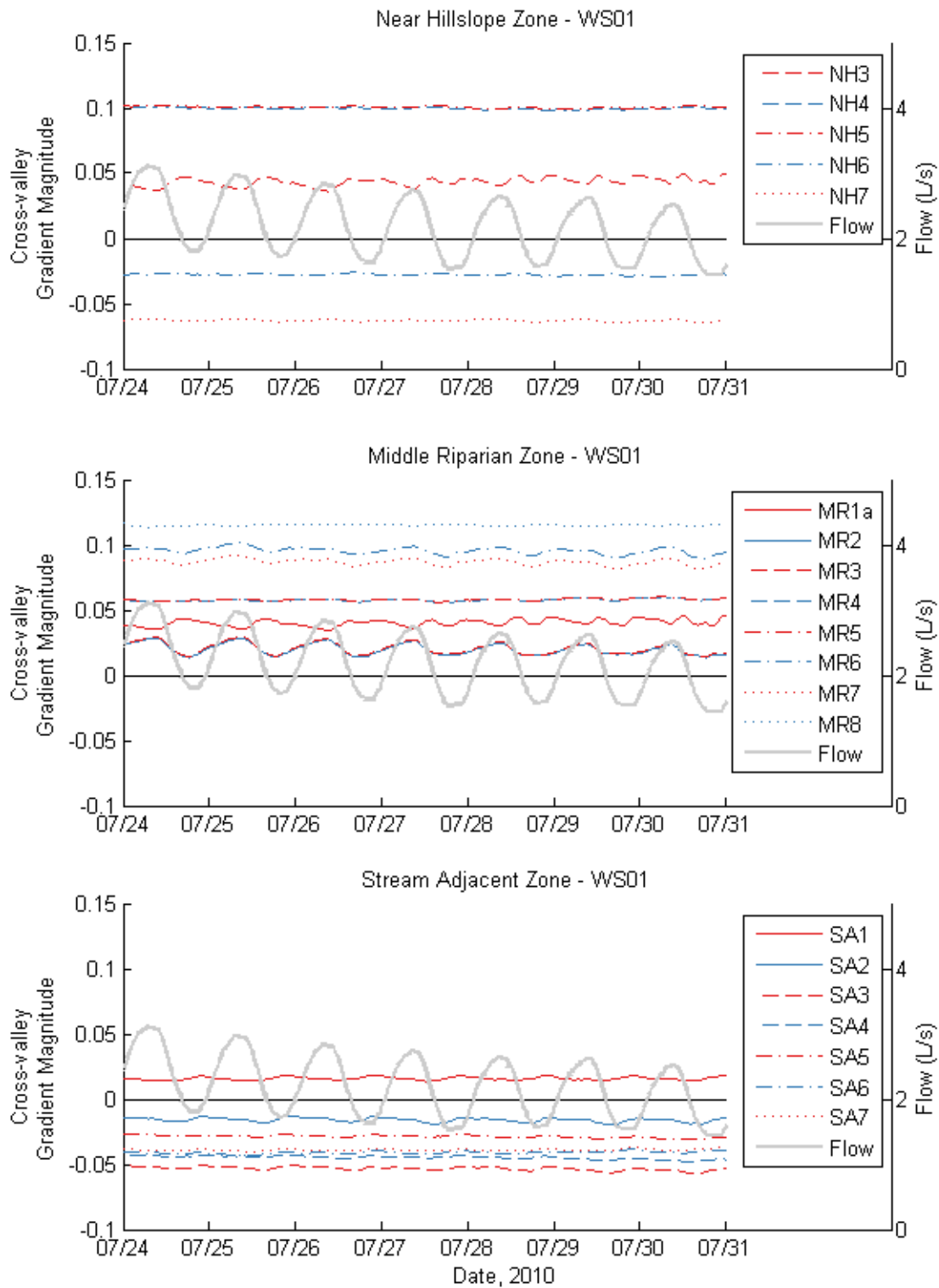


Figure B-2-3. WS01 cross-valley gradient magnitude for the week of July 24-31, plotted according to the three zones labeled in **Figure 4-2**.

B-3. WS03 – Down-valley Gradient Magnitudes

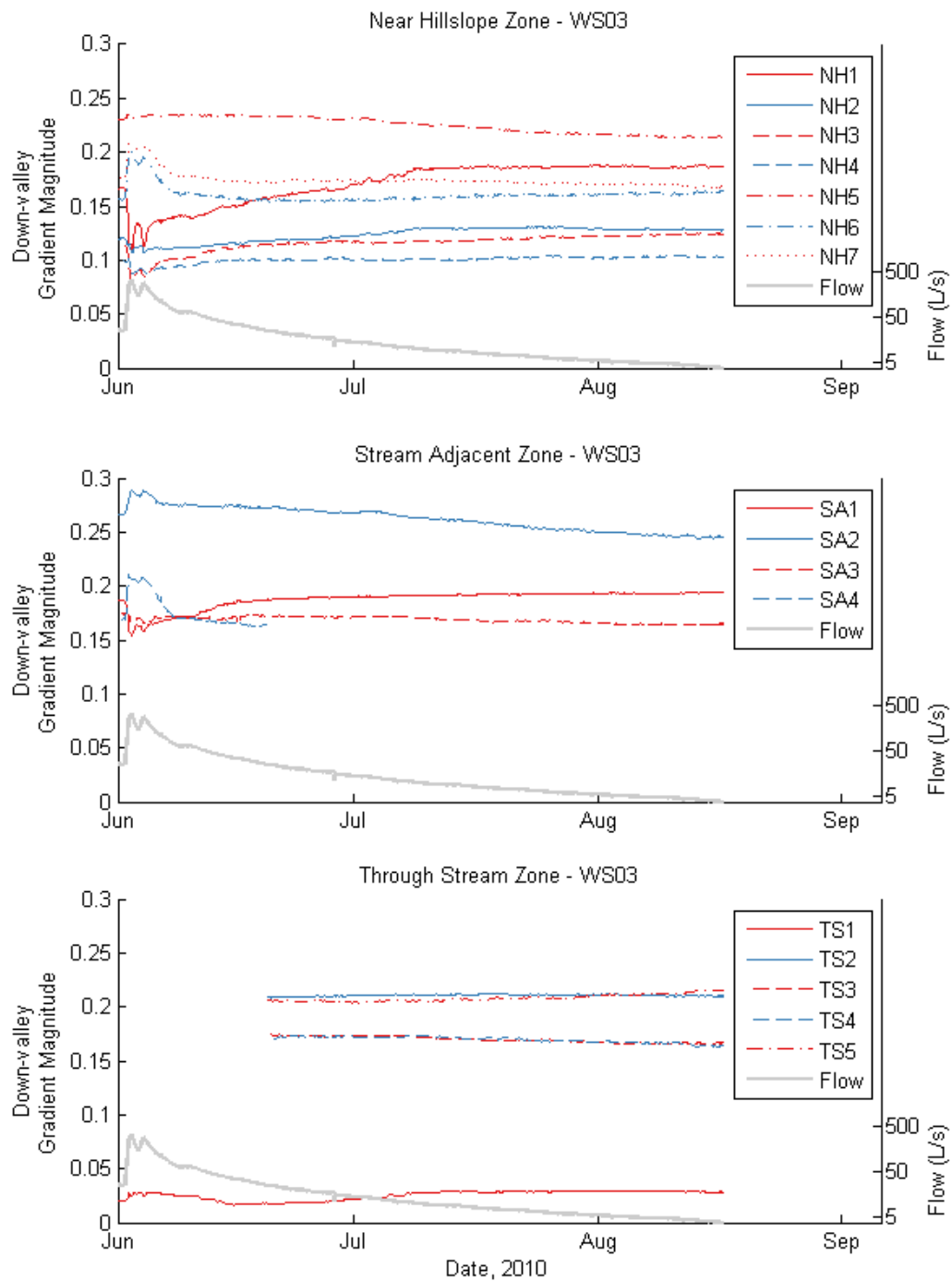


Figure B-3-1. WS03 down-valley gradient magnitude for the entire field season, plotted according to the three zones labeled in **Figure 4-3**.

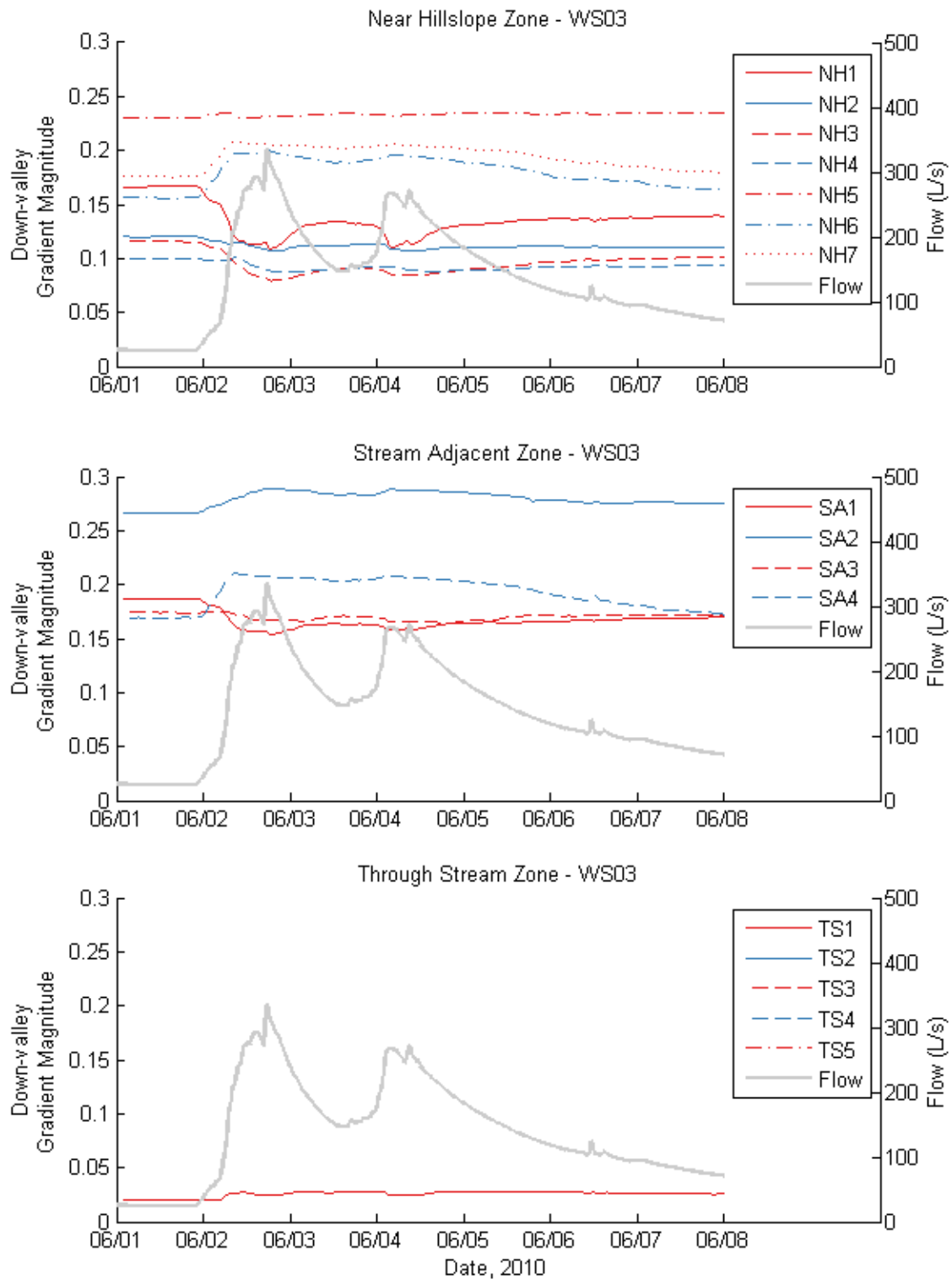


Figure B-3-2. WS03 down-valley gradient magnitude for the storm period, plotted according to the three zones labeled in **Figure 4-3**.

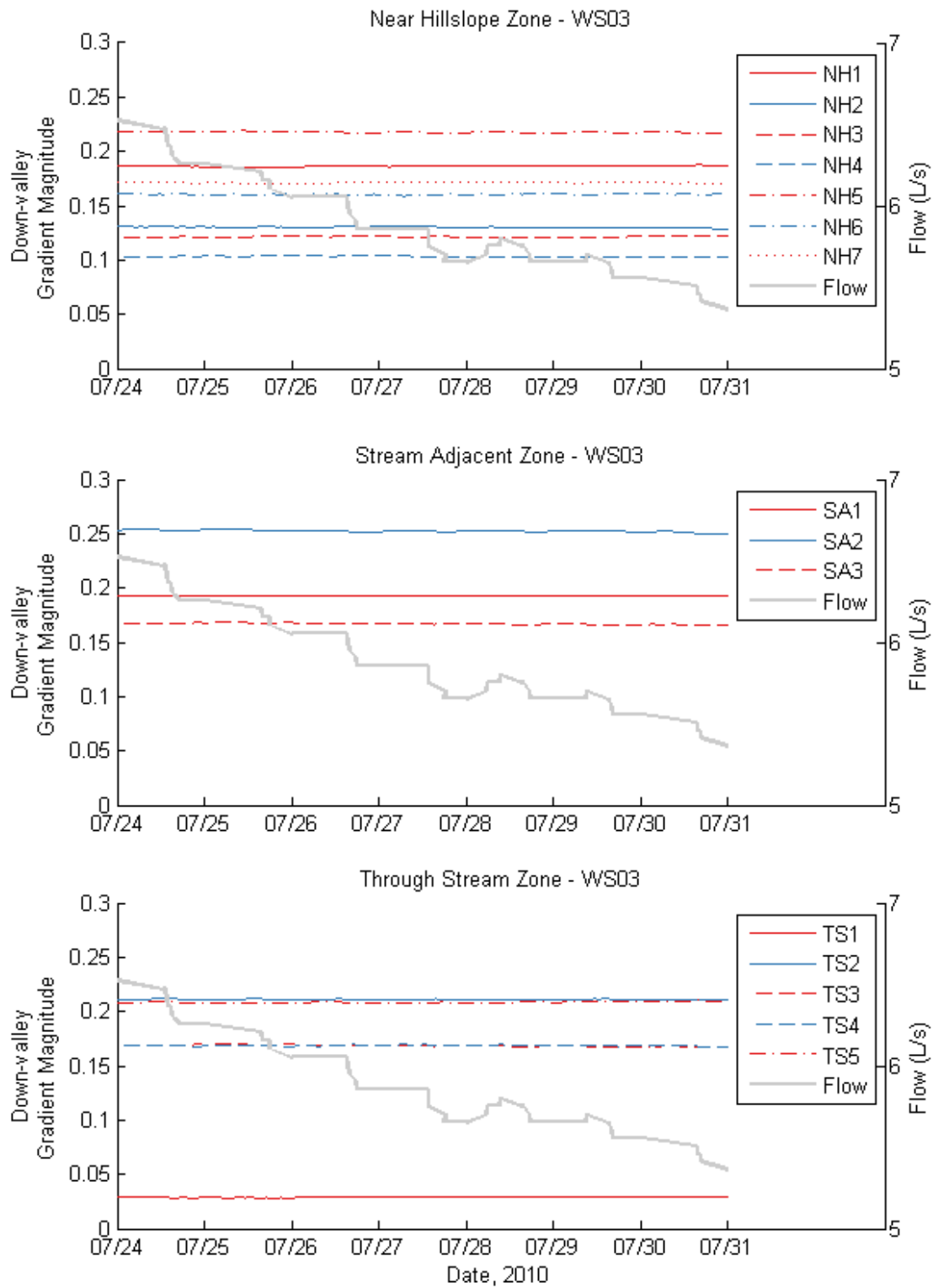


Figure B-3-3. WS03 down-valley gradient magnitude for the week of July 24-31, plotted according to the three zones labeled in **Figure 4-3**.

B-4. WS03 – Cross-valley Gradient Magnitudes

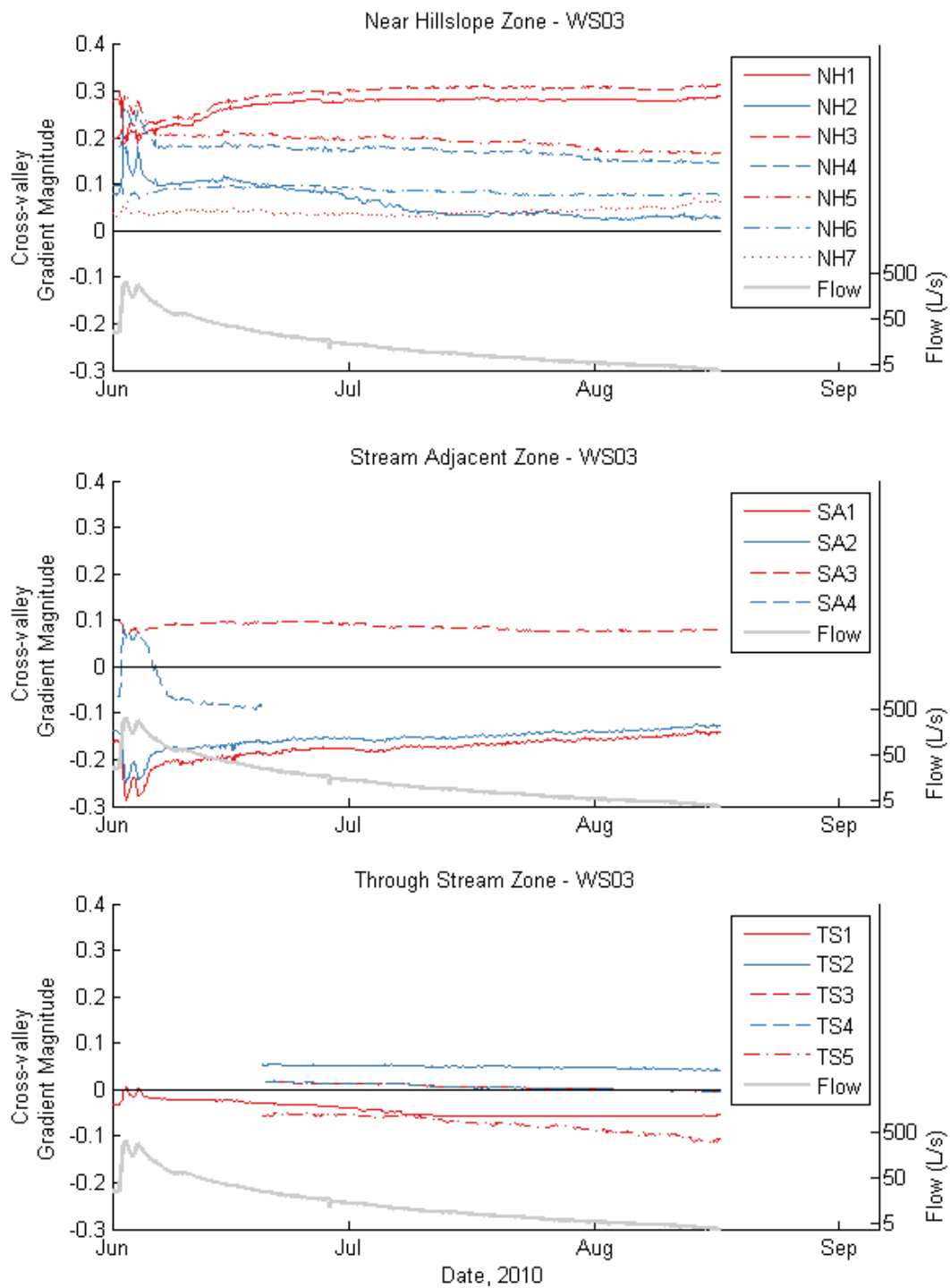


Figure B-4-1. WS03 cross-valley gradient magnitude for the entire season, plotted according to the three zones labeled in **Figure 4-3**.

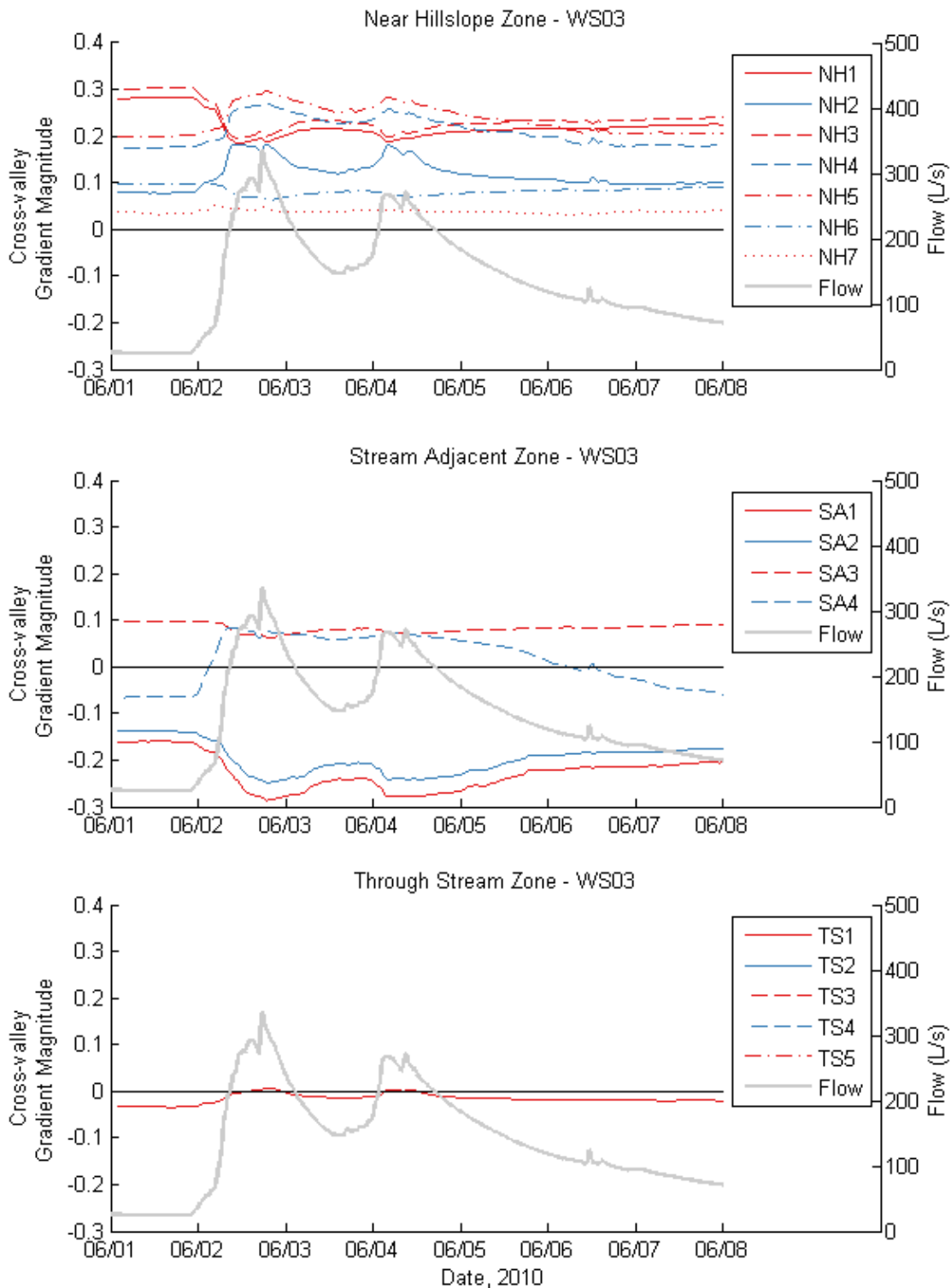


Figure B-4-2. WS03 cross-valley gradient magnitude for the storm period, plotted according to the three zones labeled in **Figure 4-3**.

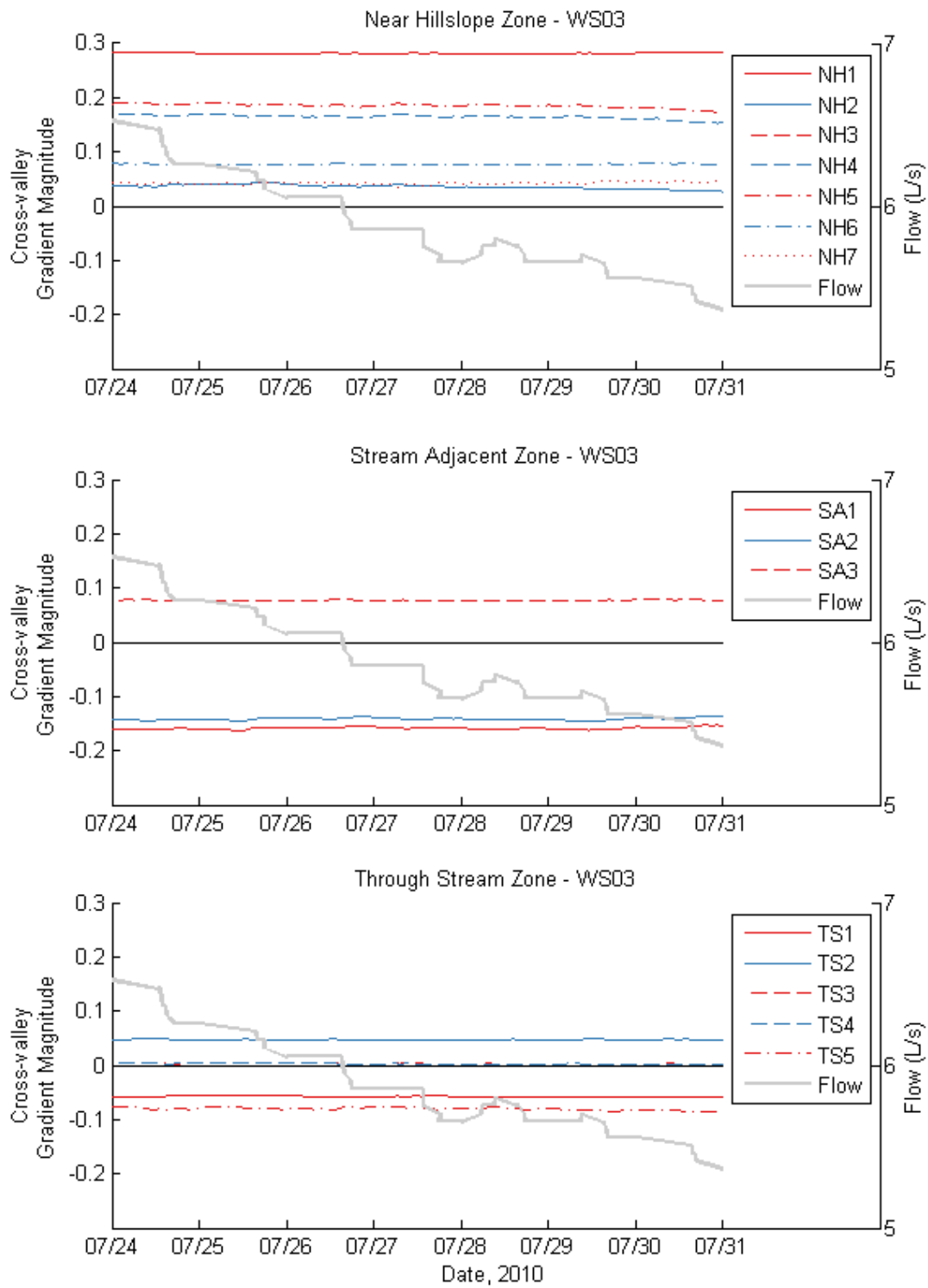


Figure B-4-3. WS03 cross-valley gradient magnitude for the week of July 24-31, plotted according to the three zones labeled in **Figure 4-3**.

Appendix C

Anomaly Magnitude vs. Vapor Pressure Deficit in WS01

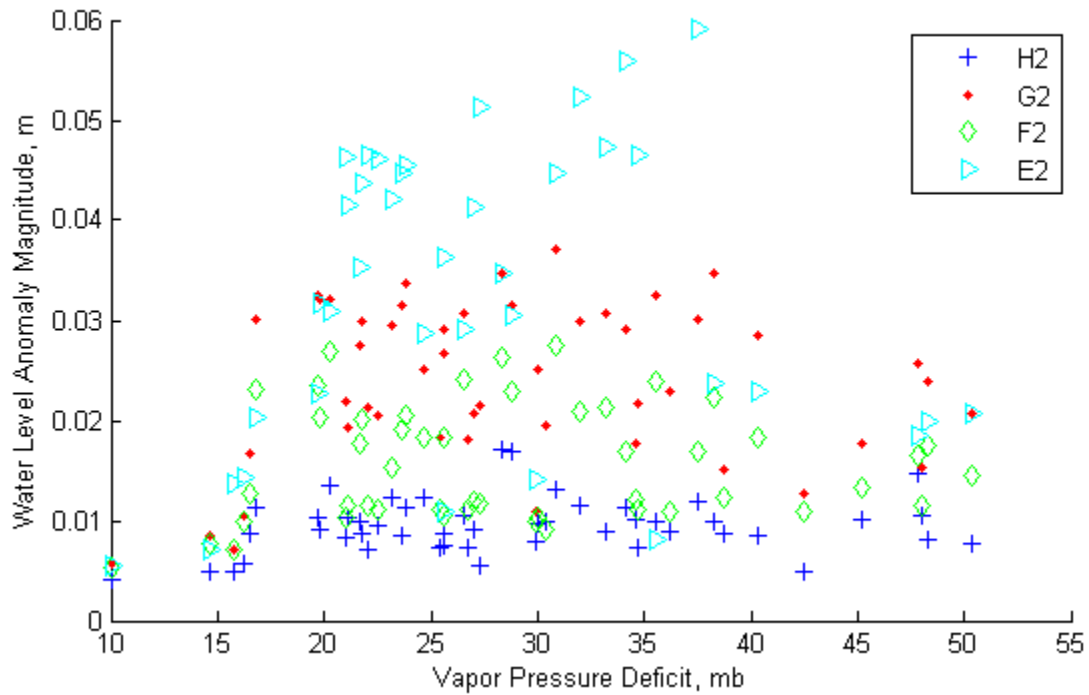


Figure C-1. Water level anomaly magnitude plotted against change in vapor pressure deficit for the same daily period in the middle-riparian (MR) zone of WS01.

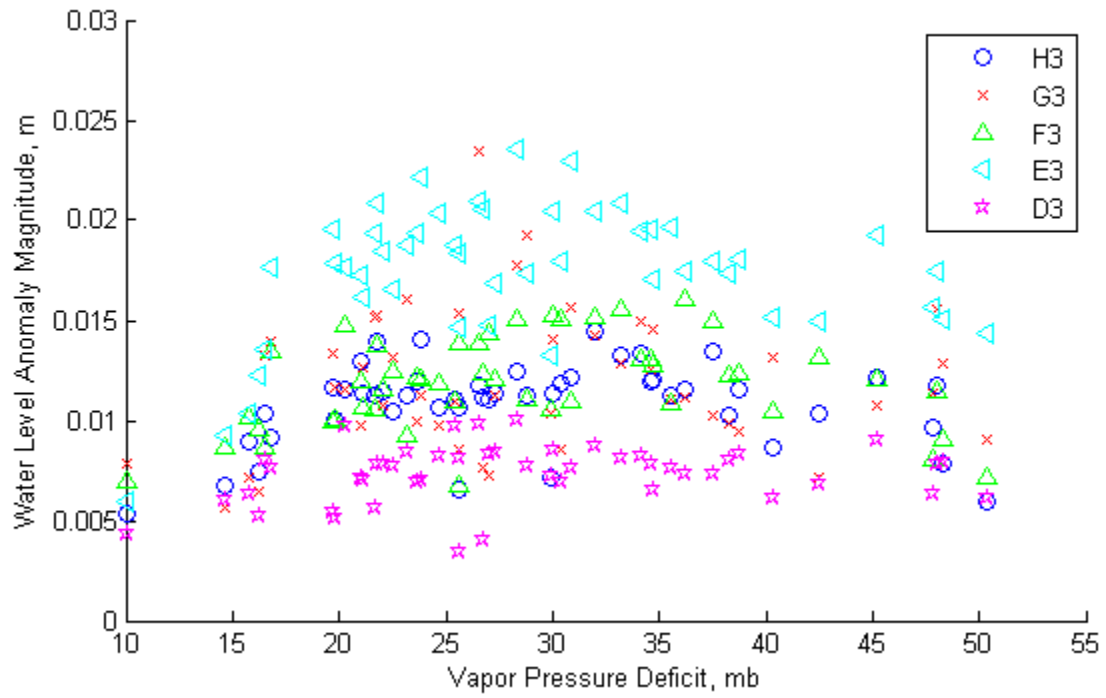


Figure C-2. Water level anomaly magnitude plotted against change in vapor pressure deficit for the same daily period in the stream-adjacent (SA) zone of WS01.

Appendix D

Water Level Anomalies in WS03

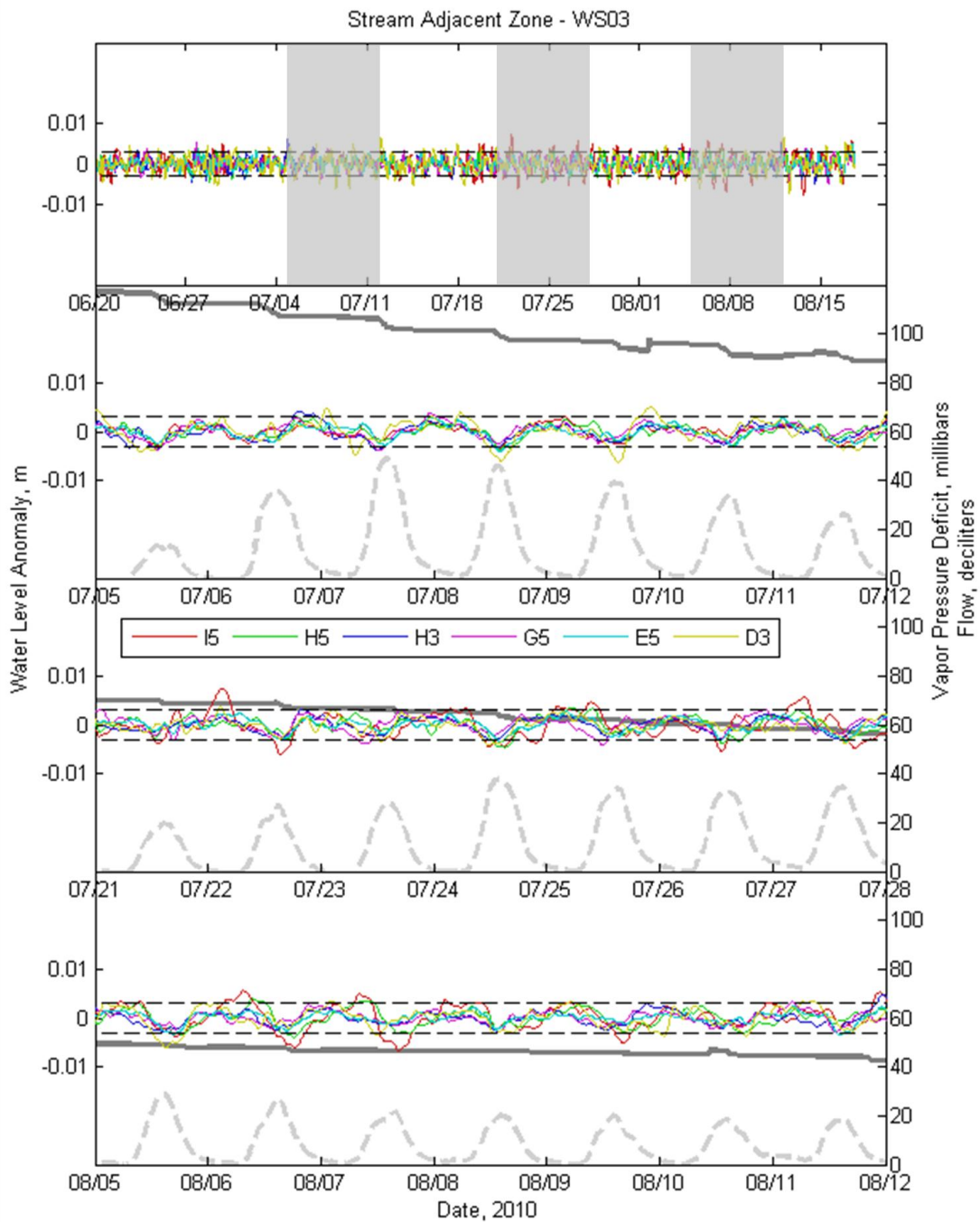


Figure D-1. Water level anomalies in the WS03 riparian wells, stream-adjacent (SA) zone. The dark grey line is flow at the weir 75 m downstream, and the light grey dashed line is vapor pressure deficit at 4.5 m above the ground, recorded at a meteorological station several hundred meters away. The grey rectangles in the top panel indicate when each of the week-long sub-periods occurs. 3-mm data logger tolerance is shown as black dashed lines.

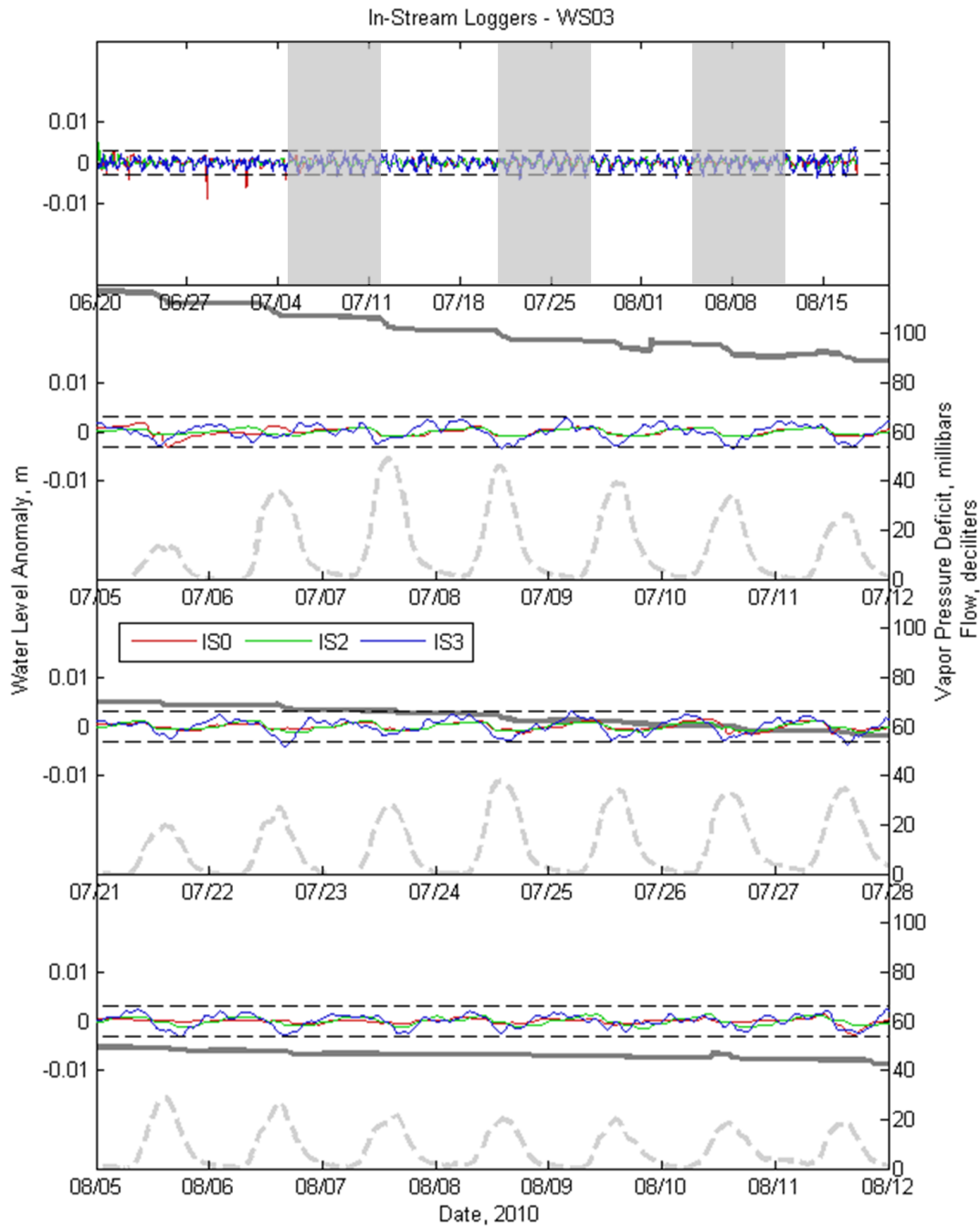


Figure D-2. Water level anomalies in the WS03 riparian wells, in-stream loggers. The dark grey line is flow at the weir 75 m downstream, and the light grey dashed line is vapor pressure deficit at 4.5 m above the ground, recorded at a meteorological station several hundred meters away. The grey rectangles in the top panel indicate when each of the week-long sub-periods occurs. 3-mm data logger tolerance is shown as black dashed lines.